Max-Planck-Institut
für Meteorologie

MAX-PLANCK-GESELLSCHAFT

Analysis of multistability and abrupt transitions - method studies with a global atmosphere-vegetation model simulating the end of the African Humid Period

Sebastian Bathiany

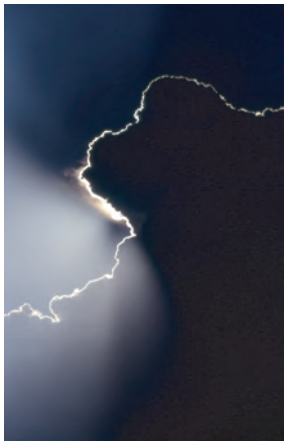

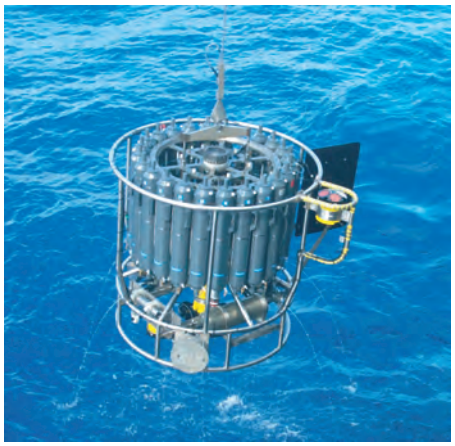

Berichte zur Erdsystemforschung 125
2013

Reports on Earth System Science

Hinweis

Die Berichte zur Erdsystemforschung werden vom Max-Planck-Institut für Meteorologie in Hamburg in unregelmäßiger Abfolge herausgegeben.

Sie enthalten wissenschaftliche und technische Beiträge, inklusive Dissertationen.

Die Beiträge geben nicht notwendigerweise die Auffassung des Instituts wieder.

Die "Berichte zur Erdsystemforschung" führen die vorherigen Reihen "Reports" und "Examensarbeiten" weiter.

Notice

The Reports on Earth System Science are published by the Max Planck Institute for Meteorology in Hamburg. They appear in irregular intervals.

They contain scientific and technical contributions, including Ph. D. theses.

The Reports do not necessarily reflect the opinion of the Institute.

The "Reports on Earth System Science" continue the former "Reports" and "Examensarbeiten" of the Max Planck Institute.

Anschrift / Address

Max-Planck-Institut für Meteorologie
Bundesstrasse 53
20146 Hamburg
Deutschland

Tel.: +49-(0)40-4 11 73-0
Fax: +49-(0)40-4 11 73-298
Web: www.mpimet.mpg.de

Layout:

Bettina Diallo, PR & Grafik

Titelfotos:
vorne:
Christian Klepp - Jochem Marotzke - Christian Klepp
hinten:
Clotilde Dubois - Christian Klepp - Katsumasa Tanaka

Berichte zur Erdsystemforschung 125/2013

Analysis of multistability and abrupt transitions - method studies with a global atmosphere-vegetation model simulating the end of the African Humid Period

Sebastian Bathiany

aus Heidelberg

Hamburg 2012

Reports on Earth System Science 125/2013

ISSN 1614-1199

Sebastian Bathiany
Max-Planck-Institut für Meteorologie
Bundesstrasse 53
20146 Hamburg

Als Dissertation angenommen
vom Department Geowissenschaften der Universität Hamburg

auf Grund der Gutachten von
Prof. Dr. Martin Claussen
und
Prof. Dr. Klaus Fraedrich

Hamburg, den 14. Dezember 2012
Prof. Dr. Jürgen Oßenbrügge
Leiter des Departments für Geowissenschaften

ISSN 1614-1199

Analysis of multistability and abrupt transitions - method studies with a global atmosphere-vegetation model simulating the end of the African Humid Period

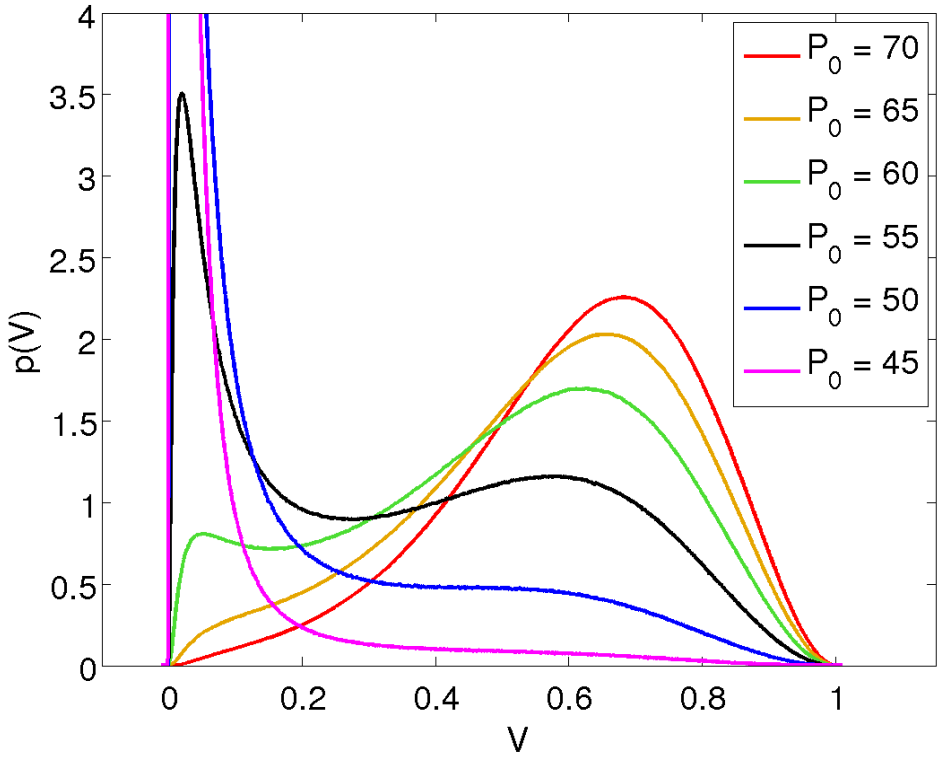

Sebastian Bathiany

Hamburg 2012

Abstract

Palaeoclimatic records and climate models indicate a decline of vegetation cover in North Africa during the mid- to late Holocene due to a change in orbital forcing. As atmosphere-vegetation feedbacks are particularly important in North Africa, the region represents a part of the climate system where sudden and non-linear responses to small changes in external conditions or even multiple equilibria may occur. Using the North African atmosphere-vegetation system as an example we assess different methods for the detection of multiple equilibria and the analysis of abrupt transitions in climate models. To this end, we couple a global atmosphere model of intermediate complexity with a simple dynamic vegetation model (PlanetSimulator-VECODE) and perform transient and stationary simulations with different orbital forcings.

We show that due to spatial complexity and temporal variability any of the assessed methods can yield misleading or inconclusive results. In particular, a detection of bistability with a stability diagram can fail because of spatial heterogeneity and spatial interactions, and the frequency distribution of a system's state, the existence of a hysteresis and the dependency on initial conditions are affected by atmospheric variability and inherent non-linearities. Mechanistic understanding is therefore essential when such diagnostic methods are applied. We also analyse the implications of climate variability for the abruptness of a vegetation decline. We find that a vegetation collapse can happen at different locations at different times. These collapses are possible despite large and uncorrelated climate variability. Because of the non-linear relation between vegetation dynamics and precipitation the green state is initially stabilised by the high variability. When precipitation falls below a critical threshold, the desert state is stabilised as variability is then also decreased.

In addition, we assess the applicability of so-called Early Warning Signals (EWS) to analyse abrupt transitions. EWS, such as rising variance and autocorrelation, can be indicators of a decrease in stability of a current equilibrium state. However, EWS are mostly applied in one-dimensional or idealised systems of predefined spatial extent. In a more general context like a complex climate system model, the critical subsystem that exhibits a loss in stability (hotspot) and the critical mode of the transition may be unknown. We document this problem with a simple stochastic model of atmosphere-vegetation interaction where EWS at individual grid cells are not always detectable before a vegetation collapse as the local loss in stability can be small. However, we suggest that EWS can be applied as a diagnostic tool to find the hotspot of a sudden transition and to distinguish this hotspot from regions experiencing an induced tipping. For this purpose we present a scheme which identifies a hotspot as a certain combination of grid cells which maximise an EWS. In a second step, we apply the method to PlanetSimulator-VECODE by using a surrogate stochastic toy model. For each of two vegetation collapses we find a hotspot of one particular grid cell. We demonstrate with additional experiments that the detected hotspots are indeed a particularly sensitive region in the model and give a physical explanation for these results. The method can thus provide information on the causality of sudden transitions and may help to improve the knowledge on the sensitivity of climate models and other systems.

Contents

List of Figures

List of Tables

List of Abbreviations

AHP	African Humid Period
EMIC	Earth System Model of Intermediate Complexity
ER	elimination rule
ESM	Earth System Model
ET	evapotranspiration
EWS	Early Warning Signal(s)
k	kiloyears before present
MOC	meridional overturning circulation
pdf	probability density function
PlaSim	Planet Simulator
RM	regression model
SD	signal definition
SST	sea surface temperature
VECODE	vegetation continuous description model
WAM	West African monsoon

Chapter 1

Introduction

1.1 Termination of the African Humid Period

The Sahara is today's largest desert, receiving only a few mm of annual rainfall in vast parts (Rudolf and Schneider, 2005). To its south, the Sahel forms the transition region to the densely vegetated tropics. Life in the Sahel crucially depends on the precipitation mainly provided by the West African monsoon (WAM). Palaeo records show that North Africa experienced several periods of moist and green conditions during the last 120 000 years (Tjallingii et al., 2008). The last of these periods, the African Humid Period (AHP), started around 14 k (kiloyears before present) at the end of the last ice age and was at its climax during the mid-Holocene. Palaeohydrological records provide vast evidence that today's Sahara and Sahel region was covered with lakes and wetlands, connected through a vast network of aquifers (Lézine et al., 2011a). Pollen records document that vegetation established under these humid conditions (Jolly et al., 1998a,b; Prentice et al., 2000), forming the so-called *Green Sahara*. Remnants of freshwater animals, mammals and human civilisation have been identified from that period (Petit-Maire and Riser, 1981).

Climate modelling studies have revealed the change in earth's orbital parameters as the crucial forcing to explain the existence of the Green Sahara. In the early to mid-Holocene, obliquity and precession lead to a larger summer insolation on the northern hemisphere compared to present-day, thus enhancing the WAM (Kutzbach, 1981) and providing energy for convection. In addition, the state of the rest of the climate system impacts North African climate, in particular the ocean's meridional overturning circulation (MOC) (Claussen et al., 1999; Tjallingii et al., 2008), the Indian monsoon (Marzin and Braconnot, 2009) and the ice sheets in higher latitudes which lag the orbital forcing by thousands of years (Claussen et al., 1999).

Apart from such external conditions, local feedbacks involving terrestrial vegetation and the ocean are crucial to explain the large climate anomaly in the mid-Holocene (Ganopolski et al., 1998; Hoelzmann et al., 1998; Braconnot et al., 1999, 2007b). While in an idealised setting the higher sea surface temperature (SST) would reduce the pressure difference between land and sea and thus the monsoon circulation, local characteristics of the spatial SST pattern and seasonality (Kutzbach and Liu, 1997; Liu et al., 1999, 2003; Braconnot et al., 2007b), as well as feedbacks involving evaporative cooling (Liu et al., 2003, 2004) and Ekman transport (Liu et al.,

2004; Braconnot et al., 2007b), lead to a positive atmosphere-ocean feedback. Regarding terrestrial vegetation cover, its low albedo as compared to the desert soil can increase the net-radiative balance at the surface and thus enhance convection as realised already by Otterman (1974) and Charney (1975). Charney (1975) and Charney et al. (1975) hypothesised that this effect could imply a positive atmosphere-vegetation feedback in the Sahara and Sahel region and also explain precipitation variability in the Sahel. However, changes in cloud cover and, most importantly, evapotranspiration (ET) need to be taken into account (Charney et al., 1977; Claussen, 1997), as water availability is determined by moisture convergence rather than precipitation alone. Consequently, changes in atmospheric circulation features such as the North African jets also need to be considered (Patricola and Cook, 2007, 2008).

Although some climate models imply a negative effect of vegetation on ET (Notaro et al., 2008; Wang and Kutzbach, 2008), the atmosphere-vegetation feedback in the Sahara and Sahel is most probably positive on timescales beyond decades due to vegetation and soil dynamics (Claussen, 2009). The magnitude of the feedback is directly related to the question of rapid transitions and multiple steady states of Saharan vegetation cover (see Section 1.2). Adopting a simple dynamical systems framework, the non-linearity introduced by a strong feedback implies a large sensitivity of a deterministic equilibrium state to changes in external conditions (Fig. 1.1b). In the extreme case, multiple stable states can emerge and the system can collapse when the external forcing passes a bifurcation point (Fig. 1.1c). This collapse would be irreversible as opposed to a simple threshold-behaviour where climate can be interpreted as an external forcing of vegetation dynamics.

Therefore, the understanding of physical processes and the knowledge on the phenomenology of the transition imply each other to some extent. Unfortunately, both aspects are still not well-known in case of the termination of the AHP as model results differ and reconstructions are sparse and uncertain. While earlier studies with models of different complexity revealed a multistability when choosing different initial conditions for certain orbital forcings (Claussen, 1994, 1997, 1998; Brovkin et al., 1998; Wang and Eltahir, 2000; Zeng and Neelin, 2000; Irizarry-Ortiz et al., 2003) and a rapid decline of vegetation cover in the mid-Holocene (Claussen et al., 1999), other models rather show a gradual decline (Schurgers et al., 2006; Renssen et al., 2003, 2006) or a collapse due to an ecological threshold (Liu et al., 2006, 2007; Lézine et al., 2011b). Current climate models indicate a rather weak atmosphere-vegetation feedback and a gradual vegetation decline, but also fail to reproduce the full extent of the Green Sahara as seen in reconstructions (Braconnot et al., 2007a; Claussen, 2009). Palaeoproxies do not reveal a precise spatio-temporal pattern of the end of the AHP due to their scarcity and dating uncertainties (Weldeab et al., 2011) and the low temporal resolution (Gasse, 2002). Although the asynchrony of the transition seems to reflect the local hydrological properties of different sites (Lézine, 2009), there is evidence that the AHP ended earlier and more gradually in the eastern Sahara as compared to the west (Kroepelin et al., 2008; Lézine et al., 2011a), where deMenocal et al. (2000) found an abrupt increase in terrigenous eolian sediment material around 5.5 k in a marine sediment core. However, model results by Hély et al. (2009) and Lézine et al. (2011a) indicate that an atmosphere-vegetation feedback is not

necessarily required to obtain a later and more abrupt transition in the western Sahara.

Apart from the strength of the atmosphere-vegetation feedback, the role of internal climate variability must also be considered in its spectrum and amplitude. Fluctuations not only affect the timing but also the abruptness of a transition on decadal to centennial timescales and can alter the steady states of a system in non-intuitive ways. In particular, Liu et al. (2006, 2007) demonstrate that a rapid transition in a weak-feedback case with threshold-behaviour is still possible when large red noise is imposed. The analysis of model results concerning multistability and abrupt transitions therefore requires awareness of the limitations of the applied methods and concepts.

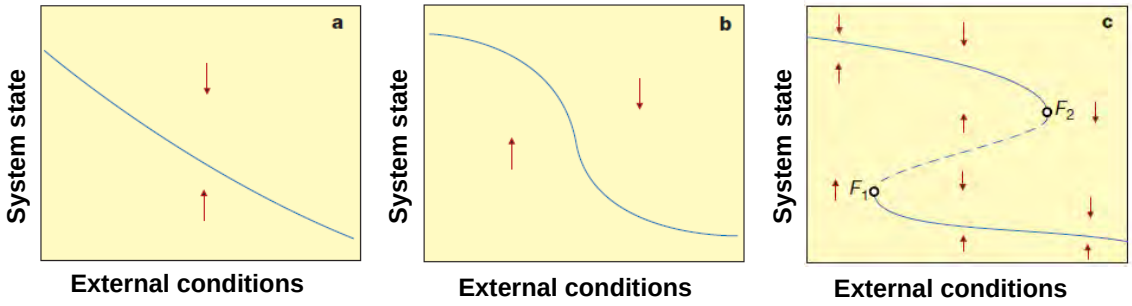

Figure 1.1: Sketch of the dependency of a system's equilibrium state on external conditions. **(a)** almost linear response due to small feedbacks, **(b)** non-linear tipping in a small parameter regime, **(c)** large feedbacks lead to bistability with bifurcations points F_1 and F_2. Solid blue lines: stable equilibria; dashed blue line: unstable equilibrium. Red arrows indicate the flow towards equilibrium when starting from a non-equilibrium state. This figure is a modification of Fig. 1 in Scheffer et al. (2001).

1.2 Tipping Points and their analysis via slowing down

Climate feedbacks in North Africa provide one example of potentially strong non-linearities in the climate system, which can generate a large sensitivity to changes in a specific forcing (external conditions in Fig. 1.1; orbital forcing in case of the Green Sahara). The phenomenon that small changes in external conditions can lead to large changes in equilibrium climate when a certain threshold is reached is often referred to as a Tipping Point (Lenton, 2011). A climate change is then called to be abrupt (Alley et al., 2003), as it happens much faster than the change in forcing (compared to the system's sensitivity at previous parameter values). In this thesis, we adopt Lenton's rather phenomenological and qualitative definition. The term Tipping Point thus does not imply anything with regard to the mechanism that causes this sudden and large sensitivity to external conditions except that it is caused by internal feedbacks which tend to destabilise a subsystem of the global climate system.

As mentioned in Sect. 1.1 very strong feedbacks can lead to the emergence of several stable equilibria for one and the same parameter value (Fig. 1.1c). We refer to such a case as *multistability*, or in the special case of two stable equilibria, *bistability*. In this deterministic context, an

equilibrium represents a stationary solution of the system's dynamic equations. When an external parameter is varied, it can happen that the deterministic solutions show a qualitative change at a threshold value where different branches of solutions touch, a phenomenon known as bifurcation (Guckenheimer and Holmes, 1983; Simonnet et al., 2009). For example, the number and/or stability (stable or unstable) of solutions suddenly changes at this bifurcation point. In practice, if a system is in some stable equilibrium and a parameter is then slowly varied across a bifurcation point (as slowly as necessary to keep the state close to equilibrium), the equilibrium can disappear and the system will approach another stable equilibrium far from the old state. Such an event is classified as a catastrophic bifurcation (Thompson et al., 1994; Thompson and Sieber, 2011b) and is a special case of a Tipping Point. Points F_1 and F_2 in Figs. 1.1 c and 1.2 provide an example.

Based on knowledge on particular feedbacks in specific regions of the earth, it can be speculated if and where subsystems with a Tipping Point exist. For example, Lenton et al. (2008) compiled a list of such potential *Tipping Elements in the earth's climate system* (while it must be noted that their definition of a Tipping Point is less specific than in Lenton (2011) and this thesis). Prominent examples of such potential Tipping Elements besides the Green Sahara are the decline of the MOC due to freshwater forcing, the loss of Arctic sea ice and the Greenland ice shield due to warming, and the dieback of Amazon rainforest due to changes in hydrology (see Lenton et al., 2008, and references therein). Although at present, a multistability in most of these potential Tipping Elements seems unlikely and projections for the coming centuries with modern earth system models show rather gradual changes (Meehl et al., 2007), an abrupt event could have devastating impacts and in the case of a bifurcation the resulting climate change can even be irreversible. The irreversibility leads to a static hysteresis when the external parameter is slowly varied forwards and backwards (a static hysteresis is due to the bistability in the system, not only due to the system's delayed response to the forcing; Bordi et al., 2012; Fraedrich, 2012). From a risk perspective, it is therefore politically advisable to study methods of stability analysis that can be applied to complex climate models or even observations. Also scientifically, it is beneficial to understand the effects of climate feedbacks and the susceptibility of the earth system to changes in external forcing.

The theory of dynamical systems provides a useful framework for such analysis (Ghil, 2001). In this framework, a climate model constitutes an (autonomous) evolution operator $f(\mathbf{x})$ which describes how the climate system's state evolves from one time to another (Strogatz, 1994). In case of a time-continuous system:

$$\frac{d\mathbf{x}}{dt} = f(\mathbf{x}) \tag{1.1}$$

The state $\mathbf{x}$ can be thought of as a location in phase space, a space that is spanned by the system's variables. In this thesis, we follow the concept of dynamical systems theory and therefore refer to the number of variables as a system's dimension (i.e. dimension of phase space in contrast to physical space). In particular, we make use of the concepts of bifurcation theory and linear stability analysis. Although the global structure of a system may be very non-linear as in Fig. 1.1 b and

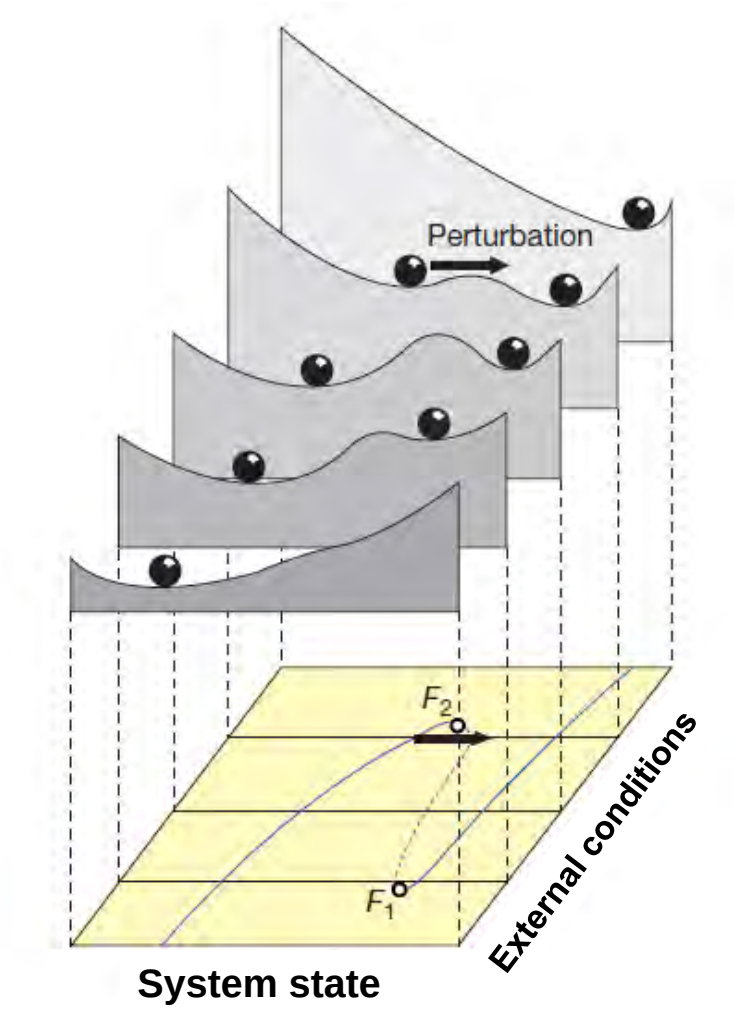

Figure 1.2: Sketch to illustrate changes in stability when approaching a bifurcation point. The bottom plane represents Fig. 1.1c. Above, a potential landscape represents the stability structure at five different conditions. Potential wells indicate the basins of attraction, potential minima represent stable equilibrium points, the maxima unstable equilibria. The (inertia-free) ball represents the system's state. When a change in external conditions drives the system towards F_1 on the lower branch, or F_2 on the upper branch, the well of the according equilibrium flattens until it disappears and the ball rolls towards the remaining minimum. Also, a random perturbation can push the ball over the threshold before the bifurcation point. This figure is a modification of Fig. 3 in Scheffer et al. (2001).

c, the dynamics close to an equilibrium $\mathbf{x}_0$ that is stable or unstable in any particular direction (a hyperbolic fixed point) can be approximated by a local linearisation. The topological equivalence between the actual and the linearised flow close to the hyperbolic fixed point is addressed by the Hartman-Grobman theorem (Guckenheimer and Holmes, 1983). Considering a one-dimensional case and denoting the small anomaly $y = x - x_0$, the linearisation reads

$$\frac{dx}{dt} = \frac{dy}{dt} = f(y) \approx \lambda y \tag{1.2}$$

and has the solution

$$y = y_{\mathrm{ini}} \exp(\lambda t). \tag{1.3}$$

The real part of the eigenvalue λ describes the linear stability of x_0. A negative real part indicates a stable fixed point, a positive real part an unstable fixed point. In case of a stable fixed point, $1/Re(\lambda)$ is the timescale of the relaxation (the time until the initial perturbation y_{ini} has decayed to a fraction of $1/e$). The smaller the absolute value of λ, the slower the relaxation. This effect is often illustrated with the prototype example of a one-dimensional potential whose shape

determines the system's deterministic dynamics, and a ball (without inertia) which characterises its state (Fraedrich, 1979; Scheffer et al., 2001). A stable equilibrium state is represented by a local minimum in the potential. In physical terms, $Re(\lambda)$ then describes the restoring force due to locally stabilising feedbacks. If by varying an external control parameter the potential becomes flatter (Fig. 1.2), the linear relaxation time increases and $Re(\lambda)$ as determined by a linear stability analysis increases in a time-continuous system. When a bifurcation point is approached where the stable equilibrium is destroyed, $Re(\lambda)$ approaches 0 from below; in the case of maps (dynamical systems discrete in time), λ crosses the unit circle. A very common case is the saddle-node bifurcation, where a stable and unstable fixed point annihilate each other (points F_1 and F_2 in Figs. 1.1 c and 1.2). In this thesis, we refer to the increase of a system's relaxation time due to a loss in stability as *slowing down*. Slowing down has been studied in many contexts, e.g. theoretically (Wolff, 1990) and observationally (Collins and Teh, 1973) in physical systems, and in ecological systems (Wissel, 1984). We do not use the popular term *critical slowing down* in this thesis because it often also addresses the phenomenon of algebraic decay and universal scaling laws in systems with second order phase transitions (Strogatz, 1994).

It must be noted that although a changing potential is a useful illustration, the existence of a potential function that can be derived from the evolution operator is not a necessary condition for slowing down (Guttal and Jayaprakash, 2008). Furthermore, the restriction to only one dimension in Eqs. (1.2) and (1.3) does not imply any loss in generality here, as we only discuss local bifurcations involving fixed points. In the case of higher dimensions, there will still be one eigenvalue of the linearised Jacobian matrix approaching 0 as there is one particular direction in phase space in which the bifurcation occurs. A suitable rotation of the coordinate system would then provide a similar view as Fig. 1.2 (Simonnet et al., 2009). Likewise, it is sufficient to assume the variation of only one external parameter (codimension-1 bifurcation) which can in fact be a fixed combination of several parameters with different physical meaning. Although there are bifurcations of higher codimension where more than two regimes of solutions meet at a cusp point (Strogatz, 1994), it is only possible to hit this one point on purpose and can practically never happen by chance in a climate model. The one-dimensionality in terms of phase space and parameter space is thus not a conceptual limitation (although we will demonstrate in this thesis some of its practical limitations).

More importantly, the climate system displays permanent and irregular fluctuations on various timescales as opposed to the concept of a deterministic stable equilibrium introduced above. In this thesis we restrict ourselves to systems where there is a clear separation of timescales (Berglund and Gentz, 2006; Kuehn, 2011) between a slow subsystem (vegetation dynamics) and a fast subsystem (the atmosphere, showing variability in precipitation). The slow subsystem (*slow manifold* in terms of dynamical systems theory) is interpreted as a set of deterministic dynamic equations. The fast subsystem, although potentially deterministic in its physical nature, is described by a white noise approximation and thus introduces a stochastic term in the model equations. It is important to note that our discussion of a model's *stability properties* (e.g. multistability) refers

to the slow deterministic part of the system. The inference of its properties from the noisy and spatially complex model output is the leitmotif of this thesis.

As the underlying dynamics are rarely known in complex systems, it has been suggested to infer stability changes of a current state from statistical indicators (Wiesenfeld, 1985a,b; Wiesenfeld and McNamara, 1986; Kleinen et al., 2003; Held and Kleinen, 2004). If the system's state is subject to external random perturbations (usually assumed as white noise of constant noise level), a loss in stability will lead to an increase in autocorrelation and (at least if the noise is additive) variance. The problem can be formulated as a first-order autoregressive process (AR(1) process), which is discrete in time. The only parameter of such a process, c, is identical to the autocorrelation at lag 1. The state at each time step t is the result of the linear decay of the previous time step $t-1$ plus a random perturbation η with noise level σ:

$$y^t = y^{t-1} \exp(\lambda\ \Delta t) + \sigma \eta^{t-1}. \tag{1.4}$$

Again, λ is the eigenvalue of the time-continuous system. As η is a random variable so is y. We address the corresponding process which generates the time series of y as Y. It can be seen directly from Eq. (1.4) that $\exp(\lambda\ \Delta t)$ (the eigenvalue of the time-discrete system) yields the autocorrelation c of the process Y. Furthermore, its variance can be shown to be

$$Var(Y) = \frac{\sigma^2}{1-c^2}. \tag{1.5}$$

Hence, when λ increases towards 0 due to a loss in stability, autocorrelation will tend to 1 and variance to infinity. In terms of Fig. 1.2, as the potential well becomes flatter, the return to equilibrium becomes slower, and the state at a certain time will thus be more similar to the previous state. In addition, the random perturbations can add up while the state is anomalously large or low, and the system is less able to absorb the regular shocks by returning close to equilibrium in between, which leads to larger excursions from the well's minimum.

It is apparent that this feature already implies a limitation of concept: As soon as variance increases considerably, two problems arise. First, the small noise approximation is not valid anymore and the relation between local stability and the system's fluctuations depends on higher order terms of the potential's shape. Second, in case of a multistability, the system can experience an *early escape* when the noise pushes it over the threshold before the deterministic equilibrium point (Scheffer et al., 2009; Ditlevsen and Johnsen, 2010). The timing of such a transition can then only be assessed in probabilistic terms (e.g. Guttal and Jayaprakash, 2008; Thompson and Sieber, 2011a). However, in many practical cases, changes in statistical indicators like autocorrelation and variance can be measured if the system is not too close to the bifurcation point and if the change in external conditions is slow enough to allow a sufficiently precise sampling. Assuming that the existence of a non-linear threshold is known, then it can be attempted to predict when a sudden transition will occur (Thompson and Sieber, 2011a,b). For this reason, statistical indicators of slowing down have been named Early Warning Signals (EWS; Dakos et al., 2008; Scheffer et al.,

2009). It must be noted though that EWS are not related to the existence of a bifurcation as any change in stability will be reflected in a change in EWS (if the underlying conceptual assumptions are met).

The generality of the concept has recently inspired the search for slowing down and EWS in various contexts such as ecological models (Carpenter and Brock, 2006; van Nes and Scheffer, 2007; Guttal and Jayaprakash, 2008; Contamin and Ellison, 2009); living populations in laboratories (Drake and Griffen, 2010; Veraart et al., 2012) and real ecosystems (Carpenter et al., 2011), geological climate records (Dakos et al., 2008; Ditlevsen and Johnsen, 2010), and climate models (Kleinen et al., 2003; Held and Kleinen, 2004; Livina and Lenton, 2007; Lenton et al., 2009; Lenton, 2011). In this thesis we add another field of application by using models of atmosphere-vegetation interaction.

1.3 Thesis outline

The motivation of this thesis is to assess and develop methods to analyse the stability properties of numerical models. The improved understanding of climate models may then contribute to reduce their shortcomings or suggest new possible ways to interpret observational or proxy data.

Simulations of the end of the AHP provide test cases to reveal the performances of the applied methods. These simulations are not designed to reproduce the termination of the AHP as realistically as possible. To perform the simulations we couple the PlanetSimulator (PlaSim; Fraedrich et al., 2005a; Fraedrich, 2012), an atmosphere model of intermediate complexity, to the dynamic vegetation model VECODE (Vegetation continuous description model; Brovkin et al., 1997, 2002). In addition, we perform experiments with simple stochastic models. They follow the tradition of simple conceptual models describing potentially bistable systems like the MOC (Stommel, 1961), Snowball Earth (Budyko, 1969; Sellers, 1969; Fraedrich, 1978; North et al., 1981; Pierrehumbert, 2010) or the atmosphere-vegetation system (Watson and Lovelock, 1983; Brovkin et al., 1998).

Strategies to identify multiple solutions in numerical models often follow the logic of such simple one-dimensional deterministic models. In particular, we will address the choice of different initial conditions (usually spatially idealised and extreme in their numerical values), the construction of a stability diagram in a plane, hysteresis experiments and the calculation of an empirical probability density function (pdf). The latter strategy is usually applied in a stochastic but still simplified framework.

In contrast to simple conceptual models, our atmosphere-vegetation model PlaSim-VECODE possesses the following properties:

- It accounts for spatial heterogeneity.
- It features climate variability. The amplitude of this variability is large as compared to common Earth system models of intermediate complexity (EMICs), and it interacts with the non-

linearities in the model.

- Atmosphere and vegetation can be coupled in a transient mode (where deviations from the equilibrium vegetation cover can occur) and in an equilibrium asynchronous mode.

Chapter 2 of this thesis addresses this contrast between the concepts of multistability and the strategies to detect multistabilities on one hand, and the properties of complex climate models on the other hand. Specifically, we investigate the question:

(I) How do strategies for the detection of multistability perform in PlaSim-VECODE?

As discussed in Section 1.1, the large variability raises the question how the state of the model depends on external conditions. We therefore also discuss:

(II) What conclusions do these strategies allow regarding the possibility of a rapid transition?

Chapter 2 has been published in *Climate Dynamics* [1]. The article is reproduced here with minor extensions.

In similarity to methods for the detection of multiple states or regimes, indicators of slowing down are basically used in a one-dimensional or spatially homogeneous framework. In contrast, complex climate models involve a vast number of degrees of freedom and the system boundaries of Tipping Elements are not known and hard to define. Again, we take the termination of the AHP as an example case of a potential Tipping Element and study the applicability of EWS as a diagnostic tool by asking:

(III) How can EWS be applied to infer information on the structural stability of PlaSim-VECODE?

Chapter 3 specifically addresses this question. In Section 3.2 we document the limitations of EWS with regard to spatial complexity. In addition, we develop a stochastic algorithm to identify the spatial origin (hotspot) of a rapid transition at a Tipping Point and apply this algorithm to PlaSim-VECODE in Section 3.3. Sections 3.2 and 3.3 have been submitted to *Earth System Dynamics* [2] [3] as companion papers. Both articles are reproduced here with minor changes for the sake of the thesis' consistency. Chapter 4 provides a final summary and discussion of our results as well as perspectives for future research on stability properties of climate models and the termination of the AHP.

[1] Bathiany, S., Claussen, M. and Fraedrich, K.: Implications of climate variability for the detection of multiple equilibria and for rapid transitions in the atmosphere-vegetation system, Clim. Dynam., 38, 1775–1790, doi:10.1007/s00382-011-1037-x, 2012.

[2] Bathiany, S., Claussen, M. and Fraedrich, K.: Detecting hotspots of atmosphere-vegetation interaction via slowing down – Part 1: A stochastic approach. Earth Syst. Dynam. Discuss., 3, 643–682, 10.5194/esdd-3-643-2012, 2012

[3] Bathiany, S., Claussen, M. and Fraedrich, K.: Detecting hotspots of atmosphere-vegetation interaction via slowing down – Part 2: Application to a global climate model. Earth Syst. Dynam. Discuss., 3, 683–713, 10.5194/esdd-3-683-2012, 2012

Chapter 2

Implications of climate variability for the detection of multiple equilibria and the possibility of rapid transitions

2.1 Introduction

Various palaeo records have revealed that the Sahara was considerably greener and wetter during the early Holocene (Prentice et al., 2000). The reason lies in the earth orbit's precessional cycle and the earth axis' obliquity, which caused an increased summer insolation and thus more precipitation. In particular, the West African Monsoon was enhanced due to an increased land-ocean temperature contrast. However, the extent of these changes can only be explained with positive feedbacks in the climate system (Braconnot et al., 2007b). According to climate models an important contribution is the atmosphere-vegetation feedback (Claussen, 2009). First, the high albedo of bare soils in the Sahara with values up to 0.5 (Pinty et al., 2000) implies a low energy input to the overlying atmosphere. Therefore, the negative atmospheric radiative budget has to be partly compensated by diabatic warming caused by sinking motion. Convection and thus precipitation are then suppressed and vegetation cannot establish, a feedback proposed by Charney (1975) for the Sahel region. Second, vegetation can act to increase evapotranspiration at the expense of drainage and runoff, thus moistening the atmosphere and allowing for more precipitation (Hales et al., 2004). In addition, the contribution of the ocean-atmosphere feedback to the strength of the Holocene West African Monsoon is also supposed to be positive (Liu et al., 2003, 2004).

Previous climate modelling studies suggested that the atmosphere-vegetation feedback in Western Africa might allow for multiple equilibria of vegetation cover. This possibility can be illustrated with the conceptual model of Brovkin et al. (1998), which consists of two equilibrium curves $V^*(P)$ and $P^*(V)$, where V stands for vegetation cover and P for precipitation in a specific area (Fig. 2.1). While $V^*(P)$ is of non-linear shape due to ecological thresholds, $P^*(V)$ is generally approximated as linear because the impact of vegetation dynamics on precipitation is often small compared to geographical influences (Zeng et al., 2002). The intersections of the two curves determine the equilibrium points of the coupled system.

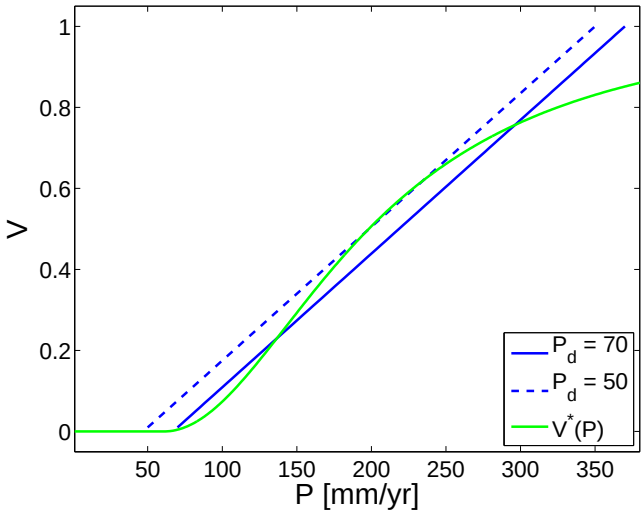

Figure 2.1: Stability diagram after Brovkin et al. (1998) for $k = 300$. The blue lines represent the equilibrium of annual precipitation, calculated from $P^*(V) = P_\mathrm{d} + kV$ for different P_d. P is in mm/year. The green line represents the equilibrium vegetation cover fraction $V^*(P)$ in VECODE for dry deserts (Eq. 2.1) with $\mathrm{GDD}_0 = 10\,000\,\mathrm{K}$.

To detect multiple equilibria of vegetation cover in models, mainly two strategies have been applied so far: the choice of idealised initial conditions (such as complete forest and desert states), and the construction of a stability diagram similar to Fig. 2.1 with various methods. By choosing different initial conditions in ECHAM3-BIOME, Claussen (1994, 1997, 1998) has found two stable states for the Western Sahara for present day orbital forcing. Similar results have been obtained in models of intermediate complexity: Zeng and Neelin (2000) have identified multiple solutions for present day, though only "in a range of parameters at the margin of realistic estimates" (Zeng and Neelin, 2000). Wang and Eltahir (2000) have found even three stable states at present day, while Irizarry-Ortiz et al. (2003) have detected two stable states in the mid-Holocene. Multiple states in vegetation cover have even been obtained in tropical South America by Oyama and Nobre (2003) in an atmospheric general circulation model coupled to a potential vegetation model.

By using the conceptual model as a graphical method of stability analysis, Brovkin et al. (1998) have explained the existence of multiple equilibria in ECHAM3-BIOME by deriving parameters for the two equilibrium curves from the model output. For ECBilt-Clio-VECODE, a stability diagram also suggests the existence of multiple solutions (Renssen et al., 2003). Based on a similar approach Levis et al. (1999) and Brovkin et al. (2003) have concluded that no multiple equilibria are possible in boreal latitudes, despite a substantial positive feedback between near surface temperature and forest cover.

The possibility of multiple states in vegetation cover suggests the occurrence of sudden transitions between these states, which are either noise-induced (caused by an external disturbance), or the result of a bifurcation at a critical parameter value (Tipping Point). Indeed, there are proxy records showing a rapid decrease in West African vegetation at the end of the African Humid Period, some thousand years before present (e.g. deMenocal et al., 2000; Salzmann and Hoelzmann, 2005). However, the timing and abruptness of this transition is site dependent. Other records indicate a more gradual transition in more easterly locations (Kroepelin et al., 2008; Lézine, 2009), and in tropical Africa (Vincens et al., 2010).

The abruptness of this decline in vegetation cover also differs among climate models. While Claussen et al. (1999) have obtained a transition that is much more rapid than the change in orbital forcing, Renssen et al. (2003, 2006) as well as Schurgers et al. (2006) have only obtained a gradual vegetation decline. Furthermore, multistability does not necessarily imply an abrupt transition, or vice versa. The reason lies in the versatile effects of climate variability. Variability can smooth the gradients in vegetation cover and even lead to steady states that are distinct from any deterministic equilibrium (Zeng and Neelin, 2000; Zeng et al., 2002; d'Odorico et al., 2005). Furthermore, variability can even lead to the establishment of multiple stable states, as has been demonstrated with a coupled climate-ecosystem model by Liu (2010), and with a box model for the MOC by Timmermann and Lohmann (2000). If it is sufficiently high, variability can obliterate a system's dependency on initial conditions (Wang, 2004) and remove hysteresis effects (Guttal and Jayaprakash, 2007). In turn, variability itself can be influenced by the stability properties. For example, a flickering between two regimes can cause low-frequency variations (Wang and Eltahir, 2000; Wang, 2004) and a bimodal probability distribution (Livina et al., 2010). The transition of a system passing a deterministic Tipping Point may then be only gradual, in the sense that the state's probability density changes only gradually when the critical parameter is varied. In contrast, rapid shifts are also possible in monostable systems: To explain the rapid vegetation decline in the complex atmosphere-ocean-land model FOAM-LPJ, Liu et al. (2006) have suggested low-frequency variations in precipitation, independent of vegetation dynamics. Due to the vegetation's non-linear dependency on soil moisture in arid regions, a rapid vegetation decline is then possible even in case of an only weak atmosphere-vegetation feedback.

In this chapter we further investigate the implications of climate variability for the detection of multiple equilibria and the possibility of rapid transitions. In Section 2.2 we describe the models and our experiment setups. We then present transient simulations of the mid-Holocene (Section 2.3), and apply and assess the methods of stability diagram analysis (Section 2.4.1) and extreme initial conditions (Section 2.4.2). We explain our results with a simple stochastic model, and in Section 2.5 apply it to document a new mechanism of vegetation collapse. Section 2.6 provides a short summary, a discussion of the implications for reality and other models, and our basic conclusions.

2.2 Model and Experiment Setup

2.2.1 Atmosphere model

The Planet Simulator (PlaSim; Fraedrich et al., 2005a,b) is a global spectral climate model of intermediate complexity, which is freely available as an open source code (http://www.mi.uni-hamburg.de/Planet-Simul.216.0.html). We run PlaSim with T21 horizontal resolution and 10 vertical layers in all experiments presented in this thesis. As we only consider biogeophysical land-atmosphere feedbacks, atmospheric CO_2 is set to 280 ppm in all experiments, and ocean sur-

face temperatures and sea ice properties are prescribed from present day observations and are the same in each year.

2.2.2 Vegetation model

Vegetation dynamics are represented by VECODE (Brovkin et al., 2002), a dynamic global vegetation model of reduced complexity. With a time step of 1 yr, the equilibrium cover fractions of trees, grass and desert are calculated from precipitation, growing degree days above 0 °C (GDD_0), and temperature. For this transformation analytical functions are used whose parameters have been tuned in order to match the observed relation between vegetation distribution and climate (Brovkin et al., 1997). For dry deserts, the equilibrium vegetation fraction V^* is calculated from annual precipitation P via

$$V^* = \begin{cases} 0 & \text{if } P < P_1 \\ 1 & \text{if } P > P_2 \\ 1.03 - \dfrac{1.03}{1+\alpha\left(\dfrac{P-P_1}{\exp(\gamma\delta)}\right)^2} & \text{otherwise,} \end{cases} \tag{2.1}$$

with

$$\begin{aligned} P_1 &= \beta \exp(\gamma\delta/2) \\ P_2 &= \beta \exp(\gamma\delta/2) + \frac{\exp(\gamma\delta)}{\sqrt{0.03\,\alpha}}. \end{aligned}$$

Parameter values are $\alpha = 0.0011$, $\beta = 28$, $\gamma = 1.7 \times 10^{-4}$, and $\delta = GDD_0 - 900$ (GDD_0 is in Kelvin, but from hereon given as a unitless number like the other parameters). The second condition corresponds to resetting d^* to 0 once it becomes negative.

For exploring abrupt vegetation dynamics, we create a second, more sensitive model by setting $\beta = 140$ and $\gamma = 1.7 \times 10^{-5}$ (Fig. 2.2, dashed line). By doing so we accept that the modified VECODE (VECODEm) is less realistic than the original one (VECODEo). As the strength of the atmosphere-vegetation feedback and the existence of multiple steady states in reality remains unclear (Liu et al., 2007; Claussen, 2009), we aim to also represent a case of a particularly large feedback. To do this, we prefer the mentioned approach because the sensitivity of VECODE can be changed much easier and more directly than the sensitivity of the atmosphere model.

2.2.3 Coupling procedure

VECODE is coupled to PlaSim in two ways, equilibrium mode (PlaSim-VECODE-eq) and transient mode (PlaSim-VECODE-tr). In equilibrium mode we run the atmosphere model for 10 yrs (if not stated otherwise), and average the climate over this period. The corresponding equilibrium

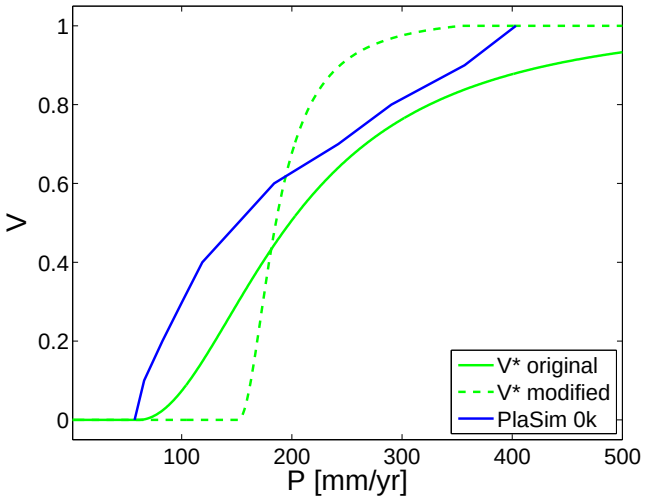

Figure 2.2: Equilibrium vegetation cover fraction $V^*(P)$ for both VECODE versions. The blue line shows the spatial mean $P^*(V)$ response of uncoupled PlaSim simulations with fixed uniform grass cover in the Sahara/Sahel region and present day orbital forcing.

cover fractions then provide the boundary conditions in PlaSim for the next iteration step. This approach is similar to previous studies like Claussen (1994) and Liu et al. (1999). In transient mode, the cover fractions are updated each year (index t in Eq. 2.2) and approach their (annually changing) equilibrium values on the basis of a linear relaxation law commonly used in simple dynamic vegetation models (e.g. Zeng and Neelin, 2000; Zeng et al., 2002; Wang, 2004; Liu et al., 2006):

$$V^{t+1} = V^t + \frac{V^*(P^t) - V^t}{\tau}. \tag{2.2}$$

A similar equation is solved for tree cover. The cover fraction of grass is then determined as the difference between vegetation and tree cover, so that there is coexistence but no competition between trees and grass. In the dry regions of the Sahara/Sahel, vegetation almost completely consists of grass so that vegetation dynamics can be described by Eq. (2.2) with τ as the timescale of grass. In the case of very dry conditions, a weighted average between the timescales of trees and grass is used, which can produce a narrow and discontinuous peak in the pdf of vegetation cover at low values. In the following, we ignore this artificial effect because it is irrelevant for the mechanisms we discuss in this thesis. In VECODE, τ is calculated from net primary production (NPP), which depends on annual precipitation, annual mean temperature and atmospheric CO_2. These dependencies are implemented as least squares fits of analytical curves to global observations of NPP, living phytomass, and climate. Interannual changes in τ are mostly due to the variability in precipitation: In wet years, vegetation dynamics are faster than in dry years (Fig. 2.3).

In each coupling step, the land cover types have to be transformed to surface parameter values. In PlaSim, the four parameters that are substantially affected by vegetation are background (snowfree) surface albedo, surface roughness length, bucket size and a parameter that controls the fraction of soil water available for evaporation (Fraedrich et al., 2005b). For each land cover type (trees, grass and desert) we assume constant parameter values (Table 2.1) that are combined by weighting with the land cover fractions in a particular grid cell. Most parameter values for trees and desert are from Fraedrich et al. (2005b), in the other cases we choose values in agreement

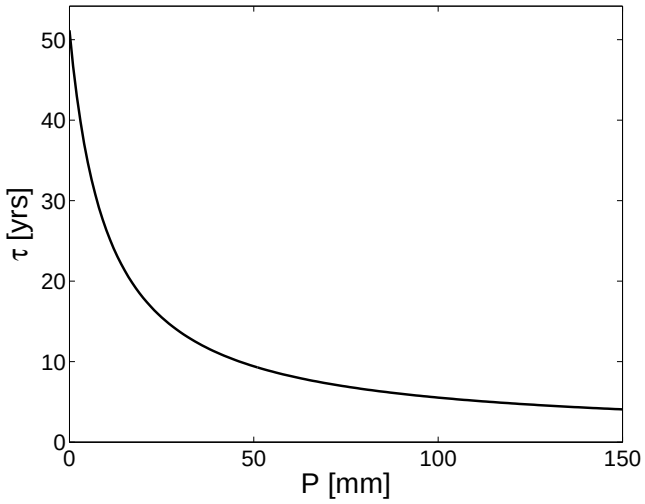

Figure 2.3: Timescale for shifts in grass fraction in dependence on annual precipitation, at a temperature of 27 °C , and 280 ppm CO_2 in VECODE.

Table 2.1: Attribution of surface parameter values to VECODE land cover types.
a) value from Fraedrich et al. (2005b), b) value from Claussen (1994).

	background albedo	roughness length [m]	bucket size [m]	fractional parameter
trees	0.12^a	1.5^b	0.5^a	0.01^a
grass	0.16^b	0.05^b	0.2	0.1
desert	0.28^a / 0.4	0.05^b	0.1^a	0.4^a

to the typical biomes in Claussen (1994). In the case of roughness length we average the corresponding momentum transfer coefficients for neutral atmospheric stability at a height of 1000 m (Stull, 1988). In addition, this bulk vegetation roughness length is combined with orographic roughness by taking the root of their summed squares (Claussen, 1994). Surface albedo, bucket size and the fractional evaporation parameter are averaged linearly. For soil albedo Fraedrich et al. (2005b) choose a value of 0.28 globally, which is the maximum surface albedo at snow- and icefree land cells in the uncoupled PlaSim. However, as the large differences in surface albedo between bare and vegetated ground in the Sahara/Sahel region are required to capture the local vegetation-atmosphere feedback, we modify the desert background albedo in Northern Africa and Arabia (Fig. 2.4). There, we assume a value of 0.4, while for the rest of the world we choose 0.28. This distinction, although very idealised, is motivated by observations (Pinty et al., 2000; Hagemann, 2002).

2.2.4 Experiments

We perform different types of experiments (Table 2.2), whose details will be explained together with the results in the following sections:

- Experiments in transient mode with continuously changing orbital parameters, corresponding to the period from 8000 yrs before present (8 k) to 2000 yrs before present (2 k)

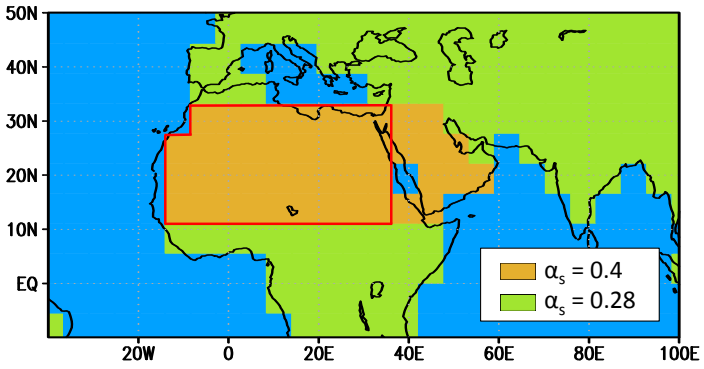

Figure 2.4: Soil albedo in PlaSim-VECODE. Green areas: 0.28 (default value in PlaSim); brown areas: 0.4; blue areas: ocean. The area enclosed in red is referred to as Sahara/Sahel region in the text and used for Figs. 2.2, 2.5, 2.9, 2.11 and 2.14.

- Experiments starting from idealised initial conditions (forest and desert world) with fixed orbital forcing, for both ways of coupling and both VECODE versions

- Uncoupled PlaSim experiments of several thousand years length, with fixed orbit year, and surface parameters fixed to the mean conditions obtained from the transiently coupled experiments (after a steady state was reached)

- Experiments with a simple stochastic model that is based on Eqs. (2.1) and (2.2), but describes atmospheric variability as a random process η with noise level σ_P. In analogy to the stability diagram of Brovkin et al. (1998) we assume a linear relation between equilibrium precipitation and vegetation cover fraction:

$$P^t = P_d + kV^t + \sigma_P \eta^t. \tag{2.3}$$

  In this regard our stochastic model is essentially the same as in Wang (2004) and Liu et al. (2006). In the following, we provide P_d, k and σ_P without units for simplicity, although the value of P represents mm/yr.

2.3 Vegetation dynamics from 8 k to 2 k

We run PlaSim-VECODE in transient mode and with both VECODE versions under changing orbital forcing from 8 k to 2 k. Each experiment is conducted twice with the same settings but different initial conditions in order to get an impression on the stochasticity of the time series. These alternative initial conditions are created by keeping the initial vegetation cover fixed for two years instead of one. In the following, we refer to the area at approx. 15° W–35° E, 12–33° N (excluding the north-western ocean grid cell) as the Sahara/Sahel region (Fig. 2.4). In this section we only use descriptive terms like *vegetation decline* regardless of the underlying mechanism, while we reserve the term *collapse* for transitions that are related to a bifurcation.

In all transient experiments, mean vegetation cover in the Sahara/Sahel remains almost stationary during the first 2000 yrs, whereas a comparatively rapid decrease occurs between 6 k and 5 k (Fig. 2.5). For VECODEo, large fluctuations occur in the 100 yrs moving averages during

Table 2.2: List of experiments with PlaSim-VECODE. *tr* = transient coupling mode, *eq* = equilibrium coupling mode. In case of the uncoupled PlaSim experiments the initial surface conditions provide the boundary conditions during the complete experiment. *Default* refers to the original surface parameters in PlaSim. The existence of multiple states was determined by eye from the according time series, like those in Fig. 2.9.

Experiment	Coupling mode and frequency	VECODE version	Orbit year	Initial surface conditions	Multiple states
T-Orig-for1	tr.	orig	8 k–2 k	default	
T-Orig-for2	tr.	orig	8 k–2 k	default	
T-Mod-for1	tr.	mod	8 k–2 k	default	
T-Mod-for2	tr.	mod	8 k–2 k	default	
T-Orig-back1	tr.	orig	2 k–8 k	default	
T-Orig-back2	tr.	orig	2 k–8 k	default	
T-Mod-back1	tr.	mod	2 k–8 k	default	
T-Mod-back2	tr.	mod	2 k–8 k	default	
E1F-Mod-8k	eq., 1 yr	mod	8 k	forest world	no
E1D-Mod-8k	eq., 1 yr	mod	8 k	desert world	
E3F-Mod-8k	eq., 3 yrs	mod	8 k	forest world	no
E3D-Mod-8k	eq., 3 yrs	mod	8 k	desert world	
E5F-Mod-8k	eq., 5 yrs	mod	8 k	forest world	yes
E5D-Mod-8k	eq., 5 yrs	mod	8 k	desert world	
E7F-Mod-8k	eq., 7 yrs	mod	8 k	forest world	yes
E7D-Mod-8k	eq., 7 yrs	mod	8 k	desert world	
E10F-Mod-8k	eq., 10 yrs	mod	8 k	forest world	yes
E10D-Mod-8k	eq., 10 yrs	mod	8 k	desert world	
E20F-Mod-7k	eq., 20 yrs	mod	7 k	forest world	yes
E20D-Mod-7k	eq., 20 yrs	mod	7 k	desert world	
E10F-Mod-7k	eq., 10 yrs	mod	7 k	forest world	no
E10D-Mod-7k	eq., 10 yrs	mod	7 k	desert world	
E10F-Mod-6k	eq., 10 yrs	mod	6 k	forest world	no
E10D-Mod-6k	eq., 10 yrs	mod	6 k	desert world	
E10F-Mod-5.5k	eq., 10 yrs	mod	5.5 k	forest world	no
E10D-Mod-5.5k	eq., 10 yrs	mod	5.5 k	desert world	
E10F-Mod-5k	eq., 10 yrs	mod	5 k	forest world	yes
E10D-Mod-5k	eq., 10 yrs	mod	5 k	desert world	
E10F-Mod-4.5k	eq., 10 yrs	mod	4.5 k	forest world	yes
E10D-Mod-4.5k	eq., 10 yrs	mod	4.5 k	desert world	
E10F-Mod-0k	eq., 10 yrs	mod	0 k	forest world	no
E10D-Mod-0k	eq., 10 yrs	mod	0 k	desert world	

Table 2.2: Continued.

Experiment	Coupling mode and frequency	VECODE version	Orbit year	Initial surface conditions	Multiple states
TF-Mod-8k	tr.	mod	8 k	forest world	no
TD-Mod-8k	tr.	mod	8 k	desert world	
TF-Mod-4.5k	tr.	mod	4.5 k	forest world	no
TD-Mod-4.5k	tr.	mod	4.5 k	desert world	
TF-Mod-0k	tr.	mod	0 k	forest world	no
TD-Mod-0k	tr.	mod	0 k	desert world	
E10F-Orig-8k	eq., 10 yrs	orig	8 k	forest world	no
E10D-Orig-8k	eq., 10 yrs	orig	8 k	desert world	
E10F-Orig-6k	eq., 10 yrs	orig	6 k	forest world	no
E10D-Orig-6k	eq., 10 yrs	orig	6 k	desert world	
E10F-Orig-5.5k	eq., 10 yrs	orig	5.5 k	forest world	no
E10D-Orig-5.5k	eq., 10 yrs	orig	5.5 k	desert world	
E10F-Orig-5k	eq., 10 yrs	orig	5 k	forest world	no
E10D-Orig-5k	eq., 10 yrs	orig	5 k	desert world	
E10F-Orig-4.5k	eq., 10 yrs	orig	4.5 k	forest world	no
E10D-Orig-4.5k	eq., 10 yrs	orig	4.5 k	desert world	
E10F-Orig-0k	eq., 10 yrs	orig	0 k	forest world	no
E10D-Orig-0k	eq., 10 yrs	orig	0 k	desert world	
T-Mod-8k	tr.	mod	8 k	default	
T-Mod-7k	tr.	mod	7 k	default	
T-Mod-4.5k	tr.	mod	4.5 k	default	
T-Mod-4k	tr.	mod	4 k	default	
T-Mod-3.6k	tr.	mod	3.6 k	default	
T-Orig-8k	tr.	orig	8 k	default	
TU-8k	uncoupled	-	8 k	yrs 300–1000 from T-Orig-8k	
T-Orig-5.5k	tr.	orig	5.5 k	default	
TU-5.5k	uncoupled	-	5.5 k	yrs 300–1000 from T-Orig-5.5k	
T-Orig-0k	tr.	orig	0 k	default	
TU-0k	uncoupled	-	0 k	yrs 300–1000 from T-Orig-0k	

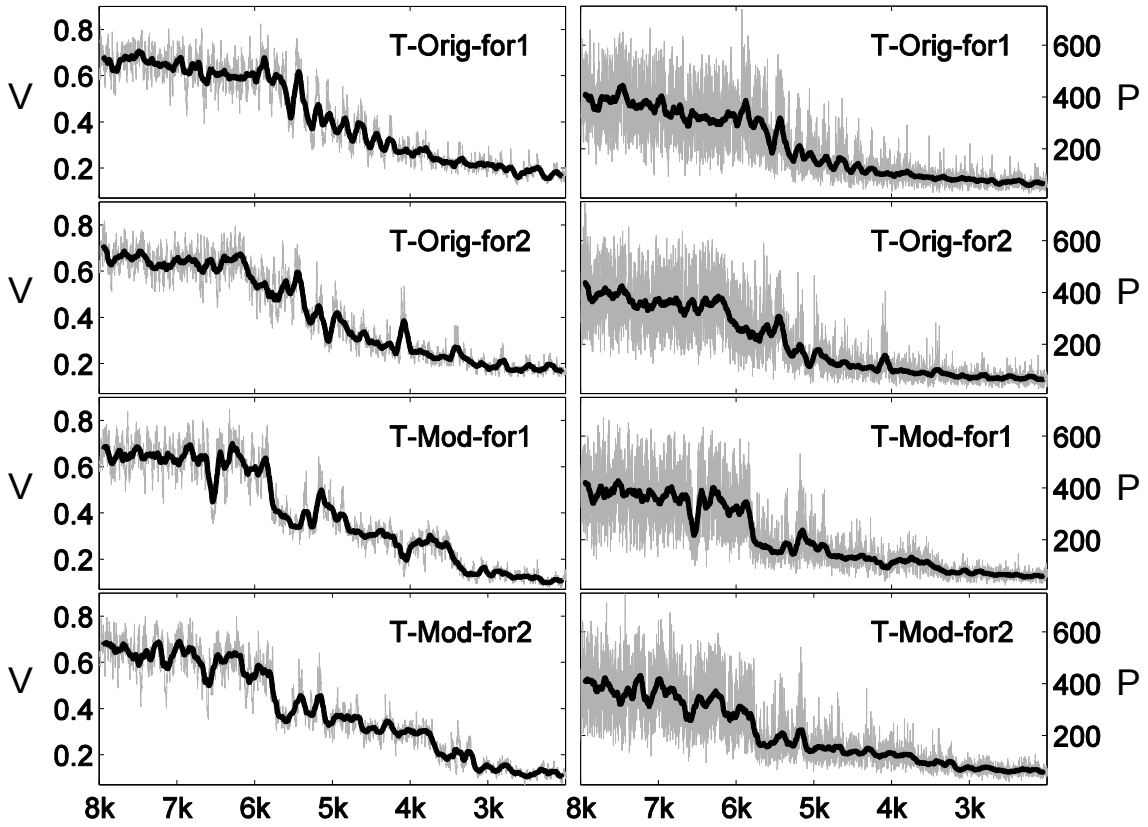

Figure 2.5: Evolution of spatial mean vegetation cover fraction (left) and precipitation in mm/yr (right) in the Sahara/Sahel region in two PlaSim-VECODE experiments with VECODEo (four top panels) and VECODEm (four bottom panels). Thin line: annual data; heavy line: 100 yrs running mean.

the transition period, until the rate of vegetation decline decreases again around 5 k. For VECODEm, this vegetation decrease is more abrupt and occurs in one major event. The evolution of spatial mean precipitation in the Sahara/Sahel region closely resembles the vegetation dynamics, although absolute changes are small between 5 k and 2 k.

An analysis of the local changes reveals that the rapid transition also occurs in Central Arabia and the Middle East. For VECODEm, a second, even more pronounced vegetation decline occurs between 4 k and 3 k in the south-western Sahara (Fig. 2.6). While these features can be seen in all experiments, the shape of each time series and the exact timing of the transitions differ among the two ensemble members.

2.4 Detection of multiple equilibria

2.4.1 On the use of stability diagrams

Stability diagrams like Fig. 2.1 illustrate the nature of multistability, but they have also been used to infer the equilibria for a particular region in a complex climate model (Brovkin et al., 2003;

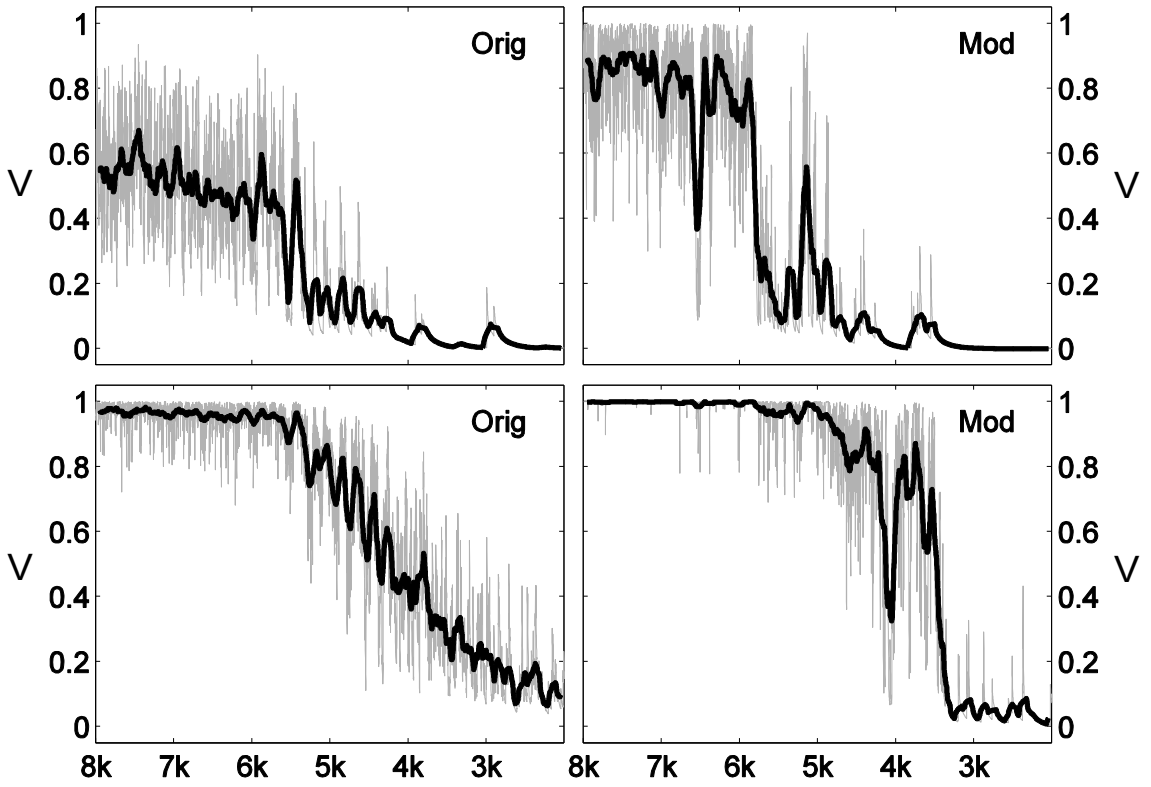

Figure 2.6: Evolution of vegetation cover fraction at two adjacent grid cells in the western Sahara (approx. 0°, 12–22° N; Fig. 2.8), for the transient experiments T-Orig-for1 (left panels) and T-Mod-for1 (right panels). Thin line: annual data; heavy line: 100 yrs running mean.

Wang, 2004). When simulating the Holocene with ECBilt-CLIO-VECODE, Renssen et al. (2003, 2006) obtained a rather gradual decline in vegetation cover in the Sahara/Sahel region, even more gradual than our result with VECODEo, considering the smaller region in their Fig. 1c (Renssen et al., 2003). However, the construction of a stability diagram lead to the conclusion that multiple equilibria exist in the early to mid-Holocene in ECBilt-CLIO-VECODE. The gradual decline in vegetation cover was explained with the large atmospheric variability that supposedly caused frequent shifts between the equilibrium states.

The specific method to construct a stability diagram differs among publications. Renssen et al. (2003) derived the $P^*(V)$-line by connecting two points in phase space: the mean state of a coupled experiment and the mean state of an uncoupled experiment with fixed vegetation cover. Both points are averages in space and time. In all cases the following limitations have to be considered:

(i) The time mean of the coupled model's state does not necessarily correspond to a deterministic equilibrium.

(ii) The effects of spatial complexity cannot be adequately represented in a simple one-dimensional model.

(iii) The equilibrium curve $P^*(V)$ is not strictly linear.

(iv) Other state variables may exist. In the case of PlaSim-VECODE, growing degree days affect V^* and depend on the location and on vegetation cover itself.

Section 2.4.2 will provide examples for argument (i). To demonstrate argument (ii) we extend the conceptual deterministic model to two spatial points (indexed $i = 1,2$) with vegetation cover (V_1, V_2) and precipitation (P_1, P_2):

$$P_i = P_{d_i} + \sum_{j=1}^{2} \mathbf{k}_{ij} V_j. \tag{2.4}$$

At each of the two points, equilibrium vegetation cover depends only on the local precipitation according to Eq. (2.1), but local precipitation P_i depends on vegetation cover at both points according to Eq. (2.4). Hence, k is now a 2×2 matrix. As examples we distinguish four systems whose stability diagrams and actual equilibria are compared in Fig. 2.7. For each system we take the original $V^*(P)$ with $\mathrm{GDD}_0 = 10000$. For system 1 and 2 we set the following parameters:

$$\text{System 1 and 2: } \mathbf{k} = \begin{pmatrix} 200 & 200 \\ 120 & 120 \end{pmatrix}$$

$$\text{System 1: } P_d = \begin{pmatrix} 0 \\ 110 \end{pmatrix} \qquad \text{System 2: } P_d = \begin{pmatrix} 110 \\ 0 \end{pmatrix}$$

In systems 1 and 2, there are no multiple equilibria. However, the stability diagram diagnoses two stable states in both cases. The reason for this contradiction lies in the spatial heterogeneity and the interactions between the two locations via the atmosphere. For example, when vegetation cover in system 2 is set to 0, the resulting mean precipitation could not sustain vegetation if it occurred at a single grid cell. Therefore, the one-dimensional stability diagram indicates a desert equilibrium. In the spatially resolved model location 1 could nonetheless maintain vegetation which in turn potentially increases precipitation also at location 2. The use of a forced climate state far from equilibrium thus turns out to be problematic. In the light of this result, the multistability in ECBilt-CLIO-VECODE postulated by Renssen et al. (2003, 2006) may be nonexistent. As we also find that a strong atmosphere-vegetation feedback with large climate variability leads to a vegetation collapse in VECODE, it is likely that ECBilt-CLIO-VECODE is monostable.

After all, is a stability diagram more reliable when only one intersection is obtained? Systems 3 and 4 show that this is not the case. In Systems 3 and 4, there is spatial heterogeneity, but no spatial interactions are involved ($k_{ij} = 0$ for $i \neq j$):

$$\text{System 3 and 4: } \mathbf{k} = \begin{pmatrix} 150 & 0 \\ 0 & 300 \end{pmatrix}$$

$$\text{System 3: } P_d = \begin{pmatrix} 50 \\ 50 \end{pmatrix} \qquad \text{System 4: } P_d = \begin{pmatrix} 180 \\ 50 \end{pmatrix}$$

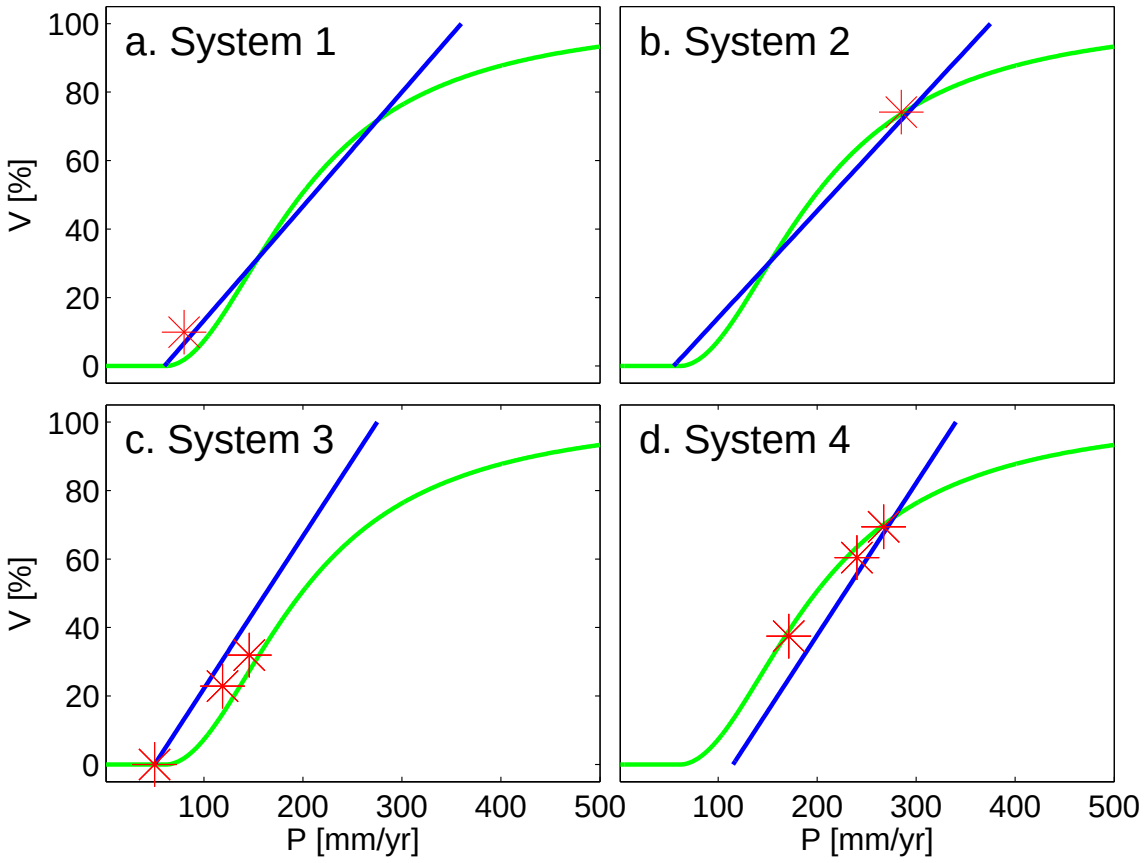

Figure 2.7: Stability diagrams for four example systems, compared to the true equilibria (red stars). In case of three equilibria, the middle red star marks the unstable equilibrium point. The state variables V and P represent the average of V_1 and V_2, and P_1 and P_2, respectively. The blue P^*-lines connect the two points $P(V=0)$ and $P(V=1)$ as obtained from Eq. (2.4).

Although one of the two spatial elements is bistable, the inclusion of monostable areas in the spatial average hides the local bistability. In this regard, the approach by Levis et al. (1999) and Brovkin et al. (2003) is also questionable, although it is physically plausible that there are no multiple equilibria in the boreal atmosphere-vegetation system.

To further illustrate our arguments (ii) and (iii), we now construct a stability diagram for PlaSim-VECODE 0 k conditions with the following method:

- In 11 different experiments we prescribe a uniform and fixed grass cover in the Sahara/Sahel region, with cover fractions ranging from 0 to 1 in steps of 0.1. Each of these uncoupled PlaSim simulations has a length of 100 yrs, of which the last 90 yrs are averaged over time and over the Sahara/Sahel region.

- The resulting mean annual precipitation values of the 11 experiments represent the equilibrium precipitation curve $P^*(V)$ in the stability diagram.

- We draw the $V^*(P)$ curve (Eq. 2.2) by assuming a fixed GDD_0-value of 10000. An analysis

which takes into account that GDD_0 differs among grid cells and among the experiments leads to a different vegetation curve, but similar results regarding the number of intersections between V^* and P^*. Hence, argument (iv) is not important in this particular case.

The resulting stability diagram (Fig. 2.2) clearly diagnoses two stable solutions for VECODEm that may also exist for VECODEo at an earlier time than 0 k. Furthermore, connecting the end points of the precipitation curve by a straight line would already suggest two stable equilibria for VECODEo. However, we will show in Section 2.4.2 that no multiple equilibria exist for 0 k orbital forcing, neither for VECODEm nor VECODEo.

Our results evoke the question of how to decide on a particular region where the stability analysis should be applied. On one hand, the land cover types of the surrounding areas can influence the climate within the region. Hence, if grid cells that are vital for the multistability are excluded, the analysis will indicate only one possible state that depends on the choice that has been made on the surrounding land cover. On the other hand, if the analysis region is large then the spatial heterogeneity might still lead to wrong conclusions as illustrated above. As all the interactions between individual grid cells are generally not known, it is not possible to a priori determine the particular region that could be appropriate for the construction of a stability diagram. In Chapter 3 we will return to this problem and propose a stochastic method for the detection of hotspots. We also note that even when the number of equilibria is not altered, our arguments (i)–(iv) imply that quantitative inferences on the stability of a certain state (e.g. in form of a potential) can still be wrong. Altogether, we conclude that the construction of a stability diagram can yield misleading results and focus on the method of different initial conditions in the next section.

2.4.2 Extreme initial conditions: desert and forest world

2.4.2.1 PlaSim-VECODE Results

In order to interpret the results of the transient experiments in terms of multiple equilibria, we run the coupled PlaSim-VECODE model starting from different initial conditions. This strategy may generally not be a trivial task, as it is not always clear how to choose the initial conditions. Also, more than two possible solutions could exist (e.g. Wang and Eltahir, 2000; Dekker et al., 2010). Putting these restrictions aside, we choose the extreme initial conditions of global desert and global forest (Fraedrich et al., 1999; Fraedrich et al., 2005b). In both cases, all land points except ice shields are initialised with the surface parameter values corresponding to complete forest or desert respectively. To bring the free variables to an equilibrium with the extreme surface parameters, we run PlaSim for 15 yrs under forest and desert world conditions. After this spin-up time the land cover types are allowed to change. We use this initialisation procedure regardless of the coupling method or VECODE version, and run the model until a steady state is obtained. The results are summarised as follows:

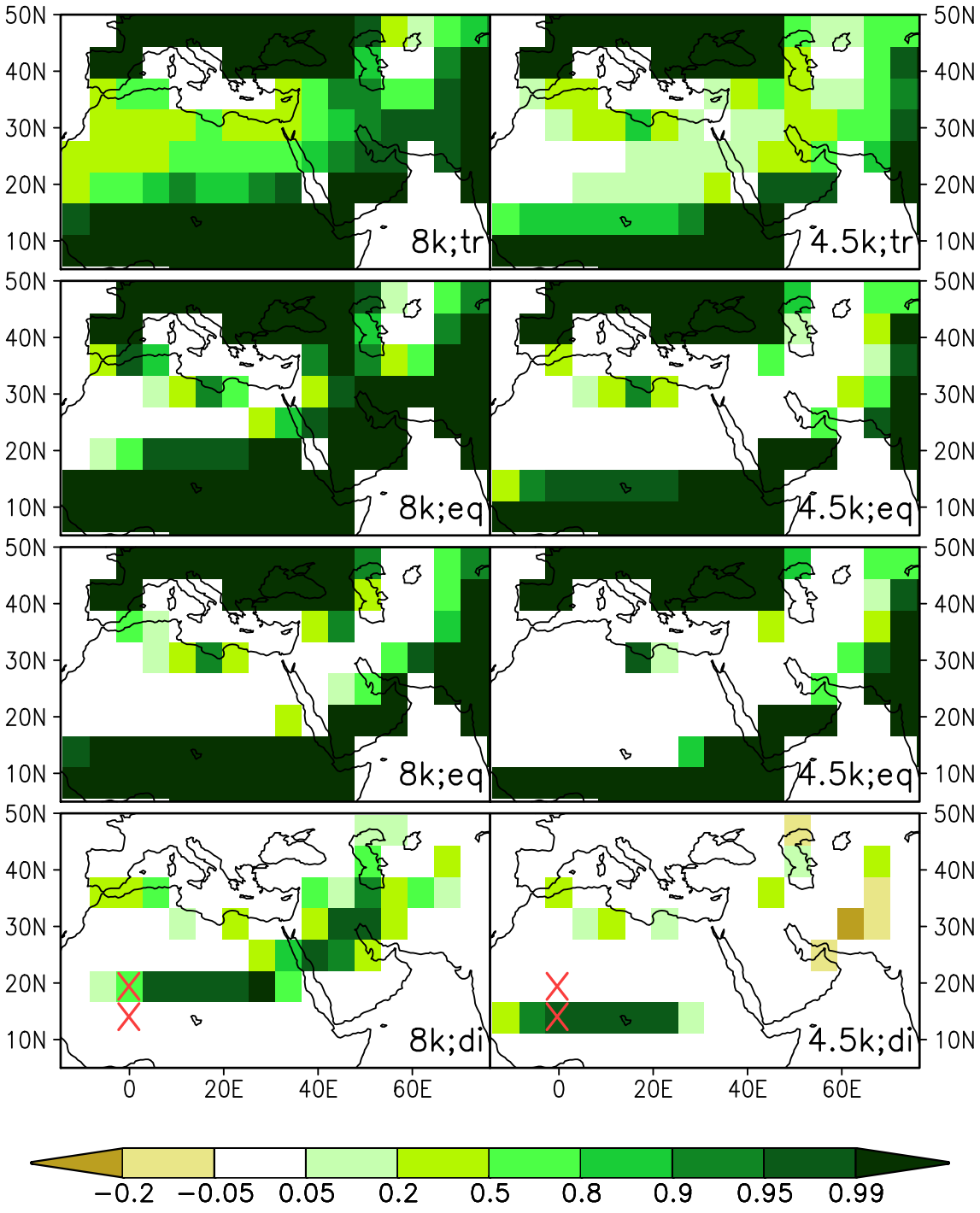

Figure 2.8: Equilibrium vegetation cover fractions for transient (tr) and equilibrium (eq) mode with VECODEm. The second row of panels shows the steady state when starting from forest world conditions, the third row shows the steady state when starting from desert world conditions (all with 10 yrs coupling frequency). In the last row, the difference (di) between these states is displayed. Results for 8 k are in the left column, results for 4.5 k in the right column. The red crosses mark the two grid boxes used for Fig. 2.6 and 2.12.

- For VECODEo we find no multiple steady states. All model trajectories lead to the same mean state. This result is independent of time (between 8 k and 0 k), the way of coupling (transient or equilibrium mode) and the coupling frequency in equilibrium mode (up to 20 yrs).

- For VECODEm in transient mode, we find no multiple steady states, independently of the orbit year (8 k, 4.5 k, and 0 k).

- For VECODEm in equilibrium mode, we find multiple steady states, whose extent and location depends on the orbit year (Fig. 2.8). In 8 k the bistable region extends from the southern margin of the Sahara desert to the central Arabian peninsula and the Middle East. In 4.5 k, the only substantial difference between forest and desert run occurs at eight grid cells at the southern desert margin, now shifted to the south-west compared to 8 k. The green state in the bistable regions resembles the steady state solution of the transient mode. However, in the monostable desert regions the transient mode produces greener conditions than the equilibrium mode.

In short, multiple steady states occur only for VECODEm in equilibrium mode, but not between approx. 7 k and 5 k (Table 2.2). The latter is probably due to low resolution of our model and the concomitant large differences in precipitation between adjacent grid cells. As Fig. 2.1 illustrates, multiple steady states can only occur for a certain range of background precipitation P_d. Following this concept, background precipitation at the grid cell line around 20° N after 7 k becomes small enough that the desert state remains the only equilibrium, while a green equilibrium is still the only possible state at the more southern grid cells around 14° N. When background precipitation is further reduced, the bistability reappears at the southern grid cell line. In case of a higher resolution we would probably obtain a continuous shift of the bistable area to the south-west until its disappearance.

When comparing the geographical position of multiple states to the vegetation dynamics of our transient runs in Section 2.3, it becomes apparent that the most rapid vegetation decline occurs exactly in the bistable regions and shortly after the green state in equilibrium mode ceases to exist. In addition, the vegetation collapse is largest where the difference between the two states is high. Hence, the collapses in the transient experiments (in the Sahara, Arabia and the Middle East after 6 k, and in the south-western Sahara after 4 k) can be interpreted as critical transitions resulting from a saddle-node bifurcation in the atmosphere-vegetation system. However, the question remains why there is nonetheless no dependency on initial conditions in transient mode.

2.4.2.2 Interpretation with the stochastic model

The behaviour of a bistable system that exhibits variability is often exemplified with stochastic motion in a potential, whose two wells correspond to the system's basins of attraction (e.g. Fraedrich, 1978, 1979; Wang and Eltahir, 2000; Renssen et al., 2006; Scheffer et al., 2001, 2009; Ditlevsen and Johnsen, 2010). If the noise level is small, the residence time in each well is very large and only one steady state can be observed in a time series. If the noise level is large compared to the

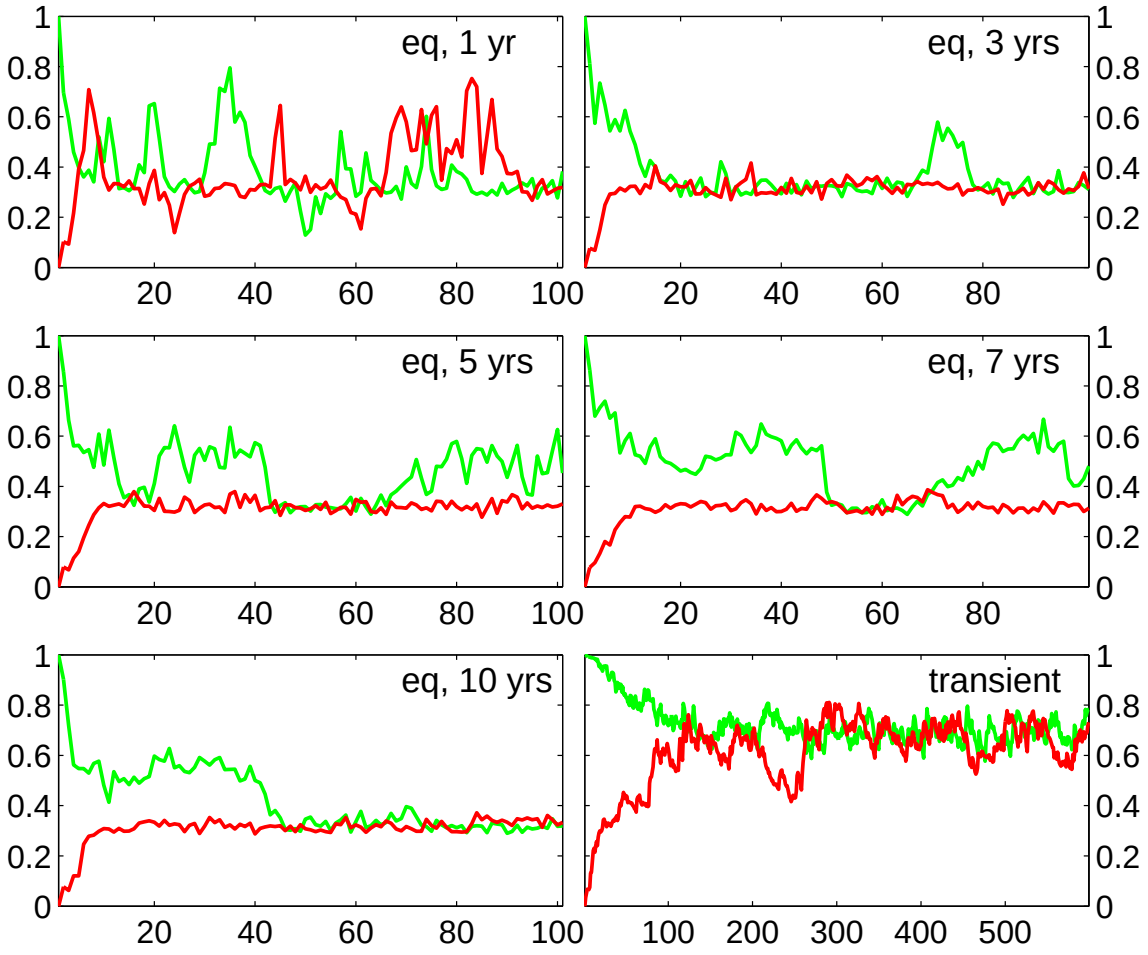

Figure 2.9: Evolution of spatial mean vegetation cover in the Sahara/Sahel region starting from forest (green) and desert world conditions (red), in equilibrium mode (eq) with different coupling frequencies, as well as transient mode (transient). The x-axis is in units of coupling iterations (1 yr in case of transient coupling). All experiments have been performed with VECODEm and under 8 k conditions.

potential barrier, a single peak is obtained in the probability density function (pdf) of the system's state variable at the potential's centre of gravity. In case of an intermediate noise level the system is supposed to flip irregularly from one regime to another, producing two separate peaks in the pdf. This behaviour is similar to PlaSim-VECODEm-eq: The more we reduce atmospheric variability by averaging over a larger number of years, the longer is the typical amount of time the system remains in the green regime (Fig. 2.9).

However, this concept is inconsistent with our PlaSim-VECODE-tr results. The Lyapunov potential following Brovkin et al. (1998) suggests two steady states for a certain range of P_d (here, we adopt the continuous equivalent to our time-discrete dynamic equation 2.2):

$$\frac{dV}{dt} = -\frac{d\Phi}{dV} = \frac{V^*(P^*(V)) - V}{\tau(P^*(V))}. \tag{2.5}$$

To obtain the potential $\Phi(V)$, Eq. (2.5) has to be integrated. As τ decreases with V, the green

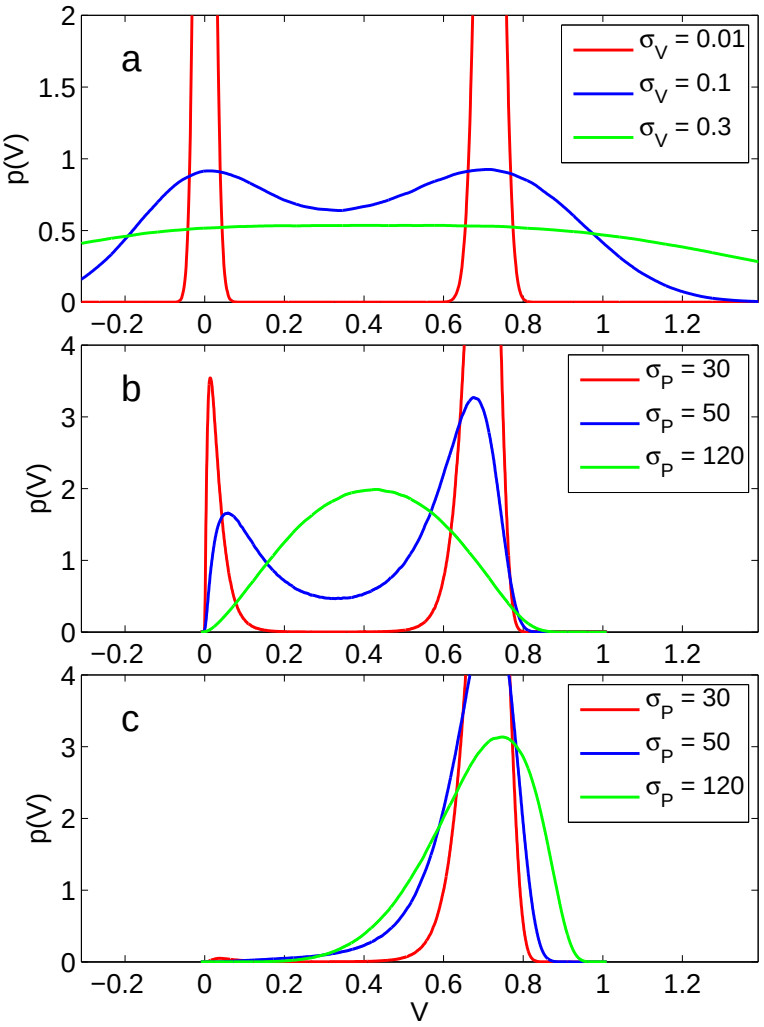

Figure 2.10: Probability density functions of vegetation cover in the stochastic conceptual model with $P_d = 60$ for different noise levels. **(a)** additive noise with $\tau = 5$ yrs, **(b)** multiplicative noise with $\tau = 5$ yrs, **(c)** multiplicative noise with interactive τ. σ_P is given in mm/yr.

regime will be stabilised in comparison with the desert regime, and the change in stability can happen faster than for constant τ. Nonetheless, the number and position of deterministic equilibria do not change. The above-mentioned inconsistency therefore remains: If the noise level is considered as small, the system's steady state would depend on initial conditions. If the noise level is intermediate, the stationary pdf should be bimodal. If the noise level is large, the mean state should lie between the deterministic equilibria, and the observed variability should be larger in amplitude than the distance between the deterministic equilibria. All this is not the case in our transiently coupled experiments (ignoring the effect of switching timescales mentioned in Section 2.2.3).

The reason is that the noise does not directly act on the changes in vegetation cover in Eq. (2.2) in the form of additive noise. Instead, a random precipitation anomaly in a particular year affects the vegetation change via the non-linear relationship $V^*(P)$, on the basis of the interactive timescale $\tau(P)$. Therefore, the noise must be interpreted as multiplicative (Horsthemke and Lefever, 1984).

We document these vital differences by calculating the empirical pdf from a time series of 10 million yrs (Fig. 2.10) with our one-dimensional stochastic model Eqs. (2.1), (2.2), and (2.3). We choose the equilibrium vegetation curve from VECODEo, $P_\mathrm{d} = 60$, and $k = 300$, so that

the corresponding deterministic system has solutions at approx. $V = 0$, and $V = 0.7$. In the following, we always choose $\mathrm{GDD}_0 = 10\,000$ and $T = 27\,^{\circ}\mathrm{C}$, as these are typical values in the Sahara/Sahel region in PlaSim-VECODE. The pdfs are calculated with an advanced Gaussian kernel density estimator for MATLAB (Botev et al., 2010). In order to always capture both possible equilibria, we start from $V = 0$ and set $V = 1$ after half the total time. The 50 yrs following each of these resets are not used for the analysis. In case a, we add Gaussian white noise directly to the dynamical equation (Eq. 2.2), while precipitation is set to its equilibrium value $P^*(V)$ in each year, and τ is fixed at 5 yrs. For small noise levels, two peaks indicate the deterministic solutions, whereas for very large noise levels the bimodality disappears. In this additive case, we allow V to be larger than 1 or smaller than 0, for the sake of simplicity. In case b, we use Eq. (2.2) directly, treat precipitation as a Gaussian white noise process (while resetting negative precipitation values to 0), but still keep τ fixed at 5 yrs. This case corresponds to the stochastic model in Liu et al. (2006). Finally, in case c we also consider the dependency of precipitation on the vegetation timescale. The stochastic conceptual model is then fully described by Eq. (2.1), (2.2), and (2.3). For sufficiently large noise levels, the only steady state is again very similar to the deterministic green equilibrium, while the desert state has disappeared. The fact that the timescale of expansion is shorter than the timescale of vegetation dieback (Fig. 2.3) results in greener conditions in comparison to the case with a fixed timescale. The reason that no multiple steady states are found in transient mode is not simply the intensity of the noise itself, but rather the effect of the noise on the stability properties of the system. This effect corresponds to the *noise-induced stability* d'Odorico et al. (2005) have found in their dryland vegetation model.

Atmospheric variability is also the reason why monostable desert regions tend to be greener in transient mode than in equilibrium mode: Although mean precipitation as such is not sufficient for vegetation, the critical threshold can be exceeded in exceptionally wet years and vegetation will temporarily establish. As vegetation cover cannot become negative, its temporal mean will thus also be positive. This effect corresponds to the *greening effect* described by Zeng et al. (2002), which adds to the general effect of an asymmetric potential (*rectifier effect*). All three mechanisms (rectification due to interactive timescale, rectification due to non-linearity in V^*, and greening effect) provide further examples for our argument (i) against the use of stability diagrams in Section 2.4.1. In equilibrium mode, however, VECODE simulates a complete desert and the boundaries between desert and grass are more pronounced. Also in similarity to Zeng et al. (2002), these boundaries are also more pronounced in VECODEm than in VECODEo because the V^*-curve is then steeper.

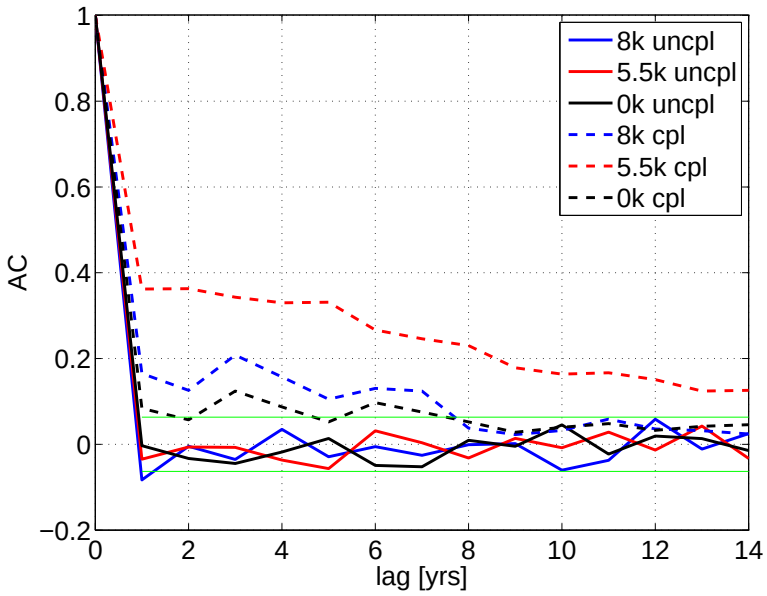

Figure 2.11: Autocorrelation function of annual precipitation averaged over the Sahara/Sahel region for uncoupled (uncpl) and coupled (cpl) experiments in transient mode. From each run, yrs 2000–3000 are used for the calculations. The 2σ-confidence bounds for white noise are indicated by the green lines.

2.5 On the mechanism of vegetation collapse

2.5.1 Relation between system state and noise level

It has been claimed that large atmospheric variability must lead to an only gradual decline in vegetation cover, for example as obtained in the intermediate complexity model of Renssen et al. (2003, 2006), and in the stochastic model of Liu et al. (2006) in the case of white noise. Nonetheless, the standard deviation of precipitation in PlaSim-VECODE is of the order of 100 mm/yr, and there can still be a vegetation collapse. Therefore, the question arises why PlaSim-VECODE can exhibit rapid vegetation changes despite the large atmospheric variability.

To explain a similar behaviour in their model, Liu et al. (2006, 2007) suggested low frequency climate variability. Due to the memory effect of soil moisture, a small but sufficiently long lasting precipitation decline can cause a collapse in vegetation cover, even without a strong feedback between atmosphere and vegetation. In the uncoupled PlaSim we do not find any substantial autocorrelation of spatial mean annual precipitation in the Sahara/Sahel region (Fig. 2.11). Very similar results are obtained for each single grid cell. It becomes obvious that the decorrelation time of the atmosphere is considerably shorter than the timescale of grass in PlaSim-VECODE. Even when we calculate the autocorrelation function of soil moisture instead of precipitation, the results look very similar to Fig. 2.11. Hence, our assumption of white noise in the stochastic model is justified and the mechanism of collapse is not the same as in Liu et al. (2006, 2007).

Instead, it has to be considered that the noise level and the state of the system affect each other. In the dry desert with very low mean precipitation, the absolute variability must also be small. For very low mean annual precipitation the distribution in PlaSim is similar to an exponential distribution but becomes more and more symmetric for increasing mean values. This property is obtained at every grid cell in the Sahara/Sahel region and is also independent of the orbit year. To capture these features as well as to avoid negative precipitation values we now represent precipitation as an

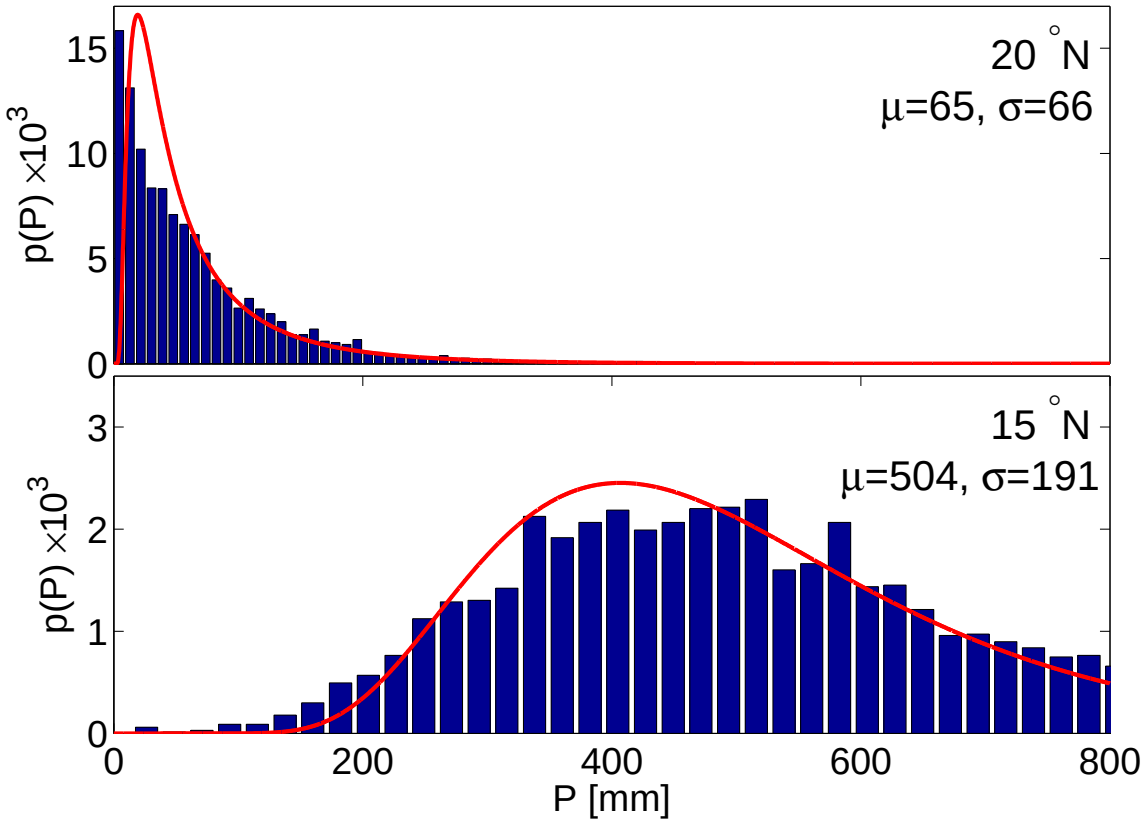

Figure 2.12: Histograms of annual precipitation in the uncoupled PlaSim experiment TU-5.5k at the two grid cells marked in Fig. 2.8. Mean μ and standard deviation σ are in mm/yr. Each red line depicts the analytical inverse normal distribution that correspond to the two moments.

inverse normal distribution in our stochastic model (Fig. 2.12). It is of further advantage that this distribution is described by the same parameters as the Gaussian distribution, mean and standard deviation. The mean μ_P still consists of the first two terms in Eq. (2.3). As the similarity between Fig. 2.10c and Fig. 2.13a,b illustrates, our results do not qualitatively depend on the choice of the distribution function.

To demonstrate the implications of the interaction between noise level and steady state we calculate the pdfs of vegetation cover fraction in our stochastic one-dimensional model for different values of background precipitation and two different noise levels σ_P (Fig. 2.13 a,b). The deterministic stability properties can be inferred from Fig. 2.1.

- For $P_d = 70$ and $P_d = 60$ two deterministic equilibria exist. The green state in this case is so stable that it is the only steady state for both noise levels. When by chance a dry event with only little vegetation occurs, and variability is reduced at the same time, the green state will only become more stable and the system returns to green conditions.

- For $P_d = 40$, the desert state is the only deterministic equilibrium, although in the presence of large noise greener conditions occur as often as dry conditions.

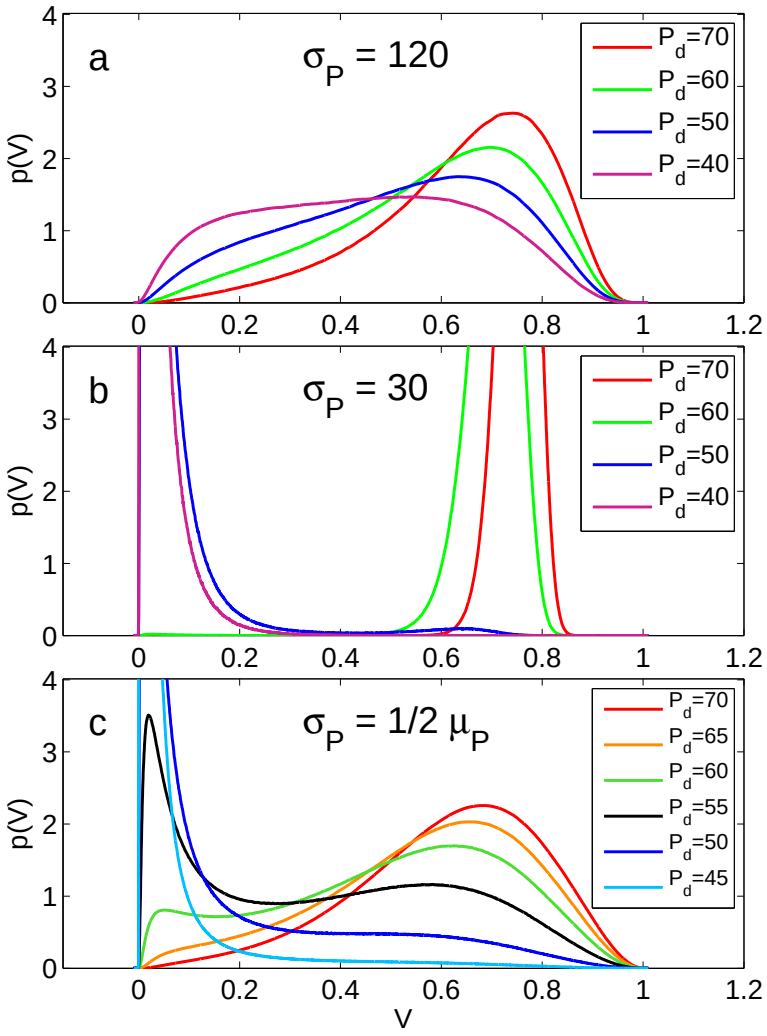

Figure 2.13: Probability density functions of vegetation cover in the stochastic conceptual model for different values of P_d. **(a)** and **(b)** at constant noise levels σ_P, **(c)** for interactive noise level. Values of P_d and σ_P are in mm/yr. The experiment length is 10^7 yrs for fixed σ_P, and 10^8 yrs for interactive σ_P. μ_P represents the mean of the precipitation probability distribution for a particular year.

- For approx. $P_d = 50$ the deterministic system is at a bifurcation point. The stability diagram then suggests a stable desert solution while the green equilibrium is only marginally stable. In the presence of large noise (Fig. 2.13a), green conditions still have maximum probability due to the noise. However, if one assumes that the noise level is reduced as soon as a state of low vegetation cover occurs, Fig. 2.13b applies. Suddenly, the desert state becomes more probable and the system may not escape from its dry state anymore.

To illustrate this concept we do not prescribe a fixed noise level anymore but calculate it from mean precipitation interactively, as suggested by our uncoupled experiments: For each single grid cell the relation between mean and standard deviation of annual precipitation is close to linear, especially under very dry conditions (Fig. 2.14). A similar relation holds in the transient experiments presented in Section 2.3, independent of the time period or grid cell. Therefore, a constant factor between mean and standard deviation of the precipitation distribution function, $r = \mu_P/\sigma_P$, seems justified, in analogy to d'Odorico et al. (2005). For the stochastic model we choose a value of $r = 2$ (Fig. 2.14).

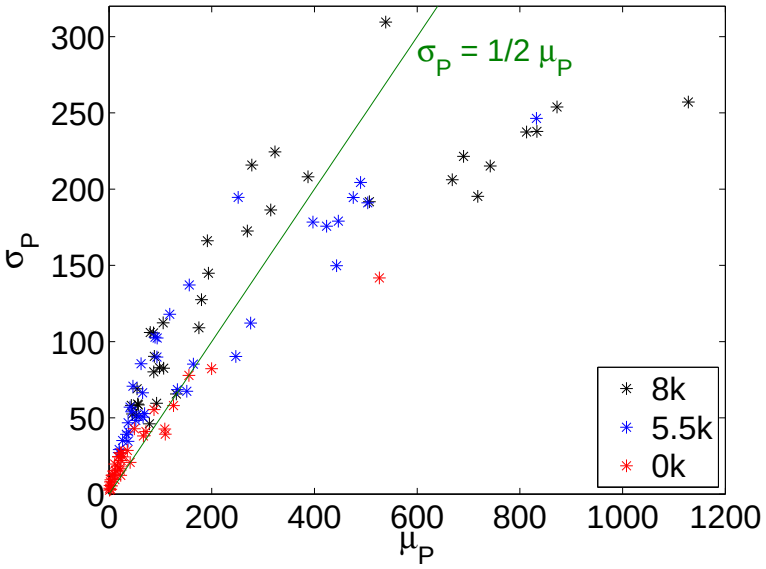

Figure 2.14: Mean μ_P and standard deviation σ_P of annual precipitation (both in mm/yr) for all individual land grid cells of the Sahara/Sahel region in three uncoupled PlaSim experiments. The dark green line shows the relation we choose for the stochastic model with interactive noise level.

2.5.2 The stochastic model with interactive noise level

As a result of coupling the noise level to vegetation cover, the pdf will not change qualitatively in a large range of P_d, whereas it responds quite sensitively to P_d around 55 mm/yr, which is slightly larger than the critical point of the corresponding deterministic system. As the mean of the distribution rapidly shifts from high to low V as P_d falls below the critical threshold, the system can tip from a green state to a desert state, in analogy to a deterministic Tipping Point. However, in contrast to a deterministic catastrophic shift, no multiple states are involved: The stochastic model only shows a bimodal pdf in a parameter range that is much smaller than the hysteresis loop of its deterministic counterpart (approx. 50–60 mm/yr, instead of 50–80 mm/yr). Furthermore, the relative size of the peaks is exchanged almost abruptly as P_d is varied (Fig. 2.13).

It must be noted that the bimodal parameter range as well as the abruptness of a shift is much dependent on our choice of r. When analysing the pdfs of vegetation cover in PlaSim-VECODE (runs T-Orig-5.5k, as well as TF-Mod-4.5k or TD-Mod-4.5k), we also do not obtain any clear bimodality, neither for the spatial mean nor at any particular grid cell. In addition, no considerable hysteresis effect becomes apparent when comparing the experiments with forward (T-Mod-for1 and T-Mod-for2) and backward (T-Mod-back1 and T-Mod-back2) orbital forcing. For values of r around 2, the conceptual stochastic model comes closest to these properties of PlaSim-VECODE. Hence, the conceptual model can explain the PlaSim-VECODE results, although we did not aim to derive precise parameter values for the conceptual stochastic model from PlaSim-VECODE. The agreement of $r = 2$ to the results from individual grid cells (Fig. 2.14) is therefore convenient, but not compelling.

As in the deterministic case, the abruptness of the vegetation decline in our stochastic model also depends on the strength of the atmosphere-vegetation feedback. However, the system's behaviour during the transition period is subject to chance. To get an impression on the different possibilities we run the stochastic model approx. 50 times for $k = 200$ (weak feedback; monos-

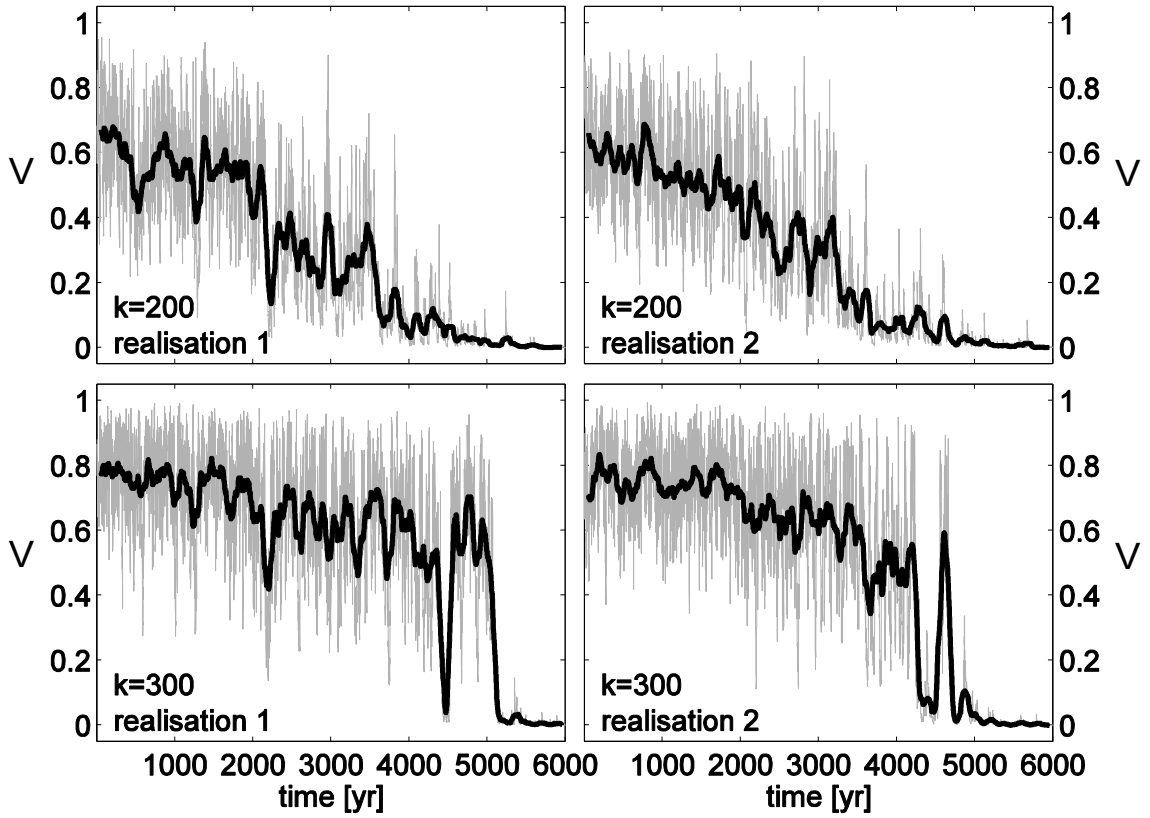

Figure 2.15: Evolution of vegetation cover fractions in the stochastic conceptual model with interactive noise level as P_d is reduced linearly over time from 120 to 30. For each feedback strength, weak ($k = 200$, upper panels) and strong ($k = 300$, lower panels), two realisations have been selected.

table) and $k = 300$ (strong feedback; bistable between approx. $P_d = 80$ and $P_d = 50$). Fig. 2.15 shows two realisations for each value of k. If the feedback is as strong as to allow for multiple equilibria, then sudden transitions always occur. Sometimes an early collapse is obtained, after which the system recovers before it finally drops into the desert state ($k = 300$, realisation 1), a behaviour that resembles our experiment T-Mod-for1 (Fig. 2.6). In other (or often the very same) cases, a short post-collapse rebound occurs ($k = 300$, realisation 2), a feature that also exists in some proxy records (e.g. deMenocal et al., 2000). In the case of the monostable system rapid changes can still occur ($k = 200$, realisation 1), but usually the decline is more gradual as the unimodal pdf smoothly shifts towards lower V ($k = 200$, realisation 2). Considering the one-dimensional concept of the stability diagram, the system must show an increased variance when the range of maximum slope in $V^*(P)$ is passed. This is due to the flattening of the corresponding Lyapunov potential (Brovkin et al., 1998), that causes slowing down of the system (Scheffer et al., 2009). The increased variability during the transition period in Renssen et al. (2003, 2006) can also be interpreted as such a temporary slowing down, instead of flickering between multiple states. In our stochastic model however, we generally do not obtain an increased variability in the weak feedback case because the level of external noise is coupled to the state V of the system

which shows an overall decrease.

If we choose a particularly small feedback parameter (below $k = 200$), the stochastic model does not simulate any collapse. The *stable collapse* of Liu et al. (2006) (which is associated with an only gradual decline in precipitation) then remains the only mechanism to explain an abrupt vegetation decline.

2.6 Summary and conclusions

By performing experiments with PlaSim-VECODE for different ways of coupling, different strengths of the atmosphere-vegetation feedback, and different orbit years in the Holocene we have investigated the stability properties of PlaSim-VECODE and the nature of the transient evolution of vegetation cover in the Sahara/Sahel region. We have also illustrated our interpretation with a conceptual stochastic model.

Our results can be summarised as follows:

- A stability diagram is a good demonstration of the concept of multistability, but it must be applied with care when inferring the stability properties of a spatially heterogeneous model. In this case, it can show equilibria that do not exist.

- The detection of multiple equilibria by choosing different initial conditions depends on the method of coupling between atmosphere and vegetation model. Atmospheric variability can obliterate a deterministic bistability, but beyond that it can act as multiplicative noise and change the stability properties themselves.

- A vegetation collapse is possible despite large and uncorrelated climate variability, provided 1. a positive and sufficiently strong atmosphere-vegetation feedback, and 2. an impact of the system's state on the intensity of variability. PlaSim-VECODEm is an example for such a mechanism: Before the vegetation collapse, the green state is stabilised by the climate-dependent timescale and the large atmospheric variability. Once the system comes close to the desert state and background precipitation is sufficiently low, the desert state is stabilised due to the decrease in variability.

Our results imply that climate variability, in interaction with non-linearities in the climate system, as well as spatial complexity must be considered for stability analysis. It also becomes apparent that the exact evolution of the system (such as abruptness of the transition, or the timing and existence of a post-collapse rebound) can strongly depend on the realisation. Even a most realistic climate model can then not be expected to agree with observations.

It also remains unclear which mechanism most appropriately describes the Saharan vegetation decline in reality. This question cannot be answered on the basis of our model results alone. Limitations arise from the low resolution and the simplicity compared to comprehensive Earth System Models. Specifically, VECODE is an empirical rather than a process-based model, and

it is lacking an annual cycle. Although soil moisture is an essential quantity of the atmosphere-vegetation system (Wang and Eltahir, 2000; d'Odorico et al., 2005), it is not represented in the model. However, as annual soil moisture in PlaSim also shows a white noise spectrum, a different coupling would probably not affect our results. However, our way of calculating surface parameters and evapotranspiration is very crude. Also, it is certainly not realistic to tie all physical surface properties that depend on vegetation cover to the same timescale.

The treatment of this timescale τ is a critical component in VECODE because of its influence on the steady state. The relation $\tau(P)$ originates from global observations of biomass turnover time in different ecosystems (Brovkin et al., 1997). According to these observations, dry ecosystems are dominated by woody plant types such as shrubs, which have a slower turnover rate than grasses in wet ecosystems. It is thus not compelling that the same relation should also hold for fast precipitation changes at a particular location. The model's response to large atmospheric variability may therefore not be appropriate. For example, a sudden interruption of all precipitation would result in an unrealistically slow dieback as between 4 k and 2 k in Fig. 2.6 (top panels). On the other hand, plant establishment and dieback in reality are due to very different biological processes and plant traits are known to adapt to changes in climate. Assuming a constant timescale as in previous conceptual studies may therefore also not be realistic. In this regard, our approach tests the implications of a climate dependent timescale for a model's stability properties such as sensitivity to initial conditions. Furthermore, our main conclusions as summarised above do not rely on the exact formulation of $\tau(P)$. In particular, a variable timescale is not an essential prerequisite for a collapse of a system that is subject to white noise. The reduction of variability after a shift has occurred can already be sufficient for a sudden transition, a feature that certainly applies to dry deserts.

Concerning climate variability the lack of ocean dynamics is another limitation in our model studies, as the ocean introduces more variability, especially at low frequencies. Including the ocean would also influence the stability properties of the model (Zeng and Neelin, 2000), for example, the SST-monsoon-feedback could enhance the effect of the atmosphere-vegetation feedback (Liu et al., 2003, 2004).

Apart from these uncertainties with regard to the real climate system, the question arises how applicable our results are to other models. It is self-evident that conceptual vegetation models with constant stochastic forcing and a fixed timescale can generally be described by the conventional approach of stochastic motion in a deterministic potential. The stability properties of the system may then be inferred from time series or even from the model formulation. However, both is not the case for models of high complexity. Whether our findings apply to any particular complex vegetation model remains an open question because such models describe many different processes on different timescales, while there is essentially only one variable and one timescale determining grass cover in VECODE. As the atmosphere model's sensitivity to land cover changes also affects the strength of the atmosphere-vegetation feedback, stability properties are not determined by the vegetation model alone. In addition, the behaviour of the coupled model depends on the

magnitude and the spectral properties of atmospheric variability. In the light of these aspects it is suggestive that properties similar to PlaSim-VECODE may also occur in other models.

Therefore, general implications for the detection of multistability and Tipping Points in climate models become apparent. Claussen (2008) summarises different methods that have been followed to identify multistable regions or subsystems in the earth system: the choice of different initial conditions, the construction of a stability diagram, the analysis of variability under stationary conditions, the application of so-called *early warning signals* for a system that approaches a bifurcation point (Scheffer et al., 2009), and the identification and quantification of mechanisms that can cause runaway feedbacks. Our results indicate that most of these methods may not be reliable under all circumstances: While variability can impede the first, and spatial complexity the second strategy, the stationary variability may also not provide the expected clues about the stability of a system. PlaSim-VECODEm is a good example: Before the vegetation collapse in experiments T-Mod-for1 and T-Mod-for2, the system can reach a state similar to post-collapse conditions at some times. However, the pdf remains unimodal. With regard to these results it is suggestive that the applicability of early warning signals should be further studied, and that a good understanding of the underlying processes may be indispensable to detect and predict Tipping Points.

Chapter 3

Detecting hotspots of atmosphere-vegetation interaction via slowing down

3.1 Introduction

The existence of potential Tipping Points in the climate system has received growing attention in recent years (Lenton et al., 2008; Lenton, 2011). In the narrower sense, a Tipping Point occurs when a system becomes very susceptible to an external forcing due to large positive feedbacks. In the extreme case the system's attractor disappears at a threshold value of the forcing (bifurcation) and the state has to approach a different attractor.

In order to predict the collapse at a preconceived bifurcation or to distinguish such changes in stability from random state transitions, it has been proposed to exploit statistical precursors of instabilities (Wiesenfeld, 1985a,b; Wiesenfeld and McNamara, 1986), also called Early Warning Signals (EWS; Scheffer et al., 2009). The fundamental assumption behind their applicability is that the system is close to a deterministic solution and perturbed by small fluctuations which can be described as white noise. In case of the climate system this approach resembles Hasselmann's concept of stochastic climate models (Hasselmann, 1976). When the system's stable fixed point loses stability when approaching a local bifurcation (e.g. a saddle-node bifurcation), an eigenvalue approaches 0 (if time is continuous). As a result, the linear relaxation time of the corresponding mode increases (Wissel, 1984). This phenomenon has recently been referred to as *critical slowing down* (Rietkerk et al., 1996; Scheffer et al., 2009; Ditlevsen and Johnsen, 2010; Dakos et al., 2010, 2011; Lenton, 2011; Lenton et al., 2012b). To avoid confusion with the phenomenon of algebraic (rather than exponential) decay in systems with second-order phase transitions (Strogatz, 1994) we will refer to the increased relaxation time simply as *slowing down*. As a consequence of slowing down, the system's autocorrelation and variance can increase (Scheffer et al., 2009), and the spectrum is reddened (Kleinen et al., 2003). Considering non-linear terms in the stability analysis, it follows that the skewness of the state variable can also increase in magnitude (Guttal and Jayaprakash, 2008).

However, the external parameter change must be slow enough for the system to stay close to equilibrium and to allow sufficiently long time series for a statistically significant detection of

EWS. A lack of detectability can thus impede any final conclusion on the existence of slowing down prior to an abrupt event. For example, Dakos et al. (2008) detected a consistent increase in autocorrelation with 95% probability in only 2 out of 8 palaeo records (see their Table S3), and the results seem to depend on the choice of the analysis method, parameter values and the particular proxy (Lenton et al., 2012a; Lenton et al., 2012b). This problem becomes worse close to the tipping point (for example see Dakos et al., 2012) because the uncertainty of an estimate from one sample of a fixed number of data points increases. In statistical terms, the sampling variances of the estimators of variance and autocorrelation increase with autocorrelation (Priestley, 1981). Better resolved time series may not always provide a solution as a sampling below the dynamic timescale of the system will not add relevant information.

Instead, the use of spatial EWS has been suggested (Guttal and Jayaprakash, 2009; Donangelo et al., 2010; Dakos et al., 2010): in analogy to the time domain, spatial variance and cross-correlations between different units of a spatially explicit system, as well as the spatial correlation length increase towards a tipping point. Such spatial EWS use each time step as a sample to infer the stability, while temporal EWS need a window of many subsequent time steps. As forcing changes over time in transient cases, temporal EWS thus involve information on previous states of the system. It is therefore often argued that spatial EWS could provide a more precise estimate of the current stability. However, the latter studies involve two simplifications: first, the analysed systems involve interactions which couple grid cells in a spatially homogeneous way. Second, the grid is constructed from identical elements with individual tipping points and the system's boundaries are well-defined. In this regard, the interactions between terrestrial ecosystems and the atmosphere pose a more difficult problem. Considering a global climate model, all land cells are globally coupled via the atmosphere, the spatial coupling is inhomogeneous, and the critical region producing a Tipping Point is embedded in a larger system with other dynamical characteristics. In such a complex setting, it is of interest not only if or when a tipping occurs, but also where it occurs and causally originates (hotspot). In previous studies on spatial EWS, the system's boundaries are known and well-defined. In addition, the application of the one-dimensional concept of EWS to high-dimensional systems, though justified by theory (Ditlevsen and Johnsen, 2010; Sieber and Thompson, 2012), in practice requires a priori knowledge on the critical mode of the transition (Held and Kleinen, 2004). This critical mode indicates in which direction in phase space the bifurcation occurs and thus how the information should be combined to yield EWS.

In this chapter, we consider the case where both, the critical mode as well as the critical subsystem, are unknown. In Section 3.2, we first demonstrate that under such general conditions EWS may not be detectable at any particular location of the system. Second, we propose an alternative application of EWS: the diagnostic detection of critical regions of slowing down (hotspots) in time series. In Section 3.2.1 we present a stochastic model of atmosphere-vegetation interaction which produces a vegetation collapse when a control parameter is varied. We then use the stochastic model to document a specific limitation of local EWS in a spatially explicit setting (Section 3.2.2). Based on this finding we explain our concept of a hotspot and present an algorithm

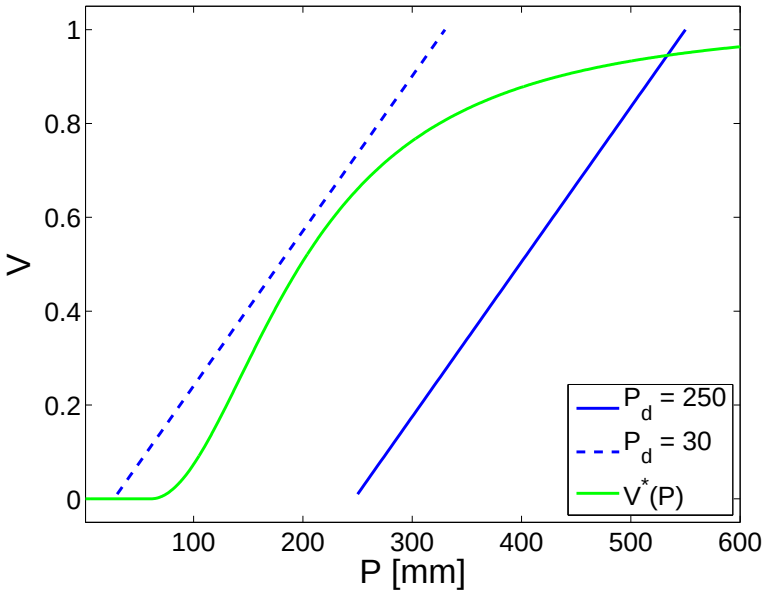

Figure 3.1: Stability diagram for the one-dimensional conceptual model with $k = 300$. Blue lines: equilibrium precipitation, calculated from $P^*(V) = P_\mathrm{d} + kV$ for different P_d. Green line: equilibrium vegetation cover $V^*(P)$ (Eq. 3.1).

for the detection of hotspots of slowing down (Section 3.2.3). We then discuss the performance of this algorithm for different properties of the analysed time series and different parameter choices and conclude in Section 3.2.4 by discussing possible applications and limitations of our approach.

In Section 3.3, we apply our method to the vegetation dynamics in PlaSim-VECODE. In Section 3.3.1, we briefly reintroduce the two models, the methods of coupling, as well as the dynamic vegetation changes simulated by PlaSim-VECODE. In Section 3.3.2 we discuss the restrictions of applying EWS to time series generated by PlaSim-VECODE, introduce a regression model, and derive parameter values to match our PlaSim-VECODE results. We then apply the hotspot detection scheme to our regression model in Section 3.3.3. In Section 3.3.4, we verify the results with PlaSim-VECODE and give a physical explanation of the model's behaviour. Section 3.3.5 provides our conclusions.

3.2 A stochastic approach to hotspot detection

3.2.1 A stochastic model of atmosphere-vegetation interaction

In order to test the performance of EWS-related methods, we generate time series with a simple stochastic model of vegetation dynamics in subtropical deserts. The structure of this model is similar to the conceptual model of Brovkin et al. (1998), Wang (2004), and Liu et al. (2006): annual precipitation P is a linear function of vegetation cover V, while equilibrium vegetation cover V^*

as a function of P is of sigmoidal shape (Fig. 3.1):

$$V^* = \begin{cases} 0 & \text{if } P < P_1 \\ 1 & \text{if } P > P_2 \\ 1.03 - \dfrac{1.03}{1+\alpha\left(\dfrac{P-P_1}{\exp(\gamma\,\delta)}\right)^2} & \text{otherwise,} \end{cases} \tag{3.1}$$

with

$$\begin{aligned} P_1 &= \beta\ \exp(\gamma\,\delta/2) \\ P_2 &= \beta\ \exp(\gamma\,\delta/2) + \frac{\exp(\gamma\,\delta)}{\sqrt{0.03\,\alpha}}. \end{aligned}$$

This function is the result of a semi-empirical fit to observations (Brovkin et al., 2002). Parameter values in all simulations of Section 3.2 are $\alpha = 0.0011$, $\beta = 28$, $\gamma = 1.7 \times 10^{-4}$ (this set of parameter values is referred to as VECODEo in Chapter 2), and $\delta = 9100$. For all time series we analyse in this chapter, P is always between P_1 and P_2.

If the conditions of a specific region are described with only one value of each, V and P, the system's deterministic equilibria can be depicted as intersections of the green and blue curve in Fig. 3.1. Reducing the external parameter P_d describes the effect of decreasing Northern Hemisphere summer insolation during the mid-Holocene, leading to a decrease in precipitation. When the green equilibrium disappears the system experiences a saddle-node bifurcation and vegetation cover has to collapse to the remaining desert state.

We extend this conceptual model by defining V and P for several elements with index i (for example to represent different grid cells in a climate model). At each of the N elements equilibrium vegetation cover depends only on the local precipitation according to $V^*(P)$. Vegetation cover is updated every (yearly) time step via the dynamic equation

$$V_i^{t+1} = V_i^t + \frac{V^*(P_i^t) - V_i^t}{\tau} + \sigma_V\,\eta_i^t. \tag{3.2}$$

Following Liu et al. (2006) we fix the timescale τ to 5 yrs. Due to atmospheric water transport and circulation changes, local precipitation P_i at a particular time t depends on vegetation cover at all elements:

$$P_i = \underbrace{P_{0_i} + s_i B}_{P_\mathrm{d}} + \sum_{j=1}^{N} \mathbf{k}_{ij} V_j + \sigma_P\,\eta_i \tag{3.3}$$

Eq. (3.2) is the multidimensional generalisation of Eq. (2.2) – extended by a stochastic term –, while Eq. (3.3) is the generalisation of Eq. (2.3). Due to the fast equilibration time of the atmosphere, Eq. (3.3) is not dynamic (singularly perturbed; Berglund and Gentz, 2006), and the V_i are all the state variables of this dynamical system. The system is globally coupled via $\mathbf{k}$ and in this

regard differs from reaction-diffusion models with interactions between adjacent elements only. The choice of $V^*(P)$ and the interaction matrix $\mathbf{k}$ determine the strength and spatial structure of the atmosphere-vegetation feedback and thus the stability properties of the system.

Brovkin et al. (1998), Wang (2004), and Liu et al. (2006) refer to the equilibrium precipitation in the absence of any vegetation as P_d. However, as P_d may differ at different elements, we split it into P_{0_i}, which is variable in space but not in time, and $s_i B$ with a scalar B as external control parameter. The local sensitivity of background precipitation to B is determined by parameters s_i, which are also variable in space, but not in time. In physical terms, B describes the effect of climate forcings, while the numbers we use are chosen arbitrarily.

The Gaussian white noise process η with small noise level σ is uncorrelated in space. We distinguish two types of noise but always use only one of them in our experiments: σ_V controls perturbations which are added to Eq. (3.2) directly (additive noise), while σ_P controls perturbations added to precipitation and whose impact on the state variable V_i depends on the system's state itself (multiplicative noise). Atmospheric variability is more realistically accounted for by the multiplicative noise case, whereas the additive noise case may describe disturbances other than atmospheric conditions, such as fire, diseases or grazing. Only the additive noise case allows rising variance to be a generic indicator of slowing down (Dakos et al., 2012), although we will show that in our specific model rising variance is also a useful indicator in the multiplicative noise case. In all our simulations we use very small noise levels of $\sigma_V = 0.00013$ or $\sigma_P = 2$.

3.2.2 Performance of Early Warning Signals (EWS) in spatially coupled systems

In the following, we address the limitations of EWS at individual elements in a spatially extended setting. All statistical indicators are calculated from time series of the state variables V_i. Autocorrelations are determined for lag 1, cross-correlations for lag 0.

3.2.2.1 First example: induced tipping

Consider the following simple system (system 1): 2 elements are coupled in a way that the first element can be bistable due to a large local feedback between P and V. Precipitation at the second element depends on vegetation cover at the first element, but not vice versa. We implement this property by choosing the interaction matrix

$$\mathbf{k} = \begin{pmatrix} 300 & 0 \\ 200 & 0 \end{pmatrix}$$

and parameters

$$P_0 = \begin{pmatrix} 0 \\ 100 \end{pmatrix} \qquad s = \begin{pmatrix} 1 \\ 0.1 \end{pmatrix}.$$

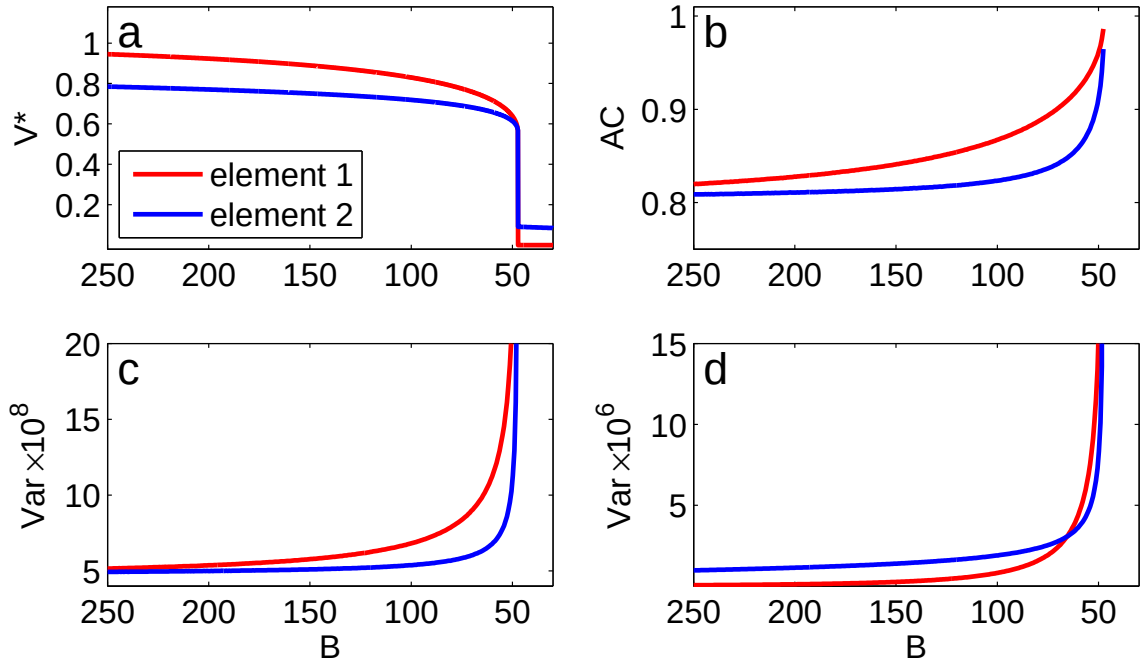

Figure 3.2: Characteristics of system 1 in dependency on parameter B. **(a)** Equilibrium vegetation cover, **(b)** autocorrelation (lag 1), **(c)** variance (additive noise only), **(d)** variance (multiplicative noise only).

As B is reduced, element 2 (blue) collapses in response to the collapse of element 1 (red; Fig. 3.2a). The curves in all our figures are derived from stationary time series. However, if B was very slowly reduced during an experiment, the transient time series of the collapse would follow the equilibrium curves like in Fig. 3.2a very closely because the noise level is small and because the timescales of both elements are identical and small compared to the parameter change. Therefore, it would not be possible to infer the causality of a transition from the timing of the collapses at different elements.

As the collapse of element 2 is induced by element 1 it is not related to a substantial loss of its own stability. It rather experiences the transition as an induced tipping caused by a sudden change in external conditions that are imposed by element 1. The stability of element 2 is hardly affected by B directly as the difference in s_1 and s_2 indicates.

Therefore, element 1 shows a clear increase in autocorrelation (Fig. 3.2b) and variance (Fig. 3.2c) in the additive noise case, but element 2 does not. Only when the noise is multiplicative the system under consideration shows an increased variance (Fig. 3.2d; note that the scale differs from Fig. 3.2c by a factor 100), but results for autocorrelation are similar to the additive noise case. The increase in variance in the multiplicative noise case is specific to the conceptual model and results from the increasing sensitivity of V^* to precipitation changes when P is reduced (Fig. 3.1). In case of a single isolated element without any P-V-feedback ($k = 0$) there would still be an increase in variance in the multiplicative noise case, but not in the additive noise case. In our system 1, the

slowing down at element 1 also affects element 2 due to the interaction term. This is the reason for the rise of the blue curve in Fig. 3.2c.

To obtain sufficiently precise estimates of the statistical properties in Fig. 3.2 we performed stationary time series of 10 million data points each for different values of B. In a transient situation where the sampling error is much larger, the collapse of element 2 would hardly be predictable with EWS.

3.2.2.2 Second example: collective bistability

To pursue this further, we now consider a system (system 2) with a different number of elements, distinguishing versions with 1, 2, 5, 10, and 20 elements, where any particular element has the identical parameters $P_{0_i} = 0$, $s_i = 1$, and $k_{ij} = 300/N$. By dividing the entries of interaction matrix $\mathbf{k}$ by the number of elements in the system, we equally distribute the P-V-feedback over all elements. When more and more elements are coupled, the spatial resolution increases but the bifurcation diagram of this globally coupled system (Fig. 3.3a) does not change. As local feedbacks (determined by k_{ii}) are weak, no single element would be bistable anymore if all other elements were fixed. This fact distinguishes our model from those in Guttal and Jayaprakash (2009), Dakos et al. (2010) and Donangelo et al. (2010), where individually bistable elements are coupled. However, the system as a whole still shows a bifurcation due to the spatial interactions k_{ij} with $i \neq j$.

As we couple more and more elements, it is evident that EWS like rising autocorrelation and variance at individual elements, as well as rising cross-correlation, tend to disappear (Fig. 3.3 b–d). Again, variance in the multiplicative noise case (Fig. 3.3e) is an exception due to the increased slope in $V^*(P)$. The one element-case here (red curves in Fig. 3.3) is identical to element 1 from system 1 (red curves in Fig. 3.2), and also to the system in Fig. 2.1. For EWS to appear properly like in this single element case, the system's time series need to be projected on the critical mode of the transition, a technique introduced as *degenerate fingerprinting* by Held and Kleinen (2004). The critical mode implies the direction in phase space in which the bifurcation occurs. Slowing down particularly occurs for this mode and can be revealed by the appropriate projection. In contrast, other modes of the system's variability are not necessarily influenced by slowing down as the changes of the stability landscape in other directions (characterised by changes of the according eigenvalues) are unrelated to the bifurcation. Hence, EWS in projections on other modes cannot be expected. The analysis of local EWS at individual elements would generally contain information on these other modes of variability and would therefore be a futile strategy. It has to be concluded that if the critical mode of the transition is not known beforehand, the tipping can be unpredictable even in cases of very long time series.

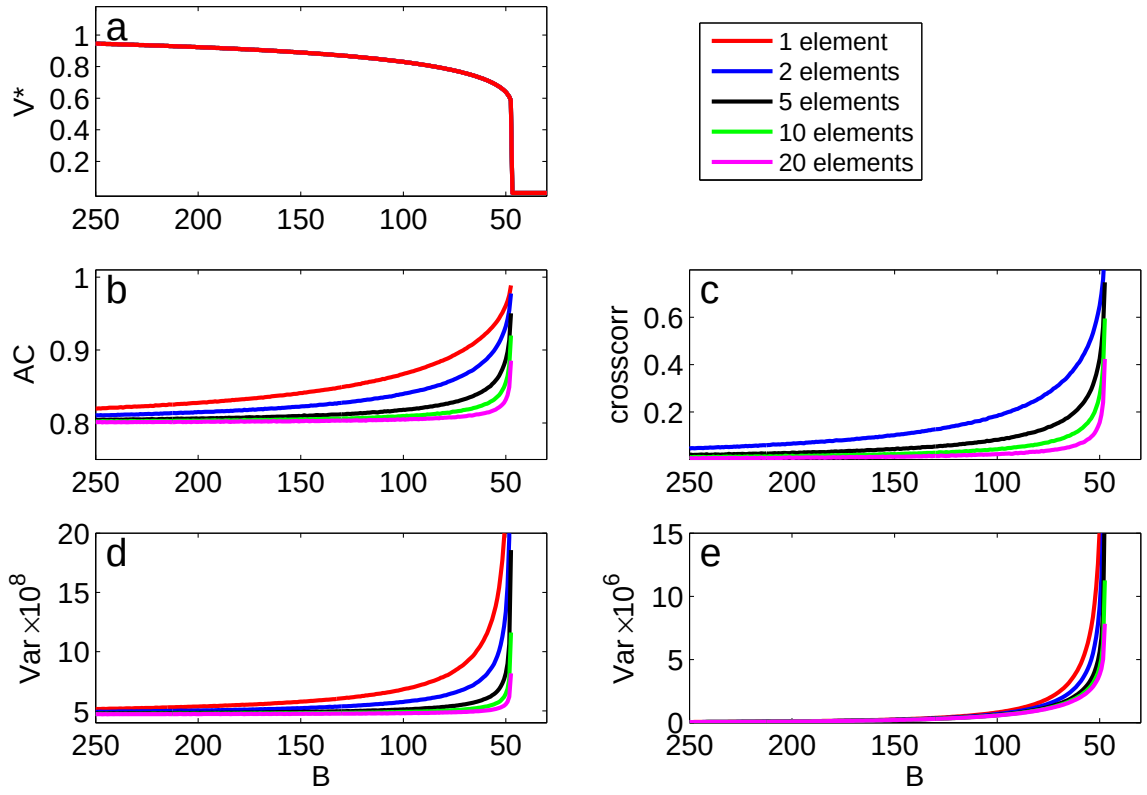

Figure 3.3: Characteristics of system 2 in dependency on parameter B for versions with a different number of elements. **(a)** Equilibrium vegetation cover (identical for any number of elements), **(b)** autocorrelation (lag 1), **(c)** cross-correlation (no lag), **(d)** variance (additive noise only), **(e)** variance (multiplicative noise only). Note that all elements of a specific system are identical and thus have the same measured indicators.

3.2.3 Early Warning Signal – based hotspot detection method

So far we have chosen systems of simple structure. In a more general case like a spatially resolved climate model, the stability structure will be more complicated. Certain subsystems of the climate may show a loss of stability during a change in external forcing while the rest of the system may respond only indirectly, or even evolve independently. In Section 3.2.2 we documented that in multidimensional settings individual elements can fail to show EWS before a sudden transition. While this constitutes a caveat for the prediction of sudden transitions, one may make a virtue out of this caveat by using EWS to diagnostically infer information on the causality of a sudden transition. In terms of system 1, we aim at finding the nucleus of slowing down (hotspot) by distinguishing elements of the red and the blue kind. This is not possible by looking at the system's state directly because red and blue elements collapse in synchrony. Of course, in complex systems there will be a continuum from red to blue and the definition of a threshold in between will be somewhat arbitrary. We expect that the hotspot can be identified as the combination of elements which (when projected on their critical mode) maximises an indicator of slowing down. In the following, we present a scheme for hotspot detection which we apply to our stochastic model.

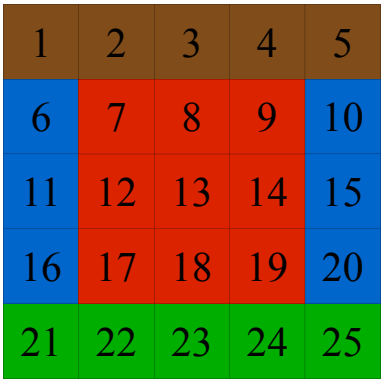

Figure 3.4: Structure of system 3. Red: area with strong P-V-feedback (hotspot), blue: passively dependent on red area, brown: dry area, green: moist area.

3.2.3.1 Highly idealised North African vegetation dynamics

As yet another example of the stochastic model framework in Section 3.2.1, consider 25 elements which can be interpreted as a highly idealised Northern Africa (Fig. 3.4). We refer to this system as system 3. Again we choose parameter values which lead to preconceived properties of the model: 5 of the 25 elements gradually become desert when B is reduced (brown elements). 5 elements stay mostly vegetated (green elements), a set of 9 elements becomes bistable and finally collapses due to a saddle-node bifurcation (red elements) and 6 elements substantially depend on the red ones but show a much weaker local atmosphere-vegetation feedback (blue elements; see Fig. 3.5). Elements with identical colours have identical parameter values and thus have the same state in equilibrium. Hence, there are 4 s_i and P_{0_i} (Table 3.1), and 16 k_{ij} (Table 3.2). In similarity to the examples in Section 3.2.2.2, no element is bistable on its own, as local feedbacks k_{ii} are too small. It is only due to the strong spatial interactions between the red elements that the system can bifurcate and thus show a vegetation collapse at $B \approx 43$.

Table 3.1: Parameters P_{0_i} and s_i in system 3 for four different types of elements. Colours correspond to those in Fig. 3.4.

	red	blue	green	brown
P_0	-50	40	210	40
s	1.7	0.8	0.2	0.9

The nucleus of the transition is the red area because this is where the system loses stability due to strong atmosphere-vegetation interaction. In the following, we refer to the red area as a hotspot.

3.2.3.2 Strategy for the detection of hotspots

We now explain our method of analysis by applying it to system 3. As several modifications of our algorithm are possible, we provide the explanation in two steps:

1. In this section we address the general strategy of our approach. This strategy sets the framework of analysis which is presented in Fig. 3.6 and is the same for all versions of our method. To

Table 3.2: Interaction matrix **k** in system 3, distinguishing four different types of elements. Colours correspond to those in Fig. 3.4. A number in some row A and column B stands for the impact of any single element of type B on any single element of type A (for example: impact of red on blue: 15, impact of blue on red: 5).

	red	blue	green	brown
red	27	5	10	10
blue	15	4	3	3
green	8	2	15	2
brown	2	3	2	5

illustrate our explanation we complement our step by step description with a simple example. This example is referred to at the end of each particular step and presented in Fig. 3.7 and Table 3.3.

2. The framework of analysis presented in this section is too general to cover all technical details as presented in Fig. 3.7 and Table 3.3. These details can differ from case to case. We therefore introduce the different versions of our algorithm together with a discussion of their advantages and disadvantages in Section 3.2.3.3.

In all cases the analysis is applied to J preferably long stationary simulations for fixed but different forcings B_j ($j = 1,2,...,J$) before the bifurcation point. In our example and for all figures which follow we choose time series of vegetation cover for $B_1 = 150$, $B_2 = 90$, $B_3 = 55$, and $B_4 = 43$ (hence $J = 4$; vertical dashed lines in Fig. 3.5). All steps that follow are an analysis of these time series and do not involve the model which generated them. We describe the individual steps of the analysis by starting with part B in Fig. 3.6, as this part of the analysis corresponds to the original degenerate fingerprinting by Held and Kleinen (2004), without time aggregation.

B1. For a given part of the system with N_p elements, we select a subset of n elements from these N_p elements. We refer to this subset as an area. Hence, there are three levels of selected elements where each set is a subset of the previous one: The number of elements in the complete system (N; here: 25), the number of elements in a part of the system (N_p), and the number of elements in an area of this part (n). Example: We choose elements 19, 20 and 25 as a part. Hence, $N_\mathrm{p} = 3$, and n can be 1 (3 possible combinations), 2 (3 possible combinations) or 3 (1 possible combination).

B2. For the n selected elements we calculate the leading empirical orthogonal function (EOF; eigenvector of the covariance or correlation matrix which represents the largest variance). To construct the EOFs we use the freely-available linear algebra package LAPACK. In our example, there are 7 combinations of the 3 elements (top left corner of panels in Fig. 3.7). The 3 cases with single elements are trivial and each EOF is 1. The 3 cases with 2 elements are also trivial ($\sqrt{1/2}, \sqrt{1/2}$) because the (symmetric) correlation matrix contains ones on its main diagonal.

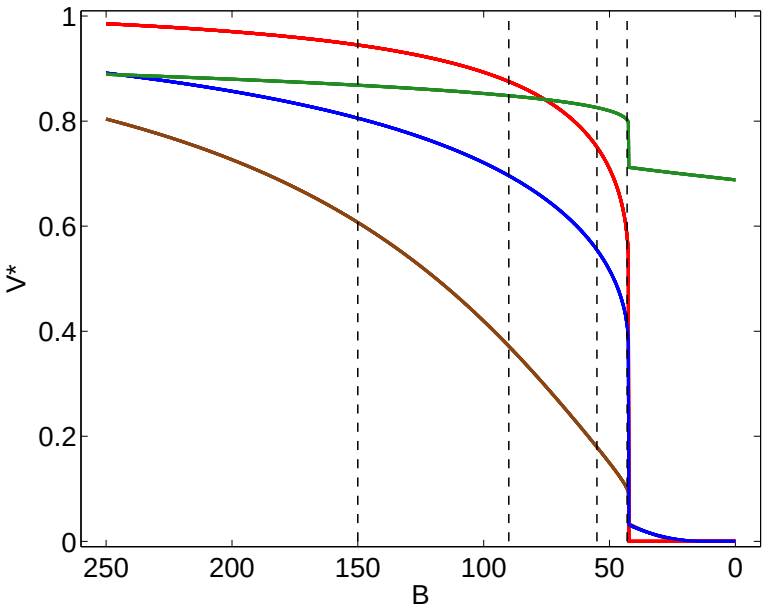

Figure 3.5: Equilibrium vegetation cover at different elements of system 3 and for different bifurcation parameter values B. The colours correspond to the elements in Fig. 3.4. The vertical black dashed lines indicate the values of B used for the four stationary simulations (the smallest one also lying above the tipping point). They correspond to BV1 in Table 3.4 and are used for Figs. 3.7–3.11 and Table 3.3.

B3. In the general case, we calculate the leading EOF for all time slices B_j from $j = 2$ to J. For every EOF_j, we project all time slices from B_1 to B_j on EOF_j. Special cases: The projection of time series B_j on EOF_j is the principal component of EOF_j. In case of areas consisting of one single element, the projections are identical with the time series themselves. The standard version of our algorithm only involves projections on EOF_J (see Section 3.2.3.3). In our example, there are therefore 4 projections for each area (small panels in Fig. 3.7).

B4. We calculate a statistical property like autocorrelation or variance of the corresponding projections to use it as an EWS. For all projections on some EOF_j the result is a curve of this EWS versus B, just like those in Figs. 3.2b–d and 3.3b–e, but less well resolved (j points only). In our example, we use $J = 4$ and autocorrelation as EWS, hence there are 4 values of AC for each of the 7 areas, shown as a line plot in each panel of Fig. 3.7.

To automatically compare the results for different areas, we expand this degenerate fingerprinting method with the following steps:

B5 As it is not the absolute value of a statistical property but its increase which indicates slowing down, we shift the curve vertically in order to be 0 at $j = 1$. Fig. 3.7 (bottom right) shows the shifted AC-curves of all 7 areas of our example.

B6 Based on the aligned curves we define a *signal* which is one number to quantify the strength of an indicator and to compare different areas. The definition of the signal can differ, but it always involves all time slices. We do so to take into account not only the difference between the first and last B, but the whole evolution of an EWS vs. B as is suggested by our results in Fig. 3.2. Table 3.3 gives an example of all areas and their associated signals for the part consisting of elements 19, 20, and 25.

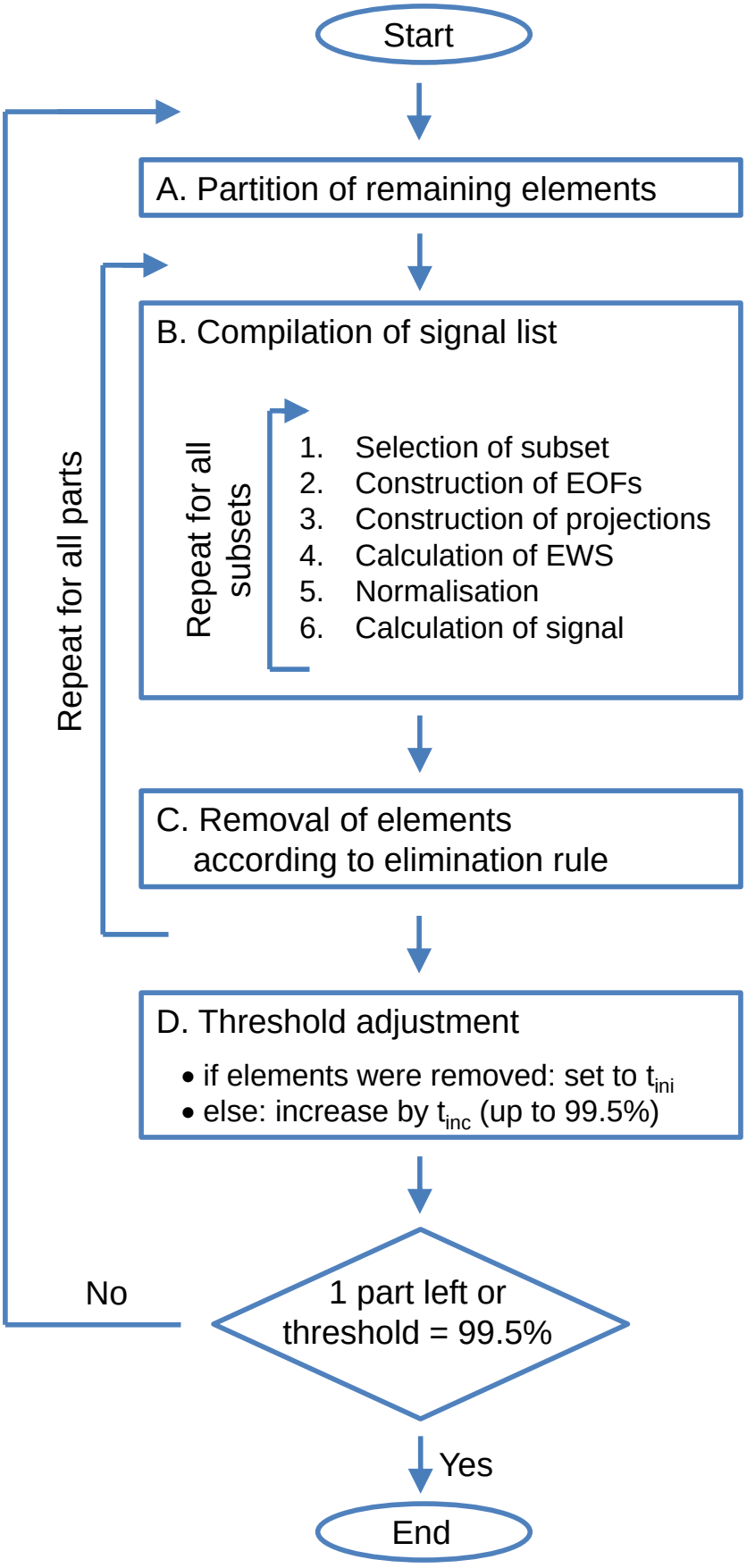

Figure 3.6: General flowchart of the hotspot detection scheme.

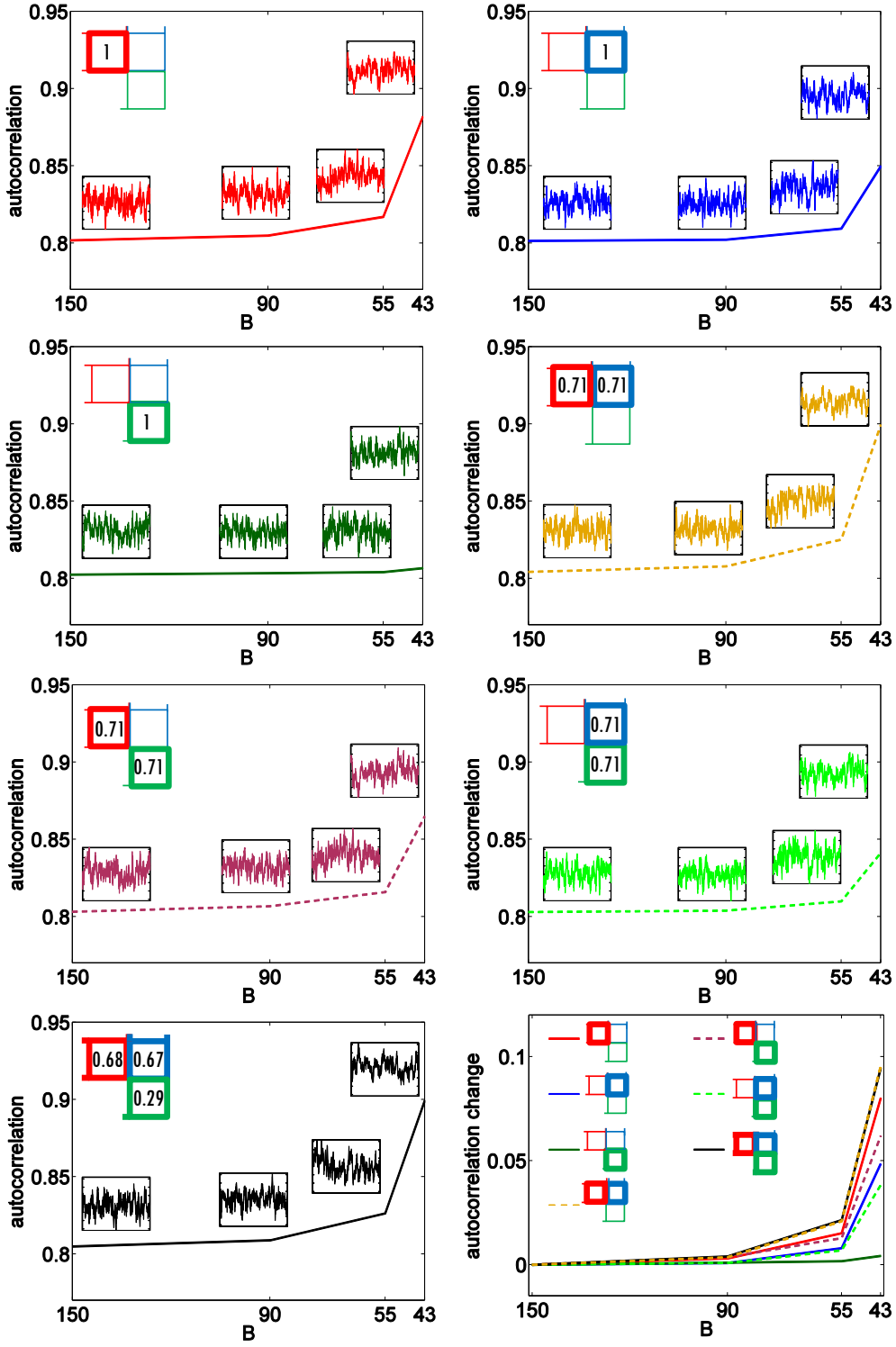

Figure 3.7: Example to illustrate the hotspot detection scheme using elements 19, 20, and 25 of system 3. All panels except bottom right: In each top left corner the particular area is highlighted by bold lines. The numbers inside the elements give the eigenvectors of the correlation matrix (EOF) for $B = 43$. All four time slices (forcings BV1 as in Fig. 3.5) are projected on this EOF. The four time series in each panel show a chunk of 500 yrs from these projections (normed to standard deviation 1 and mean 0). The autocorrelation at lag 1 for each projection is depicted as a line plot in dependency on B. Bottom right: all seven curves are shifted to 0 at $B = 150$ in order to compare the signals of the areas. Parameter settings correspond to set 1 in Table 3.4.

Table 3.3: Example signal list for elements 19, 20 and 25 in system 3. Parameter settings correspond to set 1 in Table 3.4.

area	signal × 1000
19	9.1611
20	4.8099
19, 20	11.5094
25	1.0391
19, 25	7.8746
20, 25	4.0192
19, 20, 25	11.7716
weights (19,20,25):	40.32, 32.11, 24.70

We repeat steps B1–6 for all possible combinations of elements. If the N_p elements mentioned in step 1 represent the whole system under consideration ($N_p = N$), one can then determine the area with the maximum signal, or the areas with a signal above a certain threshold. However, this requires the calculation of 2^N-1 such signals (not 2^N because selecting 0 elements is not an option). This becomes unfeasible already for N beyond 10. Therefore, not all possible combinations can be calculated and we use an iterative selection process to decide which elements can be dropped from the analysis:

A. We randomly divide the whole system into a number of non-overlapping parts. The number of parts is calculated from the fixed parameter n_{max} via the ceiling function $\lceil \frac{N}{n_{max}} \rceil$. The number of parts is thus as small as possible for a given n_{max}. The size of each part is then determined by distributing the N elements as equally as possible, so that each N_p fulfills $2 <= N_p <= n_{max}$.

B. For each part, steps 1–6 are applied. As an example, imagine that system 3 is analysed with $n_{max} = 3$. Hence, the system is subdivided into 9 parts, of which 7 parts contain 3 elements, and 2 parts contain 2 elements.

C. From a *signal list* like Table 3.3 the contribution of different elements can be disentangled, with the aim to drop unimportant elements from the analysis completely. The removal of an element means that it is not considered to be part of the system anymore and is not used from that point on. In this sense, the total system size N successively decreases and with it the number of parts is also reduced automatically.

   In principle, our selection process resembles the logic of a football world cup: each team (element) does not compete directly against every other team, but only against those of the same group (part). Only teams performing well enough in their group remain in the tournament.

The best rules of how to remove an element can depend on the system and will be discussed under the term *elimination rule* (ER) in Section 3.2.3.3.

D. As a criterion for removing elements we set a threshold which is adjusted interactively to prevent that too many elements are removed at once and too early. The threshold is a relative number in % and relates to different things depending on the elimination rule. In our example as well as all following figures we set the initial threshold t_{ini} to 5 %. As long as no element can be removed in any part, we increase the threshold by $t_{\mathrm{inc}} = 5\,\%$. If the threshold would reach or exceeded 100 %, we set the threshold to 99.5 %. If at least one element can be removed we reset the threshold to its initial value t_{ini}. In both cases, we then partition the remaining elements anew, starting from step A (large loop in Fig. 3.6).

This way, the considered number of elements is gradually reduced. After each calculation of the signals in all possible areas of all current parts and the potential removal of elements the procedure is repeated. It ends as soon as one of the following conditions is true: (1) the total number of remaining elements is not larger than $n_{\max}$, in which case the analysis is repeated one last time with one part only. (2) The relative threshold reaches 99.5 %, but still no elements can be removed because the remaining elements are too similar to be discriminated.

The algorithm serves as a sieve in order to filter out the important elements with a sufficiently small number of calculations. Without the removal of elements, the number of possible combinations would be too large to achieve a robust hotspot detection within a feasible amount of time. As the results depend on the random distribution of elements to different parts, they will be very similar but not completely identical when the analysis is repeated. The hotspot of slowing down can be identified if the time series are long enough (or if enough realisations are available) because the remaining elements at the end of the analysis tend to contribute most to slowing down.

To obtain more quantitative results, all signals calculated during the procedure can be collected in a sorted list for further analysis. Elements belonging to the hotspot tend to be part of the areas with the strongest signals and are on top of the list. However, elements that have been removed early during the analysis are not well sampled. The method therefore only provides information on the nature of the hotspot, but less on the stability properties of the rest of the system.

3.2.3.3 Parameter options and performance analysis

It has become obvious in the previous sections that the algorithm involves a number of options and parameter values which have to be chosen in advance. Also, the performance of the method will depend on properties of the original time series. For a quantitative comparison of the algorithm's performance under different conditions (parameter settings, choice of algorithm and time series properties), we perform 500 Monte Carlo experiments for each condition (Table 3.4).

In each experiment a new realisation of the time series is generated with system 3 and then analysed with the hotspot detection algorithm. Figure 3.8 shows how often each element remains until the end of each experiment for the additive noise case and a time series length of 2000 yrs.

Table 3.4: Performances of the hotspot detection algorithm for different sets of versions, parameter choices and time series properties. SD = signal definition, ER = elimination rule, BV = vector of forcings B_j. Performances are calculated from fractions f_1, italic results in parenthesis from f_2 (Section 3.2.3.3).

	parameters for hotspot detection							time series properties						
Set	EWS	SD	ER	EOF	n_{max}	t_{ini}	t_{inc}	BV	τ	noise	T=1000	T=2000	T=5000	T=10000
1	AC	1	1	corr.	5	5%	5%	BV1	5	add.	0.16 (*0.22*)	0.27 (*0.33*)	0.41 (*0.50*)	0.56 (*0.69*)
2	AC	1	1	covar.	5	5%	5%	BV1	5	add.	0.13 (*0.19*)	0.24 (*0.30*)	0.43 (*0.54*)	0.54 (*0.68*)
3	AC	1	1	corr.	5	5%	5%	BV1	2.5	add.	0.29 (*0.36*)	0.40 (*0.48*)	0.55 (*0.70*)	0.66 (*0.84*)
4	AC	1	1	corr.	3	5%	5%	BV1	5	add.	0.19 (*0.22*)	0.29 (*0.34*)	0.44 (*0.51*)	0.58 (*0.67*)
5	AC	1	1	corr.	7	5%	5%	BV1	5	add.	0.13 (*0.18*)	0.24 (*0.31*)	0.39 (*0.49*)	0.49 (*0.60*)
6	AC	1	1	corr.	5	5%	5%	BV2	5	add.	0.10 (*0.13*)	0.13 (*0.18*)	0.23 (*0.30*)	0.37 (*0.46*)
7	AC	1	1	corr.	5	5%	5%	BV3	5	add.	0.04 (*0.08*)	0.12 (*0.16*)	0.21 (*0.27*)	0.36 (*0.43*)
8	AC	1	1	corr.	5	5%	1%	BV1	5	add.	0.18 (*0.19*)	0.28 (*0.30*)	0.45 (*0.47*)	0.63 (*0.67*)
9	AC	1	1	corr.	5	5%	2,5%	BV1	5	add.	0.17 (*0.20*)	0.28 (*0.32*)	0.46 (*0.51*)	0.62 (*0.69*)
10	AC	1	1	corr.	5	5%	7,5%	BV1	5	add.	0.17 (*0.24*)	0.22 (*0.31*)	0.40 (*0.51*)	0.49 (*0.68*)
11	AC	1	1	corr.	5	5%	10%	BV1	5	add.	0.13 (*0.23*)	0.20 (*0.31*)	0.37 (*0.53*)	0.47 (*0.70*)
12	AC	1	1	corr.	5	5%	12,5%	BV1	5	add.	0.12 (*0.23*)	0.21 (*0.35*)	0.32 (*0.52*)	0.44 (*0.67*)
13	AC	1	1	corr.	5	5%	15%	BV1	5	add.	0.08 (*0.23*)	0.21 (*0.37*)	0.28 (*0.56*)	0.37 (*0.70*)
14	AC	1	1	corr.	5	5%	17,5%	BV1	5	add.	0.08 (*0.24*)	0.17 (*0.37*)	0.30 (*0.54*)	0.41 (*0.67*)
15	AC	1	1	corr.	5	5%	20%	BV1	5	add.	0.11 (*0.27*)	0.19 (*0.37*)	0.30 (*0.54*)	0.27 (*0.69*)
16	AC	1	1	corr.	5	5%	30%	BV1	5	add.	-0.01 (*0.27*)	0.11 (*0.42*)	0.26 (*0.54*)	0.36 (*0.68*)
17	AC	1	1	corr.	5	5%	40%	BV1	5	add.	0.11 (*0.28*)	0.21 (*0.39*)	0.28 (*0.54*)	0.30 (*0.68*)
18	AC	1	1	corr.	5	5%	50%	BV1	5	add.	-0.08 (*0.31*)	0.05 (*0.39*)	0.27 (*0.51*)	0.44 (*0.59*)
19	AC	1	1	corr.	5	5%	100%	BV1	5	add.	0.10 (*0.27*)	0.23 (*0.33*)	0.37 (*0.47*)	0.46 (*0.54*)
20	AC	1	1	corr.	5	80%	5%	BV1	5	add.	0.12 (*0.27*)	0.25 (*0.39*)	0.41 (*0.53*)	0.56 (*0.69*)
21	AC	2	2	covar.	5	5%	5%	BV1	5	mult.	0.60 (*0.62*)	0.66 (*0.66*)	0.87 (*0.84*)	1.10 (*0.94*)
22	AC	1	1	covar.	5	5%	5%	BV1	5	mult.	0.29 (*0.36*)	0.44 (*0.53*)	0.61 (*0.71*)	0.74 (*0.87*)

Table 3.4: Continued.

	parameters for hotspot detection							time series properties						
Set	EWS	SD	ER	EOF	n_{max}	t_{ini}	t_{inc}	BV	τ	noise	T=1000	T=2000	T=5000	T=10000
23	AC	2	2	corr.	5	5%	5%	BV1	5	mult.	0.43 (*0.46*)	0.50 (*0.53*)	0.70 (*0.64*)	0.95 (*0.70*)
24	AC	1	1	corr.	5	5%	5%	BV1	5	mult.	0.31 (*0.38*)	0.40 (*0.48*)	0.56 (*0.65*)	0.67 (*0.81*)
25	AC	2	2	covar.	5	5%	5%	BV2	5	mult.	0.57 (*0.62*)	0.64 (*0.66*)	0.71 (*0.71*)	0.82 (*0.79*)
26	AC	2	2	covar.	5	5%	5%	BV3	5	mult.	0.68 (*0.69*)	0.74 (*0.75*)	0.87 (*0.85*)	1.09 (*0.96*)
27	AC	2	2	covar.	5	5%	5%	BV1	2.5	mult.	0.64 (*0.67*)	0.79 (*0.79*)	1.12 (*0.94*)	1.63 (*0.99*)
28	var	1	1	corr.	5	5%	5%	BV1	5	add.	0.28 (*0.33*)	0.43 (*0.51*)	0.60 (*0.74*)	0.67 (*0.86*)
29	var	1	1	covar.	5	5%	5%	BV1	5	add.	0.29 (*0.36*)	0.42 (*0.51*)	0.62 (*0.75*)	0.71 (*0.87*)
30	var	1	1	corr.	5	5%	5%	BV1	2.5	add.	0.38 (*0.45*)	0.53 (*0.63*)	0.67 (*0.83*)	0.73 (*0.94*)
31	var	1	1	corr.	5	5%	1%	BV1	5	add.	0.31 (*0.33*)	0.48 (*0.50*)	0.69 (*0.72*)	0.81 (*0.85*)
32	var	1	1	corr.	5	5%	2,5%	BV1	5	add.	0.32 (*0.35*)	0.45 (*0.50*)	0.64 (*0.71*)	0.76 (*0.86*)
33	var	1	1	corr.	5	5%	7,5%	BV1	5	add.	0.27 (*0.36*)	0.41 (*0.51*)	0.57 (*0.73*)	0.62 (*0.87*)
34	var	1	1	corr.	5	5%	10%	BV1	5	add.	0.28 (*0.39*)	0.41 (*0.56*)	0.51 (*0.74*)	0.59 (*0.86*)
35	var	1	1	corr.	5	5%	12,5%	BV1	5	add.	0.22 (*0.36*)	0.35 (*0.55*)	0.48 (*0.74*)	0.60 (*0.88*)
36	var	1	1	corr.	5	5%	15%	BV1	5	add.	0.20 (*0.38*)	0.31 (*0.55*)	0.42 (*0.75*)	0.54 (*0.87*)
37	var	1	1	corr.	5	5%	17,5%	BV1	5	add.	0.19 (*0.38*)	0.28 (*0.57*)	0.45 (*0.74*)	0.56 (*0.86*)
38	var	1	1	corr.	5	5%	20%	BV1	5	add.	0.25 (*0.43*)	0.33 (*0.56*)	0.34 (*0.75*)	0.23 (*0.88*)
39	var	1	1	corr.	5	5%	30%	BV1	5	add.	0.10 (*0.42*)	0.21 (*0.51*)	0.42 (*0.74*)	0.50 (*0.85*)
40	var	1	1	corr.	5	5%	40%	BV1	5	add.	0.20 (*0.39*)	0.30 (*0.54*)	0.33 (*0.74*)	0.27 (*0.88*)
41	var	1	1	corr.	5	5%	50%	BV1	5	add.	0.06 (*0.43*)	0.24 (*0.51*)	0.45 (*0.65*)	0.54 (*0.71*)
42	var	1	1	corr.	5	5%	100%	BV1	5	add.	0.22 (*0.35*)	0.36 (*0.45*)	0.49 (*0.59*)	0.57 (*0.70*)
43	var	1	1	corr.	5	80%	5%	BV1	5	add.	0.27 (*0.43*)	0.41 (*0.55*)	0.60 (*0.74*)	0.69 (*0.87*)
44	var	2	2	covar.	5	5%	5%	BV1	5	mult.	1.70 (*1.00*)	2.04 (*1.00*)	2.22 (*1.00*)	2.25 (*1.00*)
45	var	1	1	covar.	5	5%	5%	BV1	5	mult.	0.68 (*1.00*)	0.53 (*1.00*)	0.32 (*1.00*)	0.37 (*1.00*)
46	var	2	2	corr.	5	5%	5%	BV1	5	mult.	1.59 (*1.00*)	1.99 (*1.00*)	2.21 (*1.00*)	2.25 (*1.00*)
47	var	1	1	corr.	5	5%	5%	BV1	5	mult.	0.69 (*1.00*)	0.50 (*1.00*)	0.31 (*1.00*)	0.36 (*1.00*)

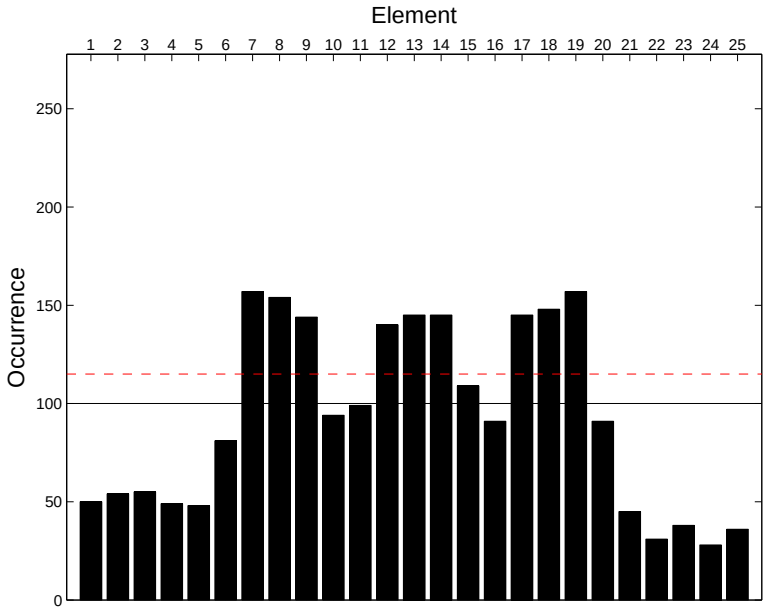

Figure 3.8: Performance of the hotspot detection algorithm for system 3 with additive noise using time series of 2000 yrs. The frequencies show the number of times a particular element remains until the end of the selection process for 500 repetitions. Each repetition involves the generation of a new time series and its analysis with the hotspot detection algorithm. The solid black line marks the expectation value for a random selection where all elements are selected with equal probability. The red dashed line marks the 95% probability threshold of the corresponding cumulative binomial distribution. Parameter settings correspond to set 1 in Table 3.4.

After the 500 repetitions we evaluate which fraction f_1 of the $500 \times n_{\max}$ potentially identified elements belongs to the hotspot, and which fraction f_2 of the actually obtained elements belongs to the hotspot. f_1 and f_2 can differ because it is not always $n_{\max}$ elements that remain in the end.

As a measure of the method's performance η we define for both variants of f:

$$\eta_{1,2} = (f_{1,2} - \frac{H}{N})/(1 - \frac{H}{N}), \tag{3.4}$$

with N as the size of the system (25) and H as the size of the hotspot (9). If we assume that all 25 elements have an equal chance to be selected, the probability for any obtained element to be part of the hotspot is $H/N = 9/25$. A detection which does not differ from this random case has performance 0.

If exactly $n_{\max}$ elements are returned in every experiment, a detection which only returns hotspot elements has performance 1 for both variants of f (which is of course only possible because we choose an $n_{\max}$ smaller than the hotspot). The expectation value for the occurrence of every element would be 100 in case of performance 0 (the solid black line in Fig. 3.8), and $500 \times 5/9$ in case of performance 1 (end of vertical scale in Fig. 3.8). Potential deviations from $n_{\max}$ elements in the output can lead to performances lower than 0 and larger than 1 if we apply f_1.

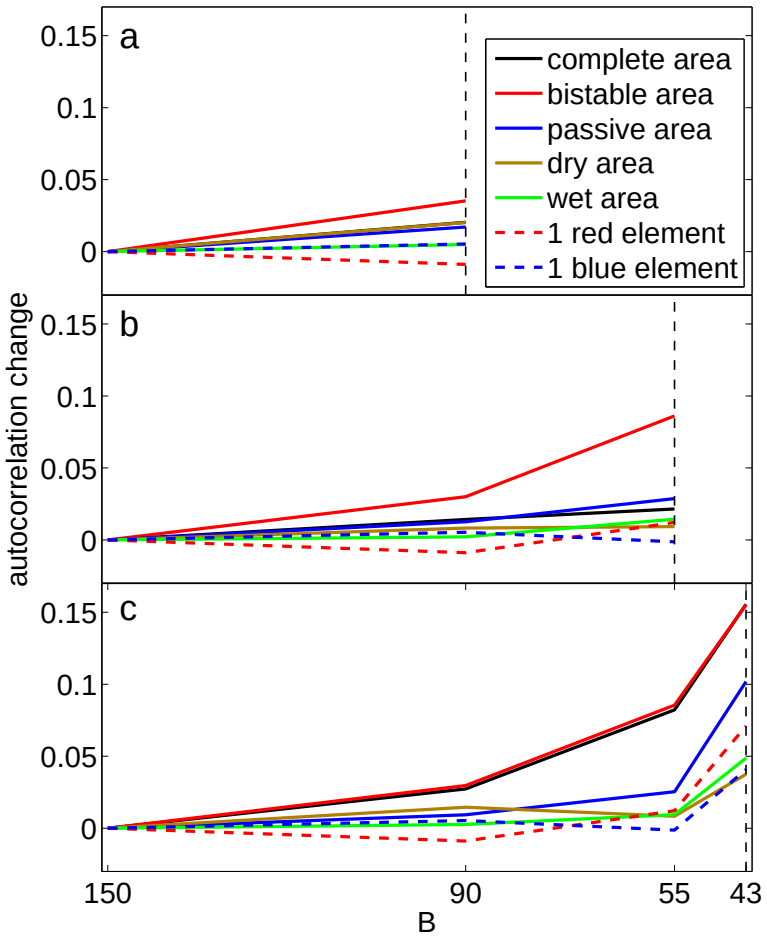

Figure 3.9: Autocorrelation changes of projections on leading EOFs for system 3 with multiplicative noise. The leading EOFs have been calculated for (a) $B_2 = 90$, (b) $B_3 = 55$, (c) $B_4 = 43$. In each case, all previous time series (including the one used for the EOF) are projected on the according EOF. The analysis is applied to the full system (black) as well as only parts of the system (other colours). The colours correspond to the elements in Fig. 3.4. Parameter settings correspond to set 21 in Table 3.4.

The decision for 500 repetitions can be justified by bootstrapping our Monte Carlo results (Efron, 1979): for any list of 500 sets of residual elements we draw n sets and measure their performances. We calculate the standard deviation of the obtained performances for many different n. It turns out that for 500 repetitions the standard deviation is approx. 0.015 and rather independent of the parameter and time series properties. Therefore, we round all performances in Table 3.4 to 2 decimal places. Above 500 repetitions, the uncertainty of the performance decreases very slowly while the computation time for the Monte Carlo experiments increases beyond feasibility.

From theoretical considerations, the performances in Table 3.4 as well as the qualitative appearance of the resulting signal lists we draw the following conclusions with regard to different parameter choices and time series properties:

- Different **EWS** can be used within the same framework. Here, we use the increase in autocorrelation (AC) and the relative increase in variance (var). Relative increases in variance usually show better performances because of a larger signal-to-noise ratio, in agreement with Ditlevsen and Johnsen (2010). However, AC is the more generic EWS and also works if multiplicative noise leads to a reduction in variance (Dakos et al., 2012). For Figs. 3.7–3.11 and Table 3.3 we use AC as an EWS.

- We distinguish two **signal definitions** (SD). The most simple approach is to only use the projections on the EOF of the last time slice (B_4 in our example). The analysis is based on the assumption that this pattern resembles the critical mode, if the selected area is the hotspot. We then integrate the EWS-curve over B (calculate the area of the $J-1$ segments). We refer to this signal definition as SD1. SD1 is used in our example Fig. 3.7 and Table 3.3.

  An alternative (referred to as SD2) is to also consider projections on previous EOFs. This approach can add information if the leading EOF smoothly approaches the critical mode when B approaches the Tipping Point. We thus obtain $J-1$ curves of an EWS vs. B (Fig. 3.9). To calculate the signal for a specific area, we perform a double integration. In terms of Fig. 3.9: first, we calculate the area under a curve with a certain colour for $\text{EOF}_{B=90}$ (Fig. 3.9a), $\text{EOF}_{B=55}$ (Fig. 3.9b), and $\text{EOF}_{B=43}$ (Fig. 3.9c). The resulting trajectory of integrated EWS is then again integrated over B. This way, not only the shape of the projection on the last EOF is accounted for, but also the shape of previous projections.

- The choice of an **elimination rule** (ER) should be adapted to the signal definition. Again, we distinguish two elimination rules, ER1 and ER2. For SD1 we use ER1, which works as follows: For each specific element, we add up the signals of all areas this element is part of (last row, second column in Table 3.3), and refer to it as the element's *weight*. The threshold to remove unimportant elements is defined relative to the maximum weight of all elements in a specific part. The absolute value of the threshold therefore depends on the maximum weight and differs among the system's parts, while the relative threshold is a parameter that is independent of the parts. For example, a threshold of 70 % means that all elements with a weight smaller than 70 % of the maximum weight are removed. In our example (Fig. 3.7 and Table 3.3), element 19 belongs to the hotspot, so it contributes more to the signal than elements 20 and 25, whose weight is therefore smaller. Element 25 has a particularly small weight (24.70) as it neither belongs to the hotspot nor is it much affected by it. Its relative weight compared to the maximum weight of 40.32 is below 70 %. It would therefore be removed from the analysis if the threshold is above 70 %.

  For SD2 we use a simpler approach, referred to as ER2: We divide the signal list in the set of signals above the current threshold and the set of signals below this threshold. All elements which are part of any area above the threshold remain, the other elements are removed. Hence, the threshold is directly applied to the signals itself without the calculation of weights. This measure allows a better discrimination of the elements. In the additive noise case it cannot be applied because there the maximum signal usually belongs to the complete area.

- **EOFs** can be calculated as an eigenvector of the system's covariance matrix or alternatively its correlation matrix. If based on the covariance matrix, elements with large variance will be emphasised. Whether this improves the performance of a hotspot detection generally depends on the system under analysis. In case of system 3 with multiplicative noise, variance

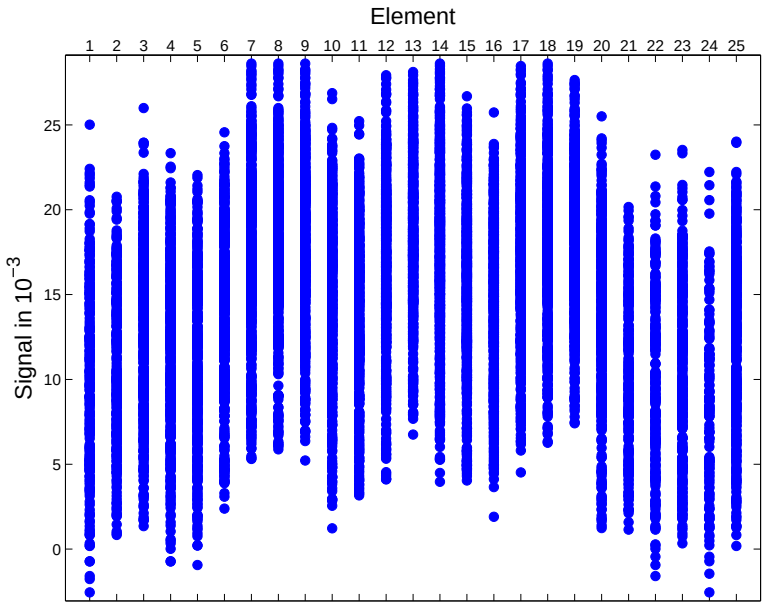

Figure 3.10: Signal list for system 3 with additive noise using time series of 100 000 yrs. Ordinate: absolute signal; abscissa: elements of the system. Any area that has been calculated during the analysis is represented at the ordinate value of its signal. All elements that are part of this area are marked as blue dots. Parameter settings correspond to set 1 in Table 3.4.

is enhanced particularly at the hotspot when B approaches the bifurcation point. Therefore, SD2 with ER2 yield the most significant results when using covariance-based EOFs.

In general, other signal definitions and elimination rules could be devised that may be tailored to a specific system.

The most generic approach is to use SD1 in combination with ER1, correlation-based EOFs and autocorrelation as EWS. The last EOF (the only one used in SD1) must resemble the critical mode in any system approaching a bifurcation (although it can be difficult to come very close to the edge of the Tipping Point in practice). In the case of additive noise, considering previous EOFs like in SD2 may not improve the signal-to-noise ratio because the signal is much weaker away from the Tipping Point. This is of particular importance if the curves of EWS vs. B do not differ substantially between different EOFs. Furthermore, autocorrelations and correlations are more generic indicators while variances can be affected by multiplicative noise in any way. When analysing a system whose variability is of unknown nature, the generic approach is thus probably the most adequate choice. Fig. 3.10 shows the resulting signal list when using time series of length 100.000 yrs and such generic options (referred to as set 1 in Table 3.4).

Although these options should be applicable to many systems, they may not lead to the most robust results. In system 3 with multiplicative noise, SD2 and ER2 in combination with covariance-based EOFs are of particular advantage. Fig. 3.11 shows the signal list for the multiplicative noise case when using time series of length 10.000 yrs and options as set 21 in Table 3.4. While for the additive noise case the AC's trajectories at the hotspot (red area) and the complete area always look alike (not shown), they differ substantially in the multiplicative case: At the hotspot the signal starts to emerge early, even when projecting on a leading EOF far from the Tipping Point (red curves in Fig. 3.9). This is not the case for the other areas because the variability of the system differs substantially from the critical mode. As variances at the hotspot are very small,

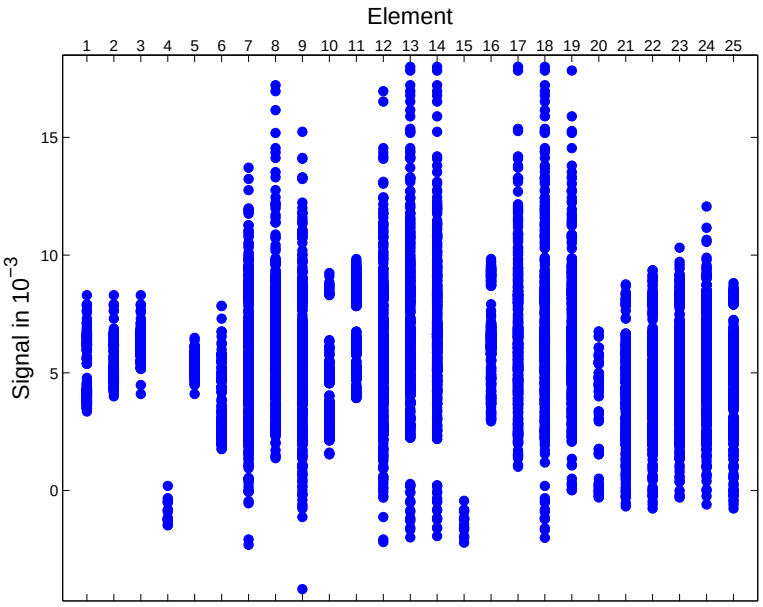

Figure 3.11: Signal list for system 3 with multiplicative noise using time series of 10 000 yrs. Ordinate: absolute signal; abscissa: elements of the system. Any area that has been calculated during the analysis is represented at the ordinate value of its signal. All elements that are part of this area are marked as blue dots. Parameter settings correspond to set 21 in Table 3.4.

the EOF pronounces other elements than the hotspot and slowing down will thus not be observed in the projection. Close to the Tipping Point, the variance at the hotspot increases not only due to slowing down, but also due to the multiplicative noise which enhances variance as vegetation cover decreases. Therefore, the relative increase in variance is particularly large at the hotspot. Close to the Tipping Point, the system's variability becomes dominated by the critical mode and slowing down can be seen in the complete as well as the hotspot area. By using SD2, ER2 and covariance-based EOFs we use this property of the system to better distinguish the elements from each other. As a result, the hotspot can be detected much easier than in the additive noise case. Using time series of 10 000 yrs each, the hotspot is clearly visible in the signal list for $n_{\max} = 5$ (Fig. 3.11). Hence, an even more robust hotspot detection can be achieved from time series ten times shorter than in the additive noise case.

In a more general case, additive and multiplicative noise may occur at the same time. In our system 3, the multiplicative noise would dominate the results if noise levels leading to similar variance in V were chosen. However, it is not a priori clear what would happen in other systems whose properties are not well-known. Under such conditions the generic approach using cross- and autocorrelations with SD1 and ER1 would be the safest option in the light of our results.

We now continue with our list of conditions:

- The choice of **time slices** should cover a range of B where the changes in steady state are already pronounced to achieve a good signal-to-noise ratio. In Table 3.4 we distinguish three different vectors of B-values:
  BV1: (150, 90, 55, 43),
  BV2: (300, 200, 100, 75, 43),
  BV3: (150, 90, 55).
  For Figs. 3.7–3.11 and Table 3.3 we use BV1 (dashed vertical lines in Fig. 3.5).

- The **initial threshold**, t_{ini}, **and increment**, t_{inc}, should be chosen small (a few percent of the maximum signal). If they are larger, the calculation is faster and not necessarily worse in performance, but the signal list will not be well sampled. A better sampling of each element's contribution to the signal allows a clearer discrimination between the elements in figures like Figs. 3.10 and 3.11. Particularly low η_1 for some larger t_{inc} result from the effect that too many elements are removed at once after increasing the threshold.

- The **maximum number of elements per part**, $n_{\max}$, can be chosen small for first results. The smaller $n_{\max}$, the faster the algorithm. When repeating the analysis with larger $n_{\max}$, the signal list gives an indication of the size of the hotspot (or hotspots). As long as the maximum signal in the list clearly increases with $n_{\max}$, the number of elements which form a common hotspot is larger than $n_{\max}$. As Figs. 3.10 and 3.11 document, the full hotspot may already be identified for $n_{\max}$ smaller than the hotspot, if t_{ini} and t_{inc} are small to allow a robustly sampled signal list.

- The **length of the time series**, T, as compared to the key variable's timescale τ has a major influence on the method's performance. As the time series provide only a limited sample, the performance will increase with T. If a single available realisation of the time series is too short, the statistical properties of the variations are insufficiently sampled and a hotspot detection can yield wrong results. It should therefore be checked whether the identified hotspot is robust to T by comparing different parts of the time series. Methods of block bootstrapping suited for time series (Politis, 2003) could in principle be applied to the full analysis to derive uncertainty estimates.

- The detectability of a hotspot, given a specific length of the time series, very much depends on intrinsic system properties like its **connectivity and the strength of the destabilising feedback**. The more elements contribute to a hotspot, the more difficult it is to detect. n_{max} should be chosen large in such a case to determine the large extent of the hotspot which slows down the algorithm. More importantly, the stronger the slowing down and the better the elements can be distinguished, the easier the hotspot detection. Our system 3 may already provide a rather demanding case as several 10 000–100 000 yr long time slices are required for a robust hotspot detection. This time is rather beyond feasibility for climate models of intermediate or high complexity and a hotspot like in system 3 would hardly be detectable. However, if hotspots of a more pronounced structure exist, they could be detected more easily. As an example, consider the most optimistic case of an univariate process where autocorrelation increases substantially over time. This increase would be detectable within the order of some 100 time steps (Ditlevsen and Johnsen, 2010). Part II of our two-part paper presents a hotspot detection from climate model time series of hundreds to thousands of years length as another example. It is therefore not possible to provide a general statement on the required length of time series. The required length depends on the nature of the potential hotspot, the exact thing that one aims to infer with the analysis.

However, this problem does not impose any restrictions to the applicability of the method, but it implies that a negative result can either be due to the non-existence of slowing down at a hotspot or to too short time series.

3.2.4 Summary and conclusions

By applying a simple stochastic model we have demonstrated that EWS at individual elements of a coupled system are no generic precursors of a sudden transition at a Tipping Point. If the local feedback of a particular element is weak or if the element's tipping is induced by other elements, EWS are not apparent until the bifurcation parameter is very close to its critical point. In this case the signal cannot be called early anymore, and a prediction of a sudden transition, together with the area where it will occur, must fail. On the other hand, we have documented that indicators of slowing down can potentially be used to infer knowledge on the causality of a sudden transition from sufficiently long time series. To this end, we have devised an algorithm to detect the hotspot or hotspots of slowing down in a many-element system. As slowing down indicates a loss in stability of the current state, the detected hotspot indicates a region where the system's susceptibility to perturbations becomes large.

Although our system is meant to represent the vegetation-atmosphere interaction in Northern Africa, the method of analysis is generic in the sense that it can be applied to any system satisfying the basic assumptions common to EWS approaches:

- The system is supposed to be close to a deterministic state (in terms of dynamical systems, a slow manifold), which loses stability.
- The system's variability results from small white noise.

It should be noted that the existence of a bifurcation is not a prerequisite of our method. Even in the case of weaker feedbacks and a more gradual transition will a change in stability be reflected in slowing down. However, the detectability of the signal tends to decrease as compared to a bifurcation where the system approaches a random walk. The main difference to previous applications of EWS is that our method does not only calculate the magnitude of slowing down but also identifies the subsystem where it occurs.

In principle, a prediction of sudden transitions could also be attempted with this approach. As new data points become available, new EOFs and projections may be constructed. As for any prediction based on EWS it must of course be known in advance which maximum signal is to be expected (Thompson and Sieber, 2011a). For example, autocorrelation only comes close to 1 when there is a bifurcation, but peaks at lower values in less extreme cases.

In addition, the very large data requirements imply a vast separation between the timescale of changing external conditions and the intrinsic timescale of the system, a condition that is not often satisified. Although we focus on autocorrelation and temporal variability, other indicators of slowing down such as spatial variability could be applied within the same iterative framework

and may lead to better performances. As our additive and multiplicative noise case illustrate, the more the analysis method is tailored to a specific system, the more a priori knowledge on the data generating process is needed. For example, variance may increase or decrease when approaching a threshold, depending on the system under consideration (Brock and Carpenter, 2010; Dakos et al., 2012).

Additional caveats are imposed by unaccounted or changing properties of the external noise, which would affect EWS (Carpenter and Brock, 2006; Scheffer et al., 2009; Ditlevsen and Johnsen, 2010). In particular, we have only used white noise which is uncorrelated in space. However, it would physically be more reasonable to account for spatial correlations in the atmospheric variability. This could reduce the detectability of hotspots because correlations between the state variables could not be attributed to spatial interactions alone, but would partly result from correlations in the noise.

Other problems may arise in cases of large noise. The local stability of the deterministic state may not be represented well anymore in EWS, and the noise can lead to an early tipping. More fundamentally, the system's mean behaviour in the large noise regime may not reflect its deterministic structure anymore due to noise-induced transitions (Horsthemke and Lefever, 1984). The link between a system's susceptibility and statistical properties of its variability breaks down under such conditions.

Within these limitations, our results suggest an alternative applicability of EWS which may contribute to a better understanding of numerical models. In this regard our study is a concretion of Lenton's recent conclusion: "Even if further research shows that early warning is unachievable in practice, it could still provide valuable information on the vulnerability of various tipping elements to noise-induced changes." (Lenton, 2011). To this end, more systematic studies on the performance of indicators of slowing down for different classes of models will be particularly beneficial.

3.3 Application to PlaSim-VECODE time series

3.3.1 Mid-Holocene vegetation dynamics in PlaSim-VECODE

To simulate mid-Holocene vegetation dynamics in this Section 3.3, we use the modified VECODE (VECODEm; Fig. 2.2) by choosing $\alpha = 0.0011$, $\beta = 140$, $\gamma = 1.7 \times 10^{-5}$, and $\delta = \mathrm{GDD}_0 - 900$ (with GDD_0 in Kelvin; see Section 2.2.2). VECODE distinguishes trees and grass as the only vegetation types. The surface cover types, trees, grass and desert, have different physical properties which are constant over time.

As explained in Section 2.2.3, PlaSim and VECODE can be coupled in two ways: in a transient mode (PlaSim-VECODEm-tr), we use an annual coupling, and vegetation cover fractions at each grid box approach their equilibrium according to a linear relaxation law using a climate dependent timescale. In equilibrium mode (PlaSim-VECODEm-eq), we iteratively run PlaSim

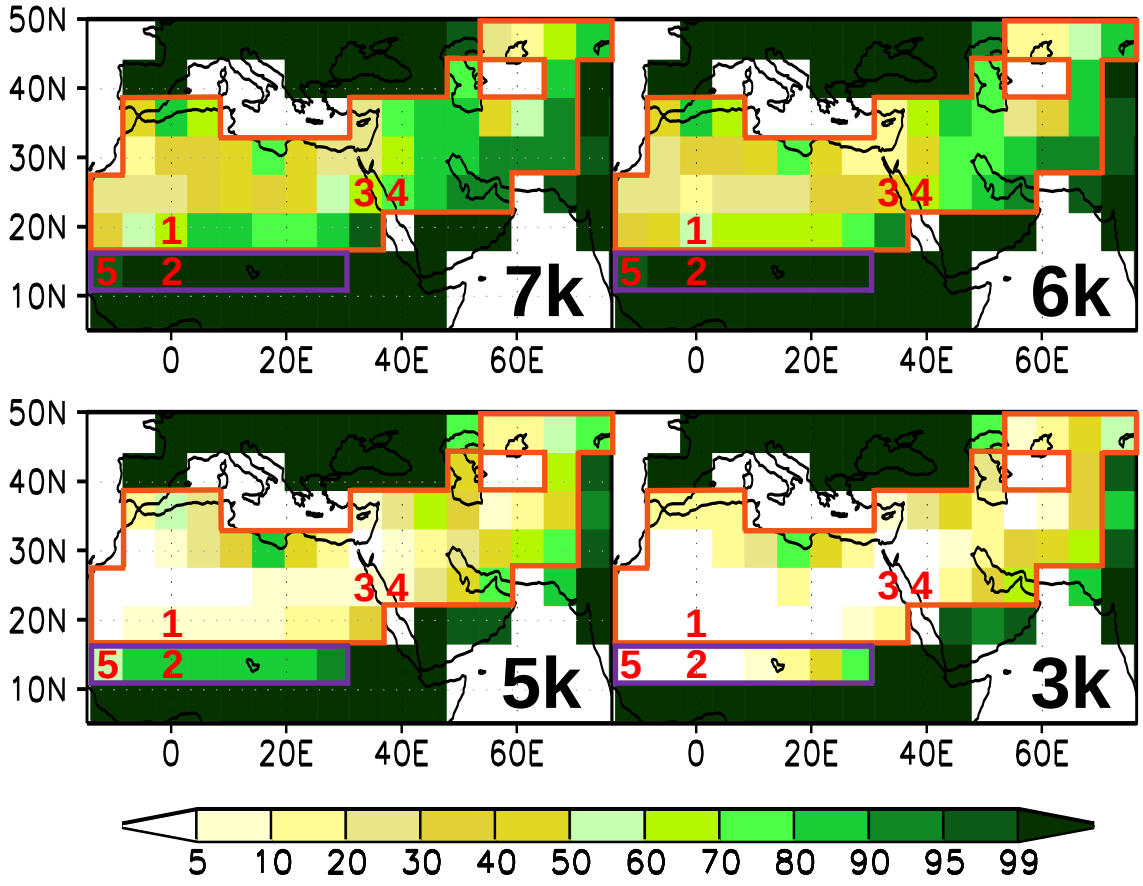

Figure 3.12: Mean vegetation cover fractions (trees + grass) in % from 9 k to 2 k in PlaSim-VECODEm-tr. Vegetation cover is averaged over 200 yrs starting from the indicated year (7 k, 6 k, 5 k, and 3 k, respectively). Numbers 1 to 5 denote the individual grid cells referred to in the text. The light red region encloses the 52 grid cells considered in RM1, the purple region encloses the 8 grid cells considered in RM2.

with fixed vegetation cover for several years, and then set vegetation cover to its new equilibrium corresponding to the multi-year average of P and GDD_0. This mode thus corresponds to an asynchronous coupling.

When running PlaSim-VECODEm-tr with orbital forcing from 9 k to 2 k, we obtain two major vegetation collapses in different regions at different times (Section 2.3). The spatial and temporal features of these transitions are presented in Figs. 3.12 and 3.13. From 9 k to 6 k, almost all land cells are at least partly covered by vegetation and cover fractions show large fluctuations due to natural climate variability but almost no trend. Around 5.5 k, vegetation cover in large parts of northern Africa and south-western Asia collapses and thereafter stays in desert-like conditions. Interestingly, the timing of this collapse corresponds to palaeoclimate time series from a sediment core (deMenocal et al., 2000) and earlier model studies (Claussen et al., 1999), despite differences in the models and our modifications to the vegetation model. Around 3.5 k, a similar abrupt event occurs in a more confined region in the Sahel region. In the following, we refer to these two

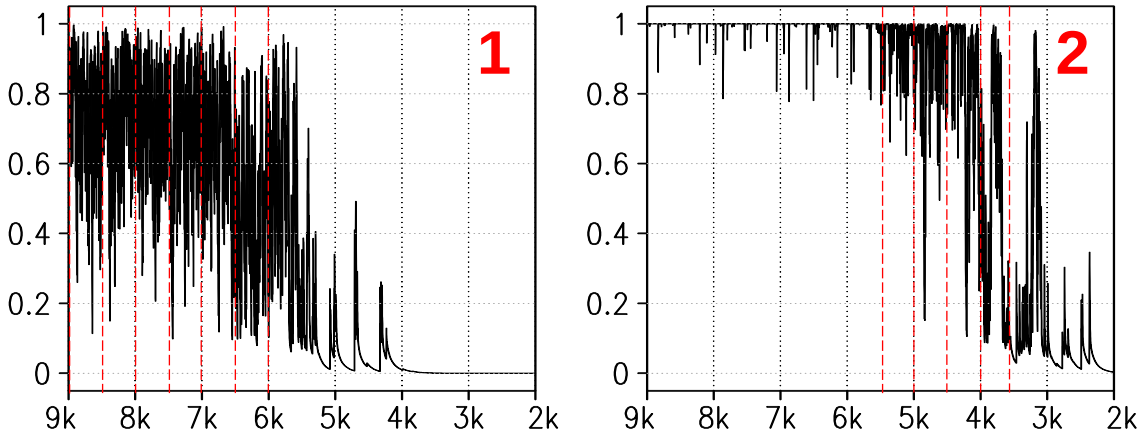

Figure 3.13: Vegetation cover fractions from 9 k to 2 k in PlaSim-VECODEm-tr. Two single grid cells are shown, indicated as grid cells 1 and 2 in Fig. 3.12. The vertical dashed lines indicate the *B*-values of the 20 000 yrs long stationary PlaSim-VECODEm-tr simulations used to construct RM1 (top) and RM2 (bottom).

sudden transitions as collapse 1 (5.5 k event) and collapse 2 (3.5 k event).

The two vegetation collapses are related to the large atmosphere-vegetation feedback in the model which can allow for multiple equilibria. In PlaSim-VECODE-eq, multiple steady states in the region of collapse 1 can be found until approx. 7 k., and in the region of collapse 2 at 4.5 k–5 k (Figs. 2.8, 2.9 and Table 2.2). For each of these orbital forcings, starting from a forest world leads to a partly vegetated state (in the following called the *green equilibrium*), while starting from desert conditions leads to a dry state (*desert equilibrium*) in PlaSim-VECODEm-eq. However, due to the large climate variability and non-linearities in the model formulation, a noise-induced transition (Horsthemke and Lefever, 1984) can occur and multiple steady states are not found in PlaSim-VECODEm-tr, where natural variability is large. The collapses presented in Figs. 3.12 and 3.13, although a result of the intrinsic multiple states in the system, thus do not exactly coincide with the deterministic bifurcation points, but rather result from a sudden change in the system's probability density function.

3.3.2 A stochastic model for EWS analysis

3.3.2.1 Idealised model setup

To further analyse the stability properties of PlaSim-VECODE and to find hotspots in the model, we apply our hotspot detection method.

In agreement with our algorithm for hotspot detection presented in Section 3.2, we first generate a number of time slices for fixed orbital forcing. To analyse collapse 1, we choose orbital forcings corresponding to 9 k, 8.5 k, 8 k, 7.5 k, 7 k, 6.5 k and 6 k (dashed red lines in Fig. 3.13, top); to analyse collapse 2 we choose 5.5 k, 5 k, 4.5 k, 4 k, and 3.6 k (dashed red lines in Fig. 3.13, bottom).

As any year is associated with a particular orbital forcing we refer to this forcing as an orbit year. Each time slice simulation consists of 20 000 yrs in transient coupling mode.

However, a direct application of the hotspot detection scheme to these time series is not adequate for the following three reasons:

1. Due to the distinction of cases in Eq. (3.1), vegetation cover fraction V does not always show free variations but is often exactly 0 or 1. The application of EWS is not suited for such a case as the stability properties of the equilibrium cannot be sampled properly. For example, before reaching a desert state, the vegetation cover fraction shows an exponential decay after a particularly wet year and stays constant afterwards (Fig. 3.13). More importantly, the same phenomenon occurs at the other limit of phase space, $V = 1$. EWS like autocorrelation or variance then depend on the frequency of such cutoff events, which are not related to the stability of a climate state.

2. The timescale τ of dynamic vegetation cover change in VECODE depends on the system's state and thus contaminates the signal of slowing down. In particular, τ is large for dry regimes and small for wet regimes (Fig. 2.3). When background precipitation is reduced, an increased timescale will be reflected in an increased autocorrelation. This state-dependent slowing down is not necessarily related to any change in stability and thus distorts the signal.

3. Atmospheric variability in PlaSim-VECODE-tr is too large to justify the small noise approximation. As explained above, the two collapses cannot be expected to coincide with a vanishing eigenvalue because they result from non-linear interactions between the amplitude of the multiplicative noise and the system's state (Chapter 2).

Insofar, the prerequisites for an application of EWS-based analysis are in conflict with the case of PlaSim-VECODE-tr. We therefore perform an intermediate step by using the stochastic model introduced in Section 3.2. In the stochastic model, vegetation dynamics are represented by Eq. (3.2) with t as the discrete time and a time step of one year. Precipitation P at any grid cell i is described as a linear function of the vegetation cover fractions V_j at all cells (Eq. 3.3, following the concept of Brovkin et al. (1998), Wang (2004), and Liu et al. (2006). The bifurcation parameter B now represents the impact of orbital forcing on northern hemisphere summer insolation and thus convective precipitation. Spatial interactions are captured by matrix k_{ij}, and climate variability is accounted for by a Gaussian white noise process η_i, which is also uncorrelated in space.

In contrast to PlaSim-VECODE, the three caveats listed above can be resolved within the framework of this stochastic model:

1. We remove the second condition in Eq. (3.1), thereby allowing for $V > 1$ which corresponds to an extrapolation of the empirical $P(V)$-relation obtained in PlaSim-VECODEm. As a maximum of $V = 1.03$ is still not exceeded, we accept the unphysical nature of cover fractions larger than 1 in the stochastic model.

2. Like in Chapter 2, we fix the dynamic timescale τ to a the climate-independent value of 5 yrs in agreement with Liu et al. (2006).

3. We prescribe a particularly small and constant noise level of $\sigma_V = 0.00013$ with $\sigma_P = 0$ (additive noise) or $\sigma_P = 2$ with $\sigma_V = 0$ (multiplicative noise).

We refer to this model as regression model 1 (RM1) when studying collapse 1, and as regression model 2 (RM2) when studying collapse 2. Both models only differ in the number of grid cells and the parameter values.

To keep the regression models as simple as possible, we only include grid cells in northern Africa and south-western Asia which show substantial fluctuations in vegetation cover. Grid cells with V permanently close to 1 or 0 in all time slices are static elements of the system under consideration and can thus be interpreted as external conditions which are indirectly reflected in the constants P_{0_i}. For RM1, we include all grid cells where V averaged over time and all time slices is between 0.1 and 0.96 (orange area in Fig. 3.12). For RM2 we select the 8 grid cells in the south-west which show substantial collapse at 3.5 k (purple area in Fig. 3.12).

Besides precipitation, growing degree days GDD_0 are also a space and time dependent variable of the system which affects V^* (Eq. 3.1). However, by choosing $\gamma = 1.7 \times 10^{-5}$, the sensitivity of V^* to changes in GDD_0 is very small in VECODEm. Differentiation of V^* with respect to δ as well as a graphical analysis reveals that shifts in P-direction do not exceed some mm/yr for typical changes in δ. As plants in arid regions are limited by water rather than temperature, the neglect of temperature fluctuations seems reasonable. Typical spatial differences in GDD_0 (time means are between 7000 and 12 000) exceed the temporal variability in North Africa (approx. 1000 at most grid cells) in PlaSim-VECODE-tr. Therefore, we prescribe a constant value of GDD_0 (and thereby δ) at each grid cell of our regression models. Each value corresponds to the average over all years and time slices (9 k–6 k for RM1, 5.5 k–3.6 k for RM2). Hence, $V_i^*(P)$ very slightly depends on the particular grid cell i, but is constant in time.

It remains to determine suitable parameter values of P_{0_i}, s_i, and k_{ij} to reproduce the stability properties of PlaSim-VECODE with the regression models. To this aim, we fit these parameters to our stationary PlaSim-VECODEm-tr simulations using a multivariate linear regression:

First, we extend the vector V_i at every year from PlaSim-VECODEm-tr by one additional dimension, assigned with the orbit year corresponding to each time slice. Although V actually consists of trees and grass cover in VECODE, we can safely neglect this distinction, as tree cover is always close to 0 in the grid cells we consider. Using the extended vector as a predictor and the corresponding PlaSim-VECODEm-tr time series of P_i as responses, we calculate regression coefficients using the MATLAB function *mvregress*. Each P_{0_i} is then obtained as the constant offset of the regression line, s_i is its slope with regard to orbit year, and k_{ij} are its slopes with regard to V_j.

3.3.2.2 Stability properties of the regression models

To investigate the stability properties of the two regression models over a range of B we numerically determine deterministic equilibria and the eigenvalues of these equilibria as obtained from a linear stability analysis (Fig. 3.14). To obtain the eigenvalues, we derive the Jacobian of the corresponding time-continuous deterministic system (for which a bifurcation is indicated by an eigenvalue approaching 0) and calculate its properties by inserting the numerically obtained equilibrium state. For the first value of B (8.8 k for RM1, and 6 k for RM2) we use $V_i = 1$ as an initial condition and run the model to equilibrium. For all subsequent steps of B, we insert the previously obtained equilibrium as an initial condition (which always results in the same solution as using $V_i = 1$ for any B in our two regression models).

In both models the obtained equilibria are stable fixed points, as indicated by the negative real parts of all eigenvalues. Before a sudden transition to a different equilibrium occurs due to a saddle-node bifurcation, one eigenvalue approaches 0. A reversed scanning of the B-range with our numeric approach to find equilibria indeed results in a static hysteresis (not shown). The equilibria coincide well with the green and desert equilibria found with PlaSim-VECODEm-eq (Chapter 2).

In RM1, there are several bifurcations along the forward branch, two in the B-range of interest: at approx. 8 k, grid cell 3 (marked in Fig. 3.12) collapses. At around 6.7 k, most other grid cells collapse in a second bifurcation. This second bifurcation clearly corresponds to the disappearance of the green equilibrium in PlaSim-VECODEm-eq (Chapter 2). Considering that the variability which is still present to some extent in PlaSim-VECODEm-eq prevents a detection of the green equilibrium close to the bifurcation point, the timing of the bifurcation also coincides well. However, the collapse of grid cell 3 at 8 k only occurs in RM1, whereas in PlaSim-VECODEm-eq vegetation cover is gradually reduced over time. In contrast, the stability structure of RM2 is much simpler and all cells collapse in synchrony.

The emergence of multiple equilibria from the noisy PlaSim-VECODEm-tr time series provides further evidence that multiple deterministic equilibria are present in PlaSim-VECODEm but do not become apparent in probability density functions due to a noise-induced transition (Chapter 2). Using an interactive noise level and an interactive vegetation timescale as in Section 2.5.2 leads to similar transitions as in PlaSim-VECODEm-tr, but in a spatially explicit way (not shown).

Altogether, the regression models therefore cannot reproduce the PlaSim-VECODEm results in every aspect but qualitatively show many similarities and provide a simple and appropriate framework for EWS analysis.

3.3.3 Hotspot detection in the regression model

We can now answer the question where each tipping in Fig. 3.14 originates by applying our hotspot detection algorithm:

1. We generate time slices of 100 000 yrs each with RM1 and RM2. The chosen values of B

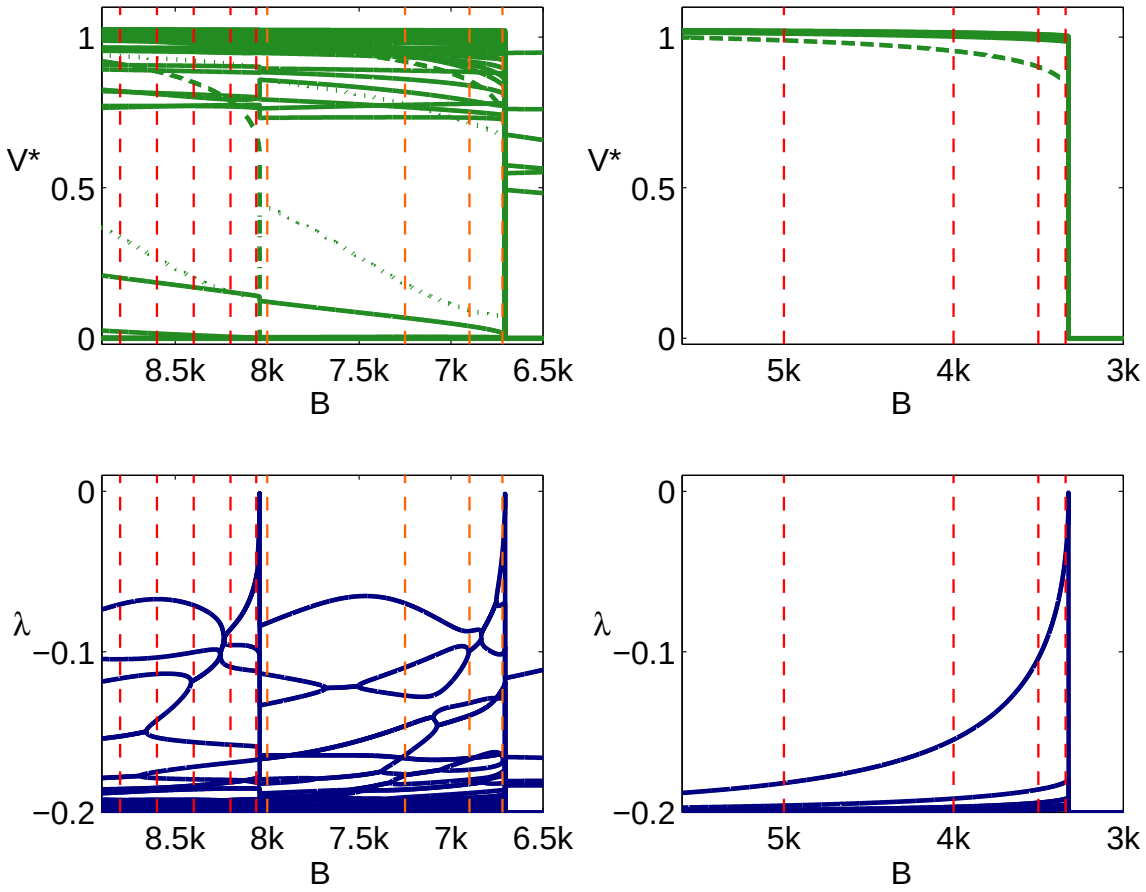

Figure 3.14: Characteristics of RM1 (left) and RM2 (right), depending on parameter B. Top: Equilibrium vegetation cover at all elements (greenest solution). The elements identified as hotspots are dashed. Some elements are dotted only to be better distinguishable from others. Bottom: real part of eigenvalues characterizing the linear stability of the corresponding solution of the time-continuous system. The vertical dashed lines indicate the B-values of the stationary simulations used for the hotspot detection (red: bifurcation 1 in RM1 and RM2, orange: bifurcation 2 in RM1).

for these time slices are again depicted as dashed vertical lines in Fig. 3.14. Two time series are generated for each forcing, one with additive noise and one with multiplicative noise.

2. As the noise level is small, some grid cells in RM1 are already unvegetated and thus can be discarded as hotspot candidates (the desert cells in PlaSim-VECODEm-eq). We therefore do not consider grid cells where V falls below 0.004 at any time step in any time slice.

3. To the rest of the grid cells we apply the hotspot detection scheme presented in Section 3.2: in short, we repeatedly apply a degenerate atmosphere-vegetation (Held and Kleinen, 2004) to a random selection of grid cells and each time determine an EWS. During this analysis we successively remove grid cells which contribute least to the signal and finally identify a hotspot from the resulting signal list as the combination of grid cells which maximises the signal.

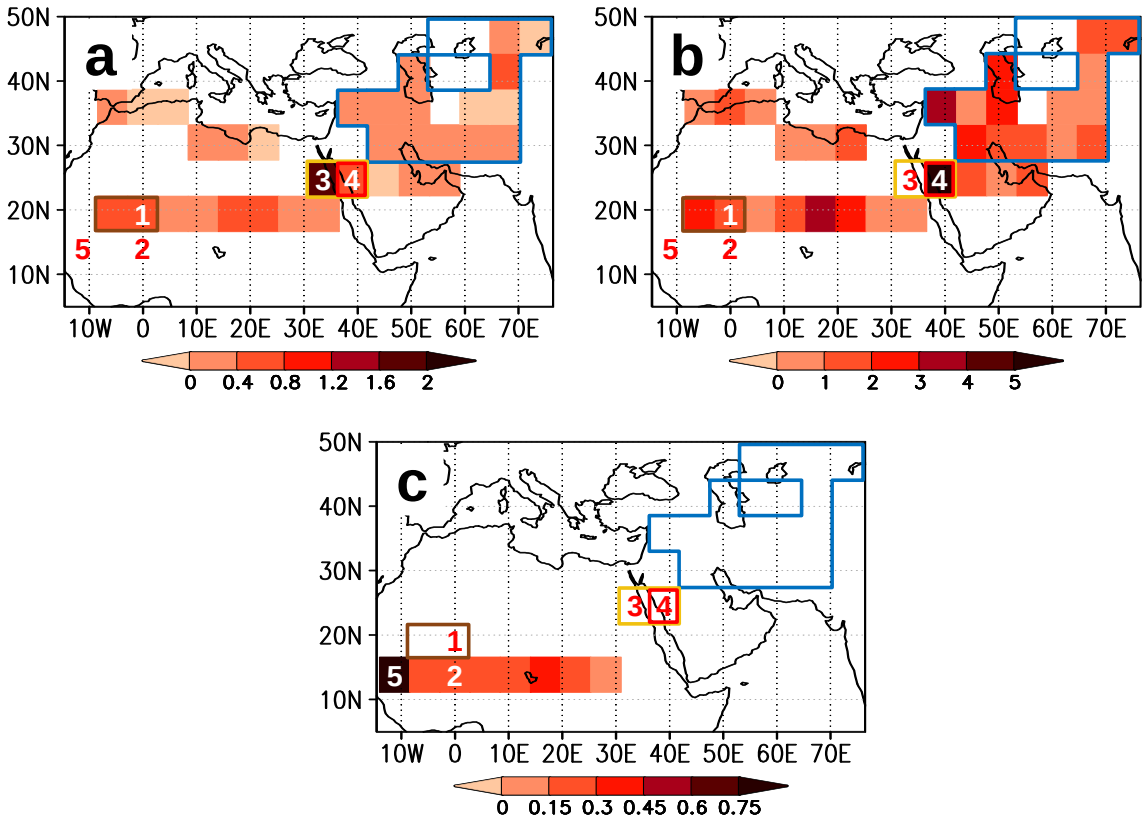

Figure 3.15: Contribution of grid cells to the increasing autocorrelation as obtained with the hotspot detection algorithm, **(a)** in RM1, tipping point 1, **(b)** RM1, Tipping Point 2, **(c)** RM2. The noise in all time series was additive, hotspot detection was applied with $n_{\max} = 3$, elimination rule 1, and covariance based EOFs. Numbers 1 to 5 denote the individual grid cells referred to in the text.

In order to illustrate the hotspots geographically, we indicate an element's weight at its corresponding grid cell (Fig. 3.15). As a weight we define the sum of signals a certain element contributes to, as illustrated by Table 3.3. It must be noted though, that the random sampling and the systematic removal of elements during the hotspot detection algorithm only allows qualitative conclusions like the position of the hotspot. The quantitative differences between the grid cells in Fig. 3.15 should therefore not be over-interpreted.

We find that before the collapse of grid cell 3 in RM1, this grid cell is detected as a hotspot of the transition. This is of course not surprising as this grid cell is the only one showing a collapse. In the more complex case of collapse 2 in RM1, its neighbouring grid cell 4 is identified as the hotspot of the transition. The collapse of the 8 grid cells in RM2 is detected to be initiated by the most western grid cell (cell 5). Hence, each collapse in our regression models originates at one single grid cell.

To investigate the robustness of these results, we apply the hotspot detection with different parameter settings: all time series are analysed with elimination rules 1 and 2. Relative thresholds t_{ini} and t_{inc} are always 5 %, for $n_{\max}$ we choose 3, 5, and 8. We construct the EOFs from the

covariance matrix as well as from the correlation matrix. As EWS we use autocorrelation and relative variance. For explanations of these parameter options see Section 3.2. We find that the determined hotspots are always the same for all combinations of these parameter settings.

Excluding certain time slices from PlaSim-VECODEm-tr (9 k, 8 k, 8.5 k, 5.5 k) to determine the regression parameters for RM1 also leads to similar results with regard to the system's stability properties and the determined hotspots. This even holds true if we replace the original PlaSim-VECODEm time series by a set of 20 000 bootstrapped pairs of P and V (Efron, 1979), although some realisations then show additional bifurcations in RM1. The tendency of RM1 to show more bifurcations than PlaSim-VECODEm may thus result from intrinsic limitations of our linear fit. For example, orbital forcing and its impact on annual precipitation certainly does not change linearly over time.

When reducing the length of the time series we generate with the regression models the hotspots clearly emerge from the noise until a total length of several 1000 yr in case of autocorrelations and several 100–1000 yr in case of variances. RM2 is even more robust: 100 yr of each time series are sufficient to detect the hotspot when using relative variance as an EWS.

In summary, our detected hotspots are a very robust characteristic of PlaSim-VECODEm. In the following section we document that they are also meaningful, in the sense that they yield information on the stability properties of PlaSim-VECODEm.

3.3.4 Evaluation of results with PlaSim-VECODEm

To verify the detected hotspots we seek evidence for their existence in PlaSim-VECODEm and an explanation in terms of the model's physics. As we apply PlaSim-VECODEm with low resolution, present day SSTs and a quite crude representation of physical surface parameters, the model cannot be expected to provide a very realistic climate of the mid-Holocene.

Despite these limitations, the large-scale features of the North African summer circulation are captured reasonably. We here focus on the conditions during July to September because in the model most precipitation in northern Africa and south-western Asia occurs during these months. The south-westerly monsoon flow is confined to the lowest model levels and advects moisture over the North African continent towards the heat low in central north-western Africa (Fig. 3.16a, b). The intertropical front is very prominently indicated by a surface convergence and a strong jump in specific moisture around 15–20° N. To the north of this front, the north-easterly trades advect dry air from the Mediterranean region.

As in observations, easterly winds prevail in all tropospheric levels above the shallow monsoon flow. Due to the low model resolution, the African Easterly Jet (AEJ), Tropical Easterly Jet (TEJ) and the low-level westerly jet (Patricola and Cook, 2007) cannot be captured well as the horizontal gradients in zonal wind are small. Since precipitation in the Sahel is related to the strength and position of these jets (Nicholson, 2009), the model cannot capture the small-scale nature of precipitation events. The seasonal migration of the rainbelt and its northward shift during the

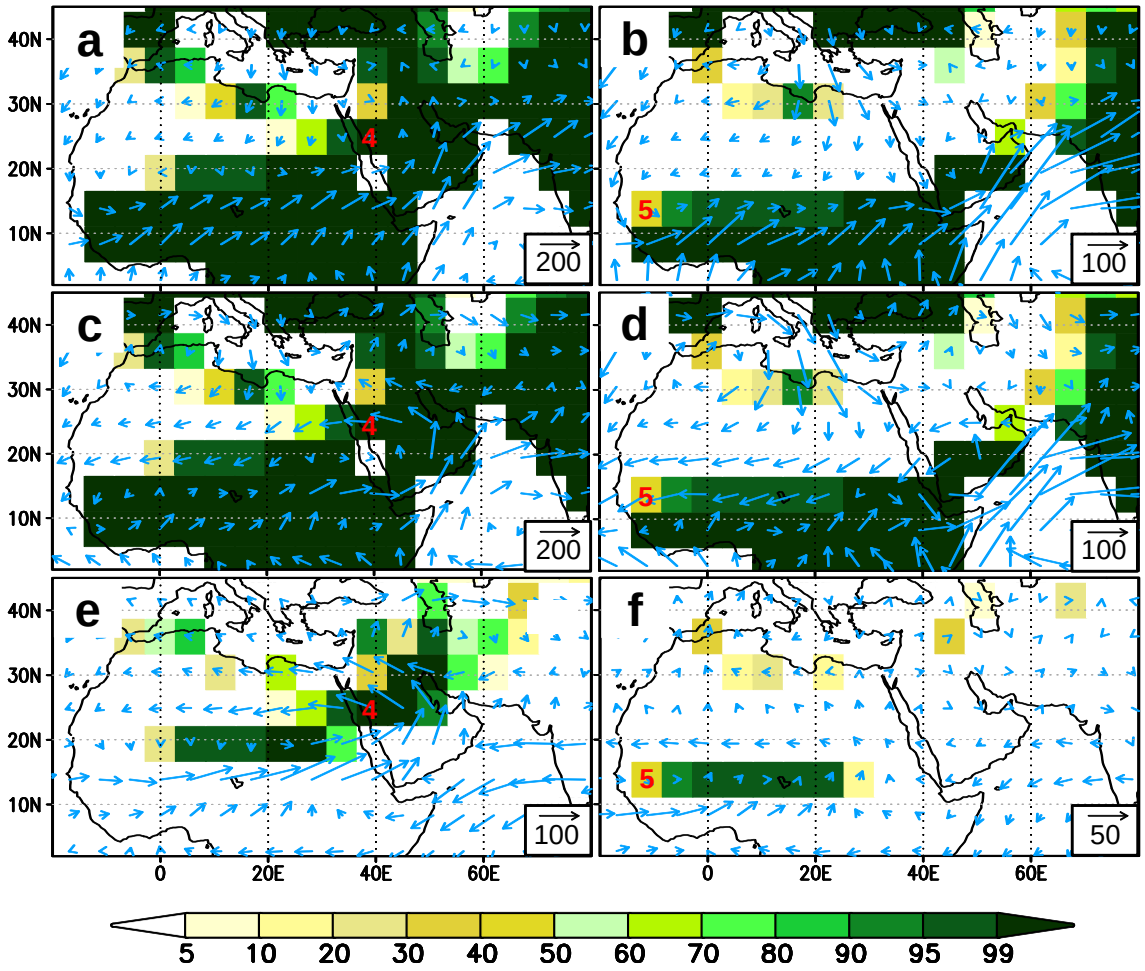

Figure 3.16: Vertically integrated horizontal moisture fluxes (arrows) and vegetation cover (colours) in PlaSim-VECODEm-eq. **(a)** green state for 8k forcing (vertical integral over two lowest atmosphere levels only), **(b)** green state for 4.5 k forcing (two lowest levels only), **(c)** green state for 8 k forcing, **(d)** green state for 4.5k forcing, **(e)** difference between green and desert states for 8 k forcing, **(f)** difference between green and desert state for 4.5 k forcing. Fluxes are in kg/(ms), vegetation cover fractions in %. Numbers 4 and 5 denote the individual grid cells referred to in the text.

mid-Holocene are nonetheless captured by PlaSim-VECODE. However, the zonal structure of the rainfall pattern is in conflict with observations. While the eastern Sahel is drier than the west in present-day observations (Andersson et al., 2010), precipitation in PlaSim-VECODE strongly increases towards the east. There, the south-westerly flow becomes even stronger and advects moisture from central Africa. This azonal structure is present in the complete Holocene.

3.3.4.1 Collapse 2

The west to east gradient in precipitation and the advection of moisture are also the key to understanding why the westernmost grid cell (grid cell 5) is a hotspot in RM2. The substantial precipitation gradient is reflected in the regression parameters P_{0_i}. In addition, the interaction

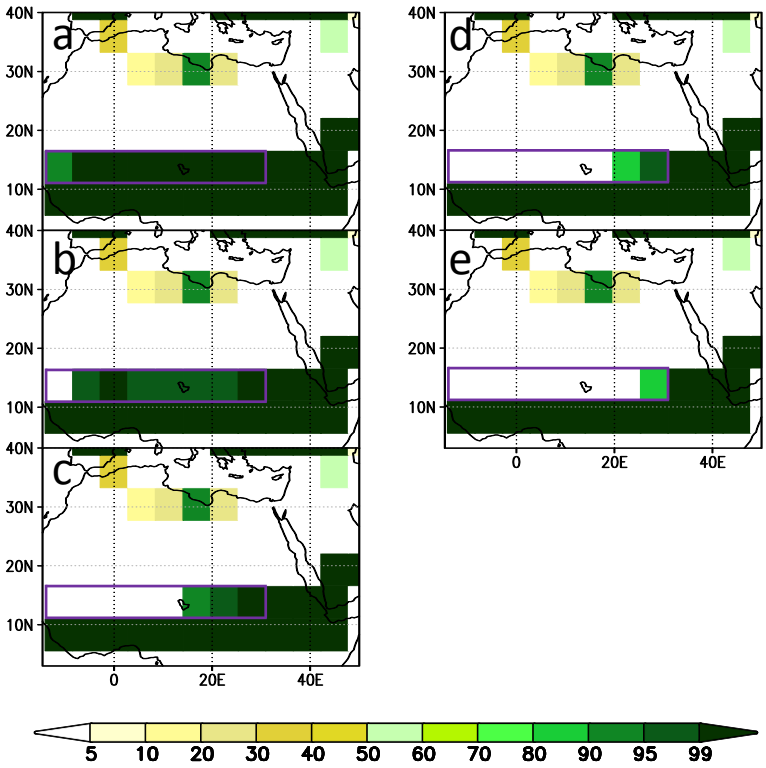

Figure 3.17: Fixed points of Eqs. (3.1), (3.3), and (3.2) for 4.5 k conditions. The regression involves the 8 grid cells enclosed in the purple box; cover fractions outside this area are set to mean conditions in PlaSim-VECODEm-eq.

matrix k_{ij} reveals that the impact of grid cell 5 on other cells is exceedingly large for reasons explained below. When orbital forcing evolves, the precipitation pattern shifts towards the east. Therefore grid cell 5 is the driest element in RM2. Its influence on its easterly neighbors due to moisture advection keeps the system green for a long time. When precipitation in cell 5 finally is too low for vegetation to be sustained, precipitation in the other cells also decreases below the critical threshold. Hence, these other elements experience an induced tipping and the hotspot is to be found at cell 5.

The non-trivial structure of interactions k_{ij} implies that more equilibria may exist in PlaSim-VECODEm than those found by choosing global forest or desert initial conditions as in Section 2.4.2. Our conceptual model framework (Eqs. 3.1, 3.3, and 3.2) is suitable to determine fixed points of the system in a more systematic way. To dispose of the deficiencies of including time in the regression model, we now apply the regression to our 4.5 k simulation with PlaSim-VECODEm-tr only, which corresponds to dropping the term $s_i B$ in Eq. (3.3). Again, we consider the same line of eight grid cells as in RM2. As it is not possible to find the fixed points analytically, we randomly select 10 million initial conditions and run RM2 (without noise) to a steady state. As a strategy to sample the initial conditions in phase space we apply a regular, completely random, and a latin hypercube sampling (using MATLAB function *lhsdesign*). Independent of

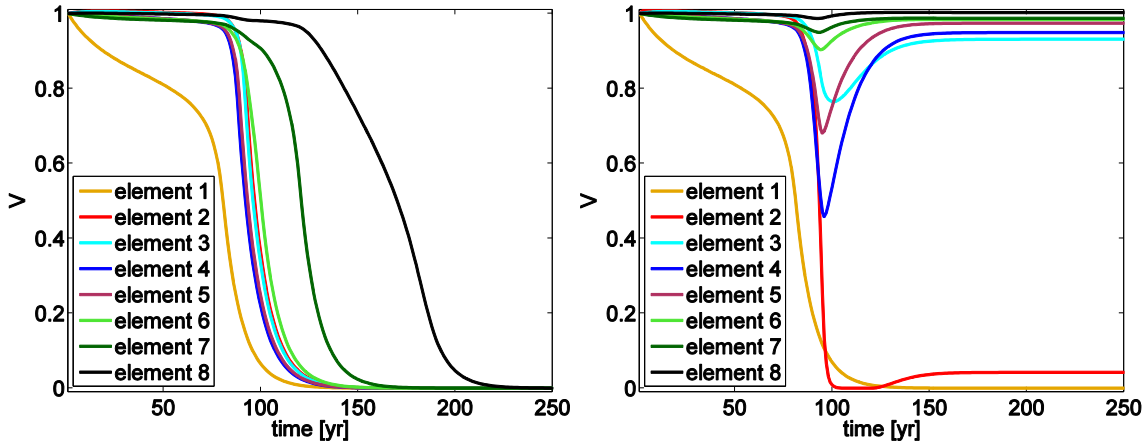

Figure 3.18: Equilibration of RM2 after choosing the initial condition $V_i = 1$. Left: all timescales $\tau_i = 10$. Right: $\tau_2 = 2$, all other $\tau_i = 10$.

the sampling method we obtain 5 deterministic solutions (Fig. 3.17). By reintroducing these fixed points as initial conditions in PlaSim-VECODEm-eq with a coupling frequency of 30 yrs we can verify the existence of all five solutions in PlaSim-VECODEm-eq.

The structure of these solutions is suggestive with regard to the position of the hotspot: all equilibria have in common that any green grid cell permits only green grid cells to its east. This feature is due to the advection of moisture with the westerly monsoon flow. In addition to this moisture recycling, the enhanced evaporation affects atmospheric stability and the circulation itself (Goessling and Reick, 2011). Also, an impact of easterly on westerly cells exists due to albedo induced changes in monsoon strength. In case of grid cell 5 both effects work in the same direction which explains its large importance: first, it supplies additional moisture to its eastward neighbors via recycling. Second, it enhances the thermal low and thus the low-level south-westerly monsoon flow which supplies the more easterly region. As this flow is overcompensated by the export of moisture towards the west in higher levels, the vertically integrated moisture flux is towards the west (Fig. 3.16d), but the difference between green and desert state (Fig. 3.16f) indicates the enhancement of low-level westerlies due to the vegetation.

In addition to this interpretation of our hotspot detection results, RM2 also provides an instructive example on the caveats of choosing initial conditions: Although the system collapses from its greenest to its driest state after 3.5 k, there are other intermediate equilibrium states. In particular, there is one solution which resembles the state in Fig. 3.17 b. During the collapse, spatial mean vegetation passes a value which is identical to this other intermediate equilibrium. However, the trajectory of the collapse from green to desert does not pass the attractor basin of the intermediate equilibrium. This intermediate equilibrium would therefore remain hidden to the modeller who chooses extreme initial conditions and varies orbital forcing. This example demonstrates that extreme initial conditions are not necessarily extreme in terms of phase space and may accidentally even lie in the same attractor basin although other basins may exist. In RM2, hidden equilibria can

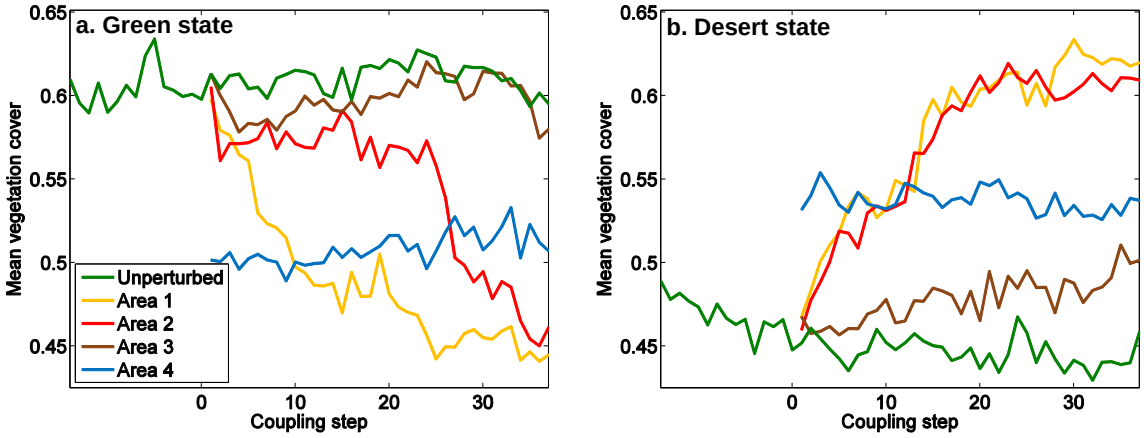

Figure 3.19: Evolution of vegetation cover fraction in PlaSim-VECODEm-eq with perturbations in different areas. All vegetation cover fractions are averaged over the complete region shown in Figs. 3.20 and 3.15 (5° N–50° N, 14.6° W–76.5° E). The colours correspond to the areas marked in Fig. 3.15, where vegetation cover is set to 0 **(a)** or 1 **(b)**.

exist due to some negative values in interaction matrix **k** (in particular, the influence of elements 2 and 8). The adequate choice of initial conditions is therefore a non-trivial task.

Furthermore, even trajectories resulting from one and the same initial condition can end up in different equilibrium states. Invoking an (imaginary) potential, a trajectory only follows the local gradient if there is one timescale for movements in all directions. This is the case in our regression models, but not in PlaSim-VECODE, where the timescale of vegetation changes at each grid cell depends on local climate. As an example, we chose the initial condition $V_i = 1$ for all i in RM2 with 3.2 k conditions. If we set all $\tau_i = 10$, the system collapses to the desert equilibrium as we know from Fig. 3.14 (Fig. 3.18 left). In contrast, if we set $\tau_2 = 2$ (keeping all other timescales at 10), element 2 collapses quicker than the other elements, which enhances rainfall P at these other elements. Although element 1 has also collapsed, vegetation can still exist at the eastern part of the region (Fig. 3.18 right). This is the intermediate state mentioned above.

As we set all $\tau_i = 5$ in our original RM2, the system stays in the greenest state for a long time when B is varied (Fig. 3.14), while some of the fixed points with intermediate vegetation cover disappear. When vegetation at the hotspot collapses, all elements collapse in synchrony, precipitation at all grid cells becomes too low to sustain vegetation and the system drops into the driest state.

3.3.4.2 Collapse 1

The zonal gradient in precipitation and its shift over time are also present from 9 k to 6 k. Like for RM2, the grid cells with the least precipitation are also at the western margin of the model region. This is the reason for the collapse of grid cell 3 in RM1, which has no consequences for the rest of the system. In contrast, our hotspot detection method identifies the rather wet grid cell

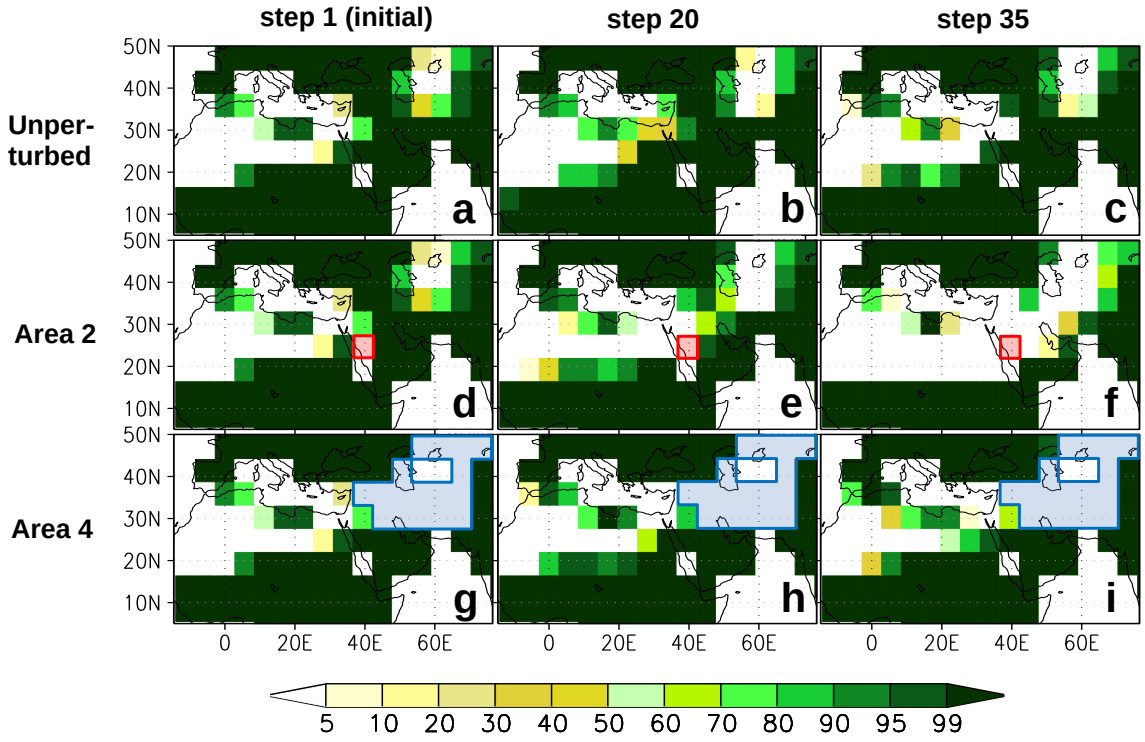

Figure 3.20: Vegetation cover fractions (in %) in PlaSim-VECODEm-eq after initialisation in the greenest equilibrium with no perturbation (**a–c**), no vegetation in area 2 (red grid box, **d–f**), and no vegetation in area 4 (blue, **g–i**).

4 as the hotspot of collapse 1 (second collapse in RM1), implying a decreasing stability and thus an increasing sensitivity to perturbations at this point. To verify this result we initialise PlaSim-VECODEm-eq with 8k forcing and a coupling frequency of 20 yrs in the green and desert equilibrium but impose a perturbation in certain test areas (enclosed by coloured boxes in Fig. 3.15). In case of the green initial state, we set the test area to desert conditions, in case of the desert initial state we set it to 100 % grass cover. In the test areas, cover fractions are kept fixed at these initial conditions, while the dynamic vegetation is still active in all other areas. As a result we find that the complete system can be forced to flip into the opposing equilibrium by a perturbation at grid cells 3 and 4 (area 1; Fig. 3.19). Even a perturbation just in grid cell 4 (area 2) has this effect, though after some time in an intermediate state in the case of green initial conditions. In contrast, the two westernmost grid cells in the Sahara (area 3) and even the complete north-eastern half of the model region (area 4) do not have a comparable effect on V in the remaining system part, which remains unaffected by the perturbations (Fig. 3.20).

An analysis of the moisture fluxes at 8 k reveals the reason for the model's vulnerability at the hotspot: North Africa, as well as south-west Asia, are both supplied by moisture which originates in the Atlantic and Indian ocean and then passes over the Arabian peninsula (Fig. 3.16 a,c). There the low-level circulation splits into an easterly part, turning back to North Africa, and a branch that extends northward over south-west Asia, and joins the mid-latitude westerlies. Therefore, the west

African part of the bistable region not only receives moisture from the direct low-level monsoon flow but also from this moistening of the easterlies aloft. The contribution of these two sources is most apparent in the difference between the green and desert equilibrium states in PlaSim-VECODEm-eq (Fig. 3.16e). With vegetation present, both sources are enhanced and contribute to the local convergence of moisture. The maximum surface pressure difference is located at the northern Red Sea, coinciding with the detected hotspot. Hence, imposing desert conditions in this key area weakens the heat low and the cyclonic circulation over Arabia and thus cuts off the moisture supply to both circulation branches. Therefore, the rest of the vegetation disappears and the resulting lack of moisture convergence leads to a rapid transition to the desert equilibrium in PlaSim-VECODEm.

3.3.5 Summary and conclusions

The possibility to use indicators of slowing down to analyse the climate system has been documented extensively in recent years (Held and Kleinen, 2004; Dakos et al., 2008; Lenton et al., 2009, 2012b). In Section 3.2 we have proposed a new method to infer the position of hotspots in a diagnostic way from model output. Here, we have applied our method to a regression model based on results from a global atmosphere-vegetation model, and have identified its hotspots.

We have thus documented that the hotspot detection method can provide information on the causality of a tipping and on the sensitivity of the model under consideration. If the model represents reality in an adequate way, an analysis with EWS can indicate where the earth system is particularly vulnerable to perturbations. On the other hand, if the model behaves in an unrealistic way, a hotspot detection analysis may improve the knowledge on its shortcomings and make its limitations more apparent. This knowledge can be beneficial for further model development. In case of PlaSim-VECODEm, a perturbation of surface parameters at a single grid cell can change the circulation on a regional to continental scale, and it remains doubtful if this result is realistic. However, we have identified the Red Sea area in the model as a crucial region for the moisture supply of Northern Africa and South West Asia at 8 k.

The application of EWS to infer this information was only possible via the somewhat technical detour of fitting a regression model to PlaSim-VECODEm-tr. A direct analysis of the model output, though technically possible, would have yielded inscrutable results as the requirements for EWS are not met. This restriction illustrates that applying EWS based tools of analysis to data of unknown origin is problematic. Instead, it should always be established if the conceptual framework of analysis is an adequate description of the processes which have generated the data. In the case of PlaSim-VECODE-tr, we have documented before that the large multiplicative noise is in conflict with this concept (Chapter 2). Although the green equilibria in PlaSim-VECODEm-eq disappear due to an instability at the corresponding hotspot, we therefore cannot draw a conclusion regarding the causality of the collapses in PlaSim-VECODEm-tr. There, the large variability eliminates the complex deterministic stability properties and the hotspots of the model are probably

much less focussed.

Another limitation of the hotspot detection method is the requirement of very long time series, a condition hardly to be fulfilled by complex earth system models. In our example system 3 in Section 3.2 we needed time series of the order of 10 000–100 000 time steps (the dynamic system's relaxation time being 5) to obtain robust results. In the case of our regression models the results are much more promising. Even in RM1 with its 52 state variables, the hotspot is detectable from several 100 to 1000 time steps, and is basically independent of parameter choices during the analysis. The reason is that the hotspots consist of one single element which is well separable from the others, in contrast to our idealised setting of 9 identical elements in Section 3.2.

It therefore seems possible that the hotspot detection method or related approaches can yield useful information on the susceptibility in other climate models.

Chapter 4

Conclusions

4.1 Summary of results

To summarise, we briefly readdress our leading research questions from Section 1.3:

(I) How do strategies for the detection of multistability perform in PlaSim-VECODE?

We have found that constructing a stability diagram from our uncoupled experiments yields misleading results regarding the number of stable equilibria. The most important reason is the spatial heterogeneity within the area under consideration. Furthermore, we conclude from our experiments with PlaSim-VECODEm-eq that the coupled model has multiple equilibria for mid-Holocene orbital forcing. Two solutions (green and desert state) are found by choosing different initial conditions in PlaSim-VECODEm-eq as this system is close to equilibrium due to small precipitation variability and the mode of coupling. Further evidence for this interpretation is provided by our regression models based on PlaSim-VECODEm-tr (Section 3.3), which verify the solutions found in PlaSim-VECODEm-eq. However, the sensitivity to initial conditions depends on the way of coupling: In PlaSim-VECODEm-tr the large variability allows only one possible steady state. Also for the reason of large variability, no hysteresis is obtained in PlaSim-VECODEm-tr when the orbital forcing is reversed in time. The shape of the pdf of vegetation cover is unimodal despite the multistability in PlaSim-VECODEm. The reason is that the timescale of vegetation dynamics directly depends on precipitation. The shape of the pdf does therefore not reflect the stability of the deterministic part of the system.

The nature of the model's variability is also the clue to our second question:

(II) What conclusions do these strategies allow regarding the possibility of a rapid transition?

Despite the lack of a static hysteresis or a multimodal pdf and despite the large climate variability there are vegetation collapses at different locations and at different times. Because of the non-linear relation between vegetation dynamics and precipitation the green state before each transition is initially stabilised by the high variability. When precipitation falls below a critical

threshold, the desert state is stabilised as variability is then also decreased. Our study with a one-dimensional stochastic model proves that this interaction between noise level and state of the system leads to a continuous but sudden change in the pdf when orbital forcing is varied. This large sensitivity to parameter changes in a certain regime is the stochastic analogy to a deterministic Tipping Point in the absence of a multistability. Therefore, transitivity and unimodality do not guarantee the absence of a Tipping Point. Due to the stochasticity the exact timing of the transition and its phenomenology are subject to chance. However, the likelihood of an abrupt change decreases with the strength of the atmosphere-vegetation feedback.

Finally, we have addressed the limitations and the potential of EWS with regard to spatial complexity by asking:

(III) How can EWS be applied to infer information on the structural stability of PlaSim-VECODE?

We have argued that in a general context like a complex climate system model, the critical subsystem that exhibits a loss in stability (hotspot) and the critical mode of the transition may be unknown. A detection of EWS at individual elements of a multidimensional-dimensional system can therefore fail when the local loss in stability is small as in cases of an induced tipping or collective multistability. However, EWS can therefore be applied as a diagnostic tool to find the hotspot of a sudden transition and to distinguish this hotspot from regions experiencing an induced tipping. For this purpose we have developed a stochastic algorithm to identify a hotspot as a certain combination of grid cells which maximises an EWS.

When applied to PlaSim-VECODEm by using a regression model, we have identified a hotspot of one particular grid cell for each vegetation collapse. We have demonstrated with additional experiments that the detected hotspots are indeed a particularly sensitive region in the model and have given a physical explanation for these results. The method can thus provide information on the causality of sudden transitions and may help to improve the knowledge on the vulnerability of certain subsystems in climate models.

4.2 Discussion

Our results as well as other studies can be brought into a broader context concerning the relation between a model's stability properties and its phenomenological behaviour (its response to initial conditions or external forcing, as well as its statistical properties). Our results demonstrate that this relation is crucially linked to spatial heterogeneity and the origin of temporal variability in the model. However, a complex climate model is usually built from fundamental laws and specific parameterisations, while spatial interactions and the nature of variability are emergent properties. It is thus a common situation in practice that these properties are not perfectly known. This is true especially if the model user is not the model developer. For the model user, the phenomenological behaviour is directly accessible and much easier to obtain than a complete mechanistic

Table 4.1: Uniqueness of strategies to detect multiple equilibria.

method	**model result**	**conclusion on existence of multiple stable equilibria**	**comments**
Construction of a stability diagram	several stable intersections	ambiguous	S1, T1
	only one stable intersection	ambiguous	S1, T1
Sensitivity to initial conditions	yes (intransitive)	yes	
	no (transitive)	ambiguous	S2, T3, T4, T5
Existence of static hysteresis	yes	yes	
	no	ambiguous	S3, T3, T4, T5
Probability density function of steady state	unimodal	ambiguous	T4, T5
	multimodal	ambiguous	T5

understanding. Essentially, the problem is similar to the inference of a data generating process from data of unknown origin.

We therefore illustrate what conclusions different methods of analysis can potentially allow regarding the existence of multiple equilibria (Table 4.1) and Tipping Points (Fig. 4.1). We also list several arguments with regard to spatial complexity (S) and different noise properties (T) which explain the possible ambiguities of this inference problem. The numeration in this list is reflected in Table 4.1 and Fig. 4.1.

Issues related to spatial heterogeneity and structural complexity:

S1. **Stability diagrams** are an unreliable tool for the detection of multiple equilibria in cases of spatial complexity (Section 2.4.1).

S2. Extreme **initial conditions** in phase space may not lie in different basins of attraction (Section 3.3.4.1), the identified equilibria may not be the only ones, and they could consist of several independent multiple equilibria (Dekker et al., 2010). In extreme cases, riddled basins of attraction may occur (Viana et al., 2009). Furthermore, the final state does not only depend on the initial condition, but also the intrinsic timescales of the system (Section 3.3.4.1).

S3. A **static hysteresis** is only found if a critical parameter is varied across a bifurcation point which involves the current state of the model and if the bifurcation is of catastrophic type (Thompson et al., 1994). Moreover, when an external parameter is varied in practice, a dynamic hysteresis is obtained (Bordi et al., 2012; Fraedrich, 2012). This can lead to drastic changes like in the case of a rate-induced tipping in a slow-fast dynamical system (Wieczorek et al., 2011; Ashwin et al., 2012) or if the system's state suddenly finds itself in another basin of attraction.

S4. **Indicators of slowing down (EWS)** may fail if the system's extent is ill-defined. The possibility of passive elements and collective bistabilities need to be addressed and can help to

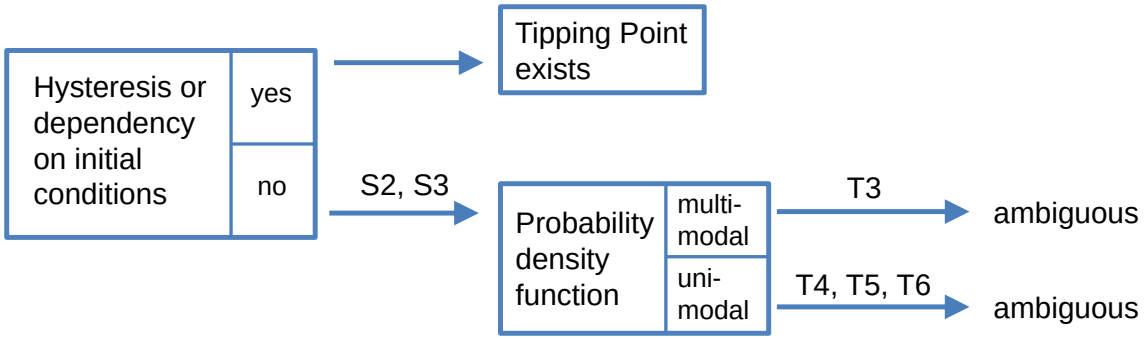

Figure 4.1: Inference of existing Tipping Points from other model properties.

Issues related to temporal variability (noise):

T1. As soon as the noise is not small anymore, the mean of a steady state is not identical to the deterministic equilibrium (Section 2.4.1). It is therefore problematic to infer the deterministic **stability diagram** from a steady state with variability.

T2. Also in all cases of substantial noise, **EWS** do not sample the local stability anymore and are not directly related to an eigenvalue of the deterministic system. Potential indicators can exist but are very system-specific (Section 3.2).

T3 – **Intermediate additive white noise.** Although the system's long-term behaviour is independent of the choice of initial conditions and shows no static hysteresis, the multimodal pdf will reveal the number (though not the position) of deterministic stable states (Horsthemke and Lefever, 1984). The abruptness of a forced transition then depends on the relation between the timescale of the external parameter change and the typical escape time (Thompson and Sieber, 2011a).

T4 – **Large additive white noise.** As before, the system is insensitive to initial conditions and lacking a static hysteresis. In addition, the pdf is unimodal and shows no Tipping Point (Horsthemke and Lefever, 1984; Liu et al., 2006) as the deterministic states are completely obliterated by the noise.

T5 – **Multiplicative white noise.** In case of sufficiently large noise, the system is transitive (independent of initial conditions) and cannot show a static hysteresis. However, as documented in Chapter 2, the multiplicative nature of the noise can lead to sudden changes in the pdf which results in a Tipping Point. The pdf does not allow direct conclusions with regard to multistability (Chapter 2; Liu, 2010).

T6 – **Additive red noise.** In the case of red noise, a Tipping Point can exist if the timescale of forcing is not too slow. This is even possible in case of a weak feedback (Liu et al., 2006).

Reverting the direction of reasoning in Fig. 4.1, the occurrence of a sudden transition does also not allow unique conclusions on a model's properties. First, a sudden transition may be the result of a large change in forcing or a large perturbation unrelated to a parameter change. Second, a Tipping Point may also exist when the feedback is not large enough to produce multiple equilibria. Third, a sudden transition in a particular time series can even occur in the absence of a large feedback due to intrinsic thresholds, red noise (Liu et al., 2006), or multiplicative white noise (Chapter 2), or even chance (though this is improbable in PlaSim-VECODE; Section 2.5.2). This stochasticity in PlaSim-VECODE and the related regression models also raises the question how much palaeoclimatic records can be expected to reveal on specific mechanisms. In our one-dimensional stochastic model it has become apparent that the existence and timing of a rebound or early collapse depends on the realisation. Unfortunately, reality only provides one realisation of the termination of the AHP. In this regard, a direct comparison between palaeoclimate proxies and model results is problematic. Furthermore, even a perfect knowledge on the phenomenology of the real transition could still allow for several interpretations. Hence, without any knowledge on the system's mechanisms and the nature of the fluctuations, one cannot infer the feedback from the transition's abruptness.

Returning to climate modelling, our compilation of results documents that apparently contradictory results can be obtained when different methods are applied to a model. It therefore seems problematic to infer anything on multistability on the basis of one particular method. Instead, only an appropriate combination of methods can provide knowledge on the intrinsic properties of a complex climate model. To this end, the specific advantages and disadvantages of methods should be taken into account. For example, in cases of small noise and long time series indicators of slowing down can be applied to investigate whether a sudden transition is due to a loss in stability or rather due to a threshold-behaviour or a random perturbation. In contrast, EWS can also indicate a loss in stability in the absence of a Tipping Point (*safe bifurcation*; Thompson et al., 1994). In cases of large noise, the phenomenology of a sudden transition such as the potential overlapping of states can provide suggestions as to the nature of the variability. As documented in

Section 3.3, a regression can contribute to the full picture, if the results are statistically robust and if there is sufficient knowledge on the model's structure. As we have shown in Chapter 2, an asynchronous coupling of models, although originally invented primarily due to technical limitations, can also be a fruitful strategy of analysis.

In addition, a fundamental mechanistic understanding is crucial to explain model results, and the methods of analysis discussed in this thesis can only provide a complementary but no exclusive strategy. It must also be considered that our list of methods and cases is by no means complete: The interaction of noise with the slow variables of a system may give rise to phenomena that are not addressed in this thesis, and global bifurcations for which EWS cannot be applied can also exist in climate models (Simonnet et al., 2009). Moreover, our discussion is mostly restricted to systems which can be separated into a slow deterministic part (involving stable fixed points) and a fast stochastic part. If this is not the case, the task to determine the generating process behind the time series becomes much more difficult. For example, even the cosine produced by a simple linear equation yields a bimodal pdf. At the other extreme of complexity, chaotic dynamics can give rise to a vast number of phenomena such as the existence of multiple regimes or sudden state changes related to intermittency, which arise from the intrinsic dynamics and do not require any external parameter perturbations.

4.3 Research perspectives

It is often stated that current earth system models do not show the multiple equilibria that have been found in simpler models in the past, at least for the MOC (Drijfhout et al., 2010), North African vegetation cover (Brovkin et al., 2009) and Arctic sea ice cover (Notz, 2009; Tietsche et al., 2011). Our conclusions illustrate that there is no fail-proof method for the detection of multiple equilibria in complex climate models. This fact could well be one reason for the failure to find multistabilities in modern ESMs, where potential multistabilities are much harder to reveal.

To test this speculation, more studies involving a variety of methods are required. In addition to the methods addressed in this thesis, other numerical methods of bifurcation analysis such as continuation methods (Dijkstra, 2007; Simonnet et al., 2009; den Toom et al., 2012) can be useful, and all methods should be supplemented with a thorough mechanistic understanding of a model's properties. In particular, it needs to be established how the fast variability interacts with the slower parts of the system and what determines the spectral properties of the variables under consideration. If their applicability can thus be established, EWS may play a role in identifying the structural stability of climate models. To this end, more systematic studies on the performance of EWS in different model frameworks would be beneficial as previous modelling studies on EWS have been based on only a few principle models such as logistic growth equations to describe population dynamics (May, 1977) or ocean circulation models of intermediate complexity to simulate changes in the MOC (Held and Kleinen, 2004; Livina and Lenton, 2007; Lenton et al., 2009).

We consider the application of EWS analysis to climate observations or proxies where the generating processes are badly understood as particularly problematic. In many cases, the system under consideration may be too badly understood to establish the validity of the concept (Hastings and Wysham, 2010; Dakos et al., 2011). For example, the phenomenology of Dansgaard-Oeschger events (Crucifix, 2012) and glacial cycles (de Saedeleer et al., 2012) can be reproduced by a number of different dynamical systems. An increase in autocorrelation of temperature fluctuations may then be completely unrelated to the phenomenon of slowing down. An increase in mixed layer depth (T. M. Lenton, personal communication) or the interactive timescale of grass in VECODE provide simple examples. In addition, changes in the spectrum of the externally imposed perturbations have to be considered (Scheffer et al., 2009).

The use of EWS in the case of climate records is also limited by a lack of statistical significance and robustness (Dakos et al., 2008; Lenton et al., 2012a,b), the question of spatial complexity (particularly in the case of single proxy records), irregular sampling and dating uncertainties. If EWS were to be used as a method to predict sudden changes, a reference system would be needed, as it is otherwise unknown what maximum signal is to be expected, what constitutes the external forcing to the tipping element and how this forcing will evolve in the future.

We therefore argue that the promise of an Early Warning System for Tipping Points based on a general *toolbox* cannot be fulfilled. The application of EWS in a diagnostic framework, although less popular, may therefore be more promising. Our hotspot detection algorithm provides one example in this direction and could potentially be applied to other problems such as fluctuations of sea ice cover close to a snowball earth instability. However, other methods with better performance or a more stringent logic in terms of a physical interpretation may provide alternatives in the future.

In order to link such studies with fast (and thus rather simple) climate models to the real climate system, a model hierarchy (as promoted by Ghil, 2001; Claussen et al., 2002; Fraedrich, 2012, and others) is required. In such a setting it will be a crucial challenge to establish that the essential stability properties carry over from complex to simple models and that they also represent reality adequately (for example by using data assimilation).

As to the nature of the real termination of the AHP and the role of the atmosphere-vegetation feedback, the possibilities to resolve this issue seem limited. First, palaeoclimate and palaeovegetation data for model evaluation are sparse, and will remain sparse as the North African soils from the mid-Holocene have been eroded away. Second, the number of possible hypotheses is not easy to be reduced. Even in the absence of stochastic effects addressed in the previous section, spatial heterogeneity could have influenced the timing of the transition at different locations. In PlaSim-VECODEm-tr, the two collapses in different areas are most probably a result of the low model resolution. However, local characteristics such as topography are important for the establishment of vegetation (Waller et al., 2007) and could have produced a similar effect in reality.

It has been argued by Williams et al. (2011) that the asynchronous termination of the AHP at different sites suggests a weak atmosphere-vegetation feedback in North Africa. In the light of the

arguments presented above this is not a compelling deduction. Although the spatial heterogeneity does suggest a weak coupling between sites, the possibility of strong feedbacks on smaller than continental or regional scales, in similarity to the hotspots in Chapter 3, cannot be excluded. The modelling of reaction-diffusion equations on heterogenous grids by van Nes and Scheffer (2005), Donangelo et al. (2010) and Dakos et al. (2010) provide simple examples of such desynchronised tippings. There is also evidence from models and observations that small-scale feedbacks between vegetation and environmental conditions, such as water and nutrient availability, can play an important role in the determination of critical thresholds and the formation of vegetation patterns on a larger scale (von Hardenberg et al., 2001; Kéfi et al., 2007; Rietkerk et al., 2002, 2004; Rietkerk and van de Koppel, 2008). We therefore agree with Scheffer et al. (2005) and Rietkerk et al. (2011) that such ecological feedbacks and their potential impact on larger scales should be further investigated. However, our results indicate that the role of temporal variability needs to be addressed also in the context of small-scale feedbacks.

Bibliography

Alley, R. B., Marotzke, J., Nordhaus, W. D., Overpeck, J. T., Peteet, D. M., Pielke Jr., R. A., Pierrehumbert, R. T., Rhines, P. B., Stocker, T. F., Talley, L. D., and Wallace, J. M.: Abrupt Climate Change, Science, 299, 2005–2010, doi:10.1126/science.1081056, 2003.

Andersson, A., Bakan, S., and Grassl, H.: Satellite derived precipitation and freshwater flux variability and its dependence on the North Atlantic Oscillation, Tellus A, 62, 453–468, doi: 10.1111/j.1600-0870.2010.00458.x, 2010.

Ashwin, P., Wieczorek, S., Vitolo, R., and Cox, P.: Tipping points in open systems: bifurcation, noise-induced and rate-dependent examples in the climate system, Phil. Trans. R. Soc. A, 370, 1166–1184, doi:10.1098/rsta.2011.0306, 2012.

Berglund, N. and Gentz, B.: Noise-Induced Phenomena in Slow-Fast Dynamical Systems. A Sample-Paths Approach, Springer, 2006.

Bordi, I., Fraedrich, K., Sutera, A., and Zhu, X.: Transient response to well-mixed greenhouse gas changes, Theor. Appl. Climatol., 109, 245–252, doi:10.1007/s00704-011-0580-z, 2012.

Botev, Z. I., Grotowski, J. F., and Kroese, D. P.: Kernel density estimation via diffusion, Ann. Stat., 38, 2916–2957, doi:10.1214/10-AOS799, 2010.

Braconnot, P., Joussaume, S., Marti, O., and de Noblet, N.: Synergistic feedbacks from ocean and vegetation on the African Monsoon response to Mid-Holocene insolation, Geophys. Res. Lett., 26, 2481–2484, doi:10.1029/1999GL006047, 1999.

Braconnot, P., Otto-Bliesner, B., Harrison, S., Joussaume, S., Peterchmitt, J. Y., Abe-Ouchi, A., Crucifix, M., Driesschaert, E., Fichefet, T., Hewitt, C. D., Kageyama, M., Kitoh, A., Laine, A., Loutre, M. F., Marti, O., Merkel, U., Ramstein, G., Valdes, P., Weber, S. L., Yu, Y., and Zhao, Y.: Results of PMIP2 coupled simulations of the mid-Holocene and Last Glacial Maximum - Part 1: experiments and large-scale features, Clim. Past, 3, 261–277, doi:10.5194/cp-3-261-2007, 2007a.

Braconnot, P., Otto-Bliesner, B., Harrison, S., Joussaume, S., Peterchmitt, J.-Y., Abe-Ouchi, A., Crucifix, M., Driesschaert, E., Fichefet, T., Hewitt, C. D., Kageyama, M., Kitoh, A., Loutre, M.-F., Marti, O., Merkel, U., Ramstein, G., Valdes, P., Weber, L., Yu, Y., and Zhao, Y.: Results of PMIP2 coupled simulations of the Mid-Holocene and Last Glacial Maximum – Part 2: feedbacks with emphasis on the location of the ITCZ and mid- and high latitudes heat budget, Clim. Past, 3, 279–296, doi:10.5194/cp-3-279-2007, 2007b.

Brock, W. A. and Carpenter, S. R.: Interacting regime shifts in ecosystems: implication for early warnings, Ecol. Monogr., 80, 353–367, doi:10.1890/09-1824.1, 2010.

Brovkin, V., Ganopolski, A., and Svirezhev, Y.: A continuous climate-vegetation classification for use in climate-biosphere studies, Ecol. Model., 101, 251–261, doi:10.1016/S0304-3800(97)00049-5, 1997.

Brovkin, V., Claussen, M., Petoukhov, V., and Ganopolski, A.: On the stability of the atmosphere-vegetation system in the Sahara/Sahel region, J. Geophys. Res.-Atmos., 103, 31 613–31 624, doi:10.1029/1998JD200006, 1998.

Brovkin, V., Bendtsen, J., Claussen, M., Ganopolski, A., Kubatzki, C., Petoukhov, V., and Andreev, A.: Carbon cycle, vegetation, and climate dynamics in the Holocene: experiments with the CLIMBER-2 Model, Global Biogeochem. Cy., 16, 1139, doi:10.1029/2001GB001662, 2002.

Brovkin, V., Levis, S., Loutre, M. F., Crucifix, M., Claussen, M., Ganopolski, A., Kubatzki, C., and Petoukhov, V.: Stability analysis of the climate-vegetation system in the northern high latitudes, Climatic Change, 57, 119–138, doi:10.1023/A:1022168609525, 2003.

Brovkin, V., Raddatz, T., Reick, C. H., Claussen, M., and Gayler, V.: Global biogeophysical interactions between forest and climate, Geophys. Res. Lett., 36, L07 405, doi:10.1029/2009GL037543, 2009.

Budyko, M. I.: The effect of solar radiation variations on the climate of the earth, Tellus, 21, 611–619, doi:10.1111/j.2153-3490.1969.tb00466.x, 1969.

Carpenter, S. R. and Brock, W. A.: Rising variance: a leading indicator of ecological transition, Ecol. Lett., 9, 308–315, doi:10.1111/j.1461-0248.2005.00877.x, 2006.

Carpenter, S. R., Cole, J. J., Pace, M. L., Batt, R., Brock, W. A., Cline, T., Coloso, J., Hodgson, J. R., Kitchell, J. F., Seekell, D. A., Smith, L., and Weidel, B.: Early warnings of regime shifts: a whole-ecosystem experiment, Science, 332, 1079–1082, doi:10.1126/science.1203672, 2011.

Charney, J., Stone, P. H., and Quirk, W. J.: Drought in Sahara: a biogeophysical feedback mechanism, Science, 187, 434–435, doi:10.1126/science.187.4175.434, 1975.

Charney, J., Quirk, W., Chow, S., and Kornfield, J.: A comparative study of the effects of albedo change on drought in semi-arid regions, J. Atmos. Sci., 34, 1366—1385, doi:10.1175/1520-0469(1977)034<1366:ACSOTE>2.0.CO;2, 1977.

Charney, J. G.: Dynamics of deserts and drought in the Sahel, Q. J. Roy. Meteor. Soc., 101, 193–202, doi:10.1002/qj.49710142802, 1975.

Claussen, M.: On coupling global biome models with climate models, Clim. Res., 4, 203–221, doi:10.3354/cr004203, 1994.

Claussen, M.: Modeling bio-geophysical feedback in the African and Indian monsoon region, Clim. Dynam., 13, 247–257, doi:10.1007/s003820050164, 1997.

Claussen, M.: On multiple solutions of the atmosphere-vegetation system in present-day climate, Global Change Biol., 4, 549–559, doi:10.1046/j.1365-2486.1998.t01-1-00122.x, 1998.

Claussen, M.: Holocene rapid land cover change - evidence and theory, in: Natural Climate Variability and Global Warming, edited by Battarbee, R. and Binney, H., pp. 232–253, Blackwell Publishing, 2008.

Claussen, M.: Late Quaternary vegetation-climate feedbacks, Clim. Past, 5, 203–216, doi:10.5194/cp-5-203-2009, 2009.

Claussen, M., Kubatzki, C., Brovkin, V., Ganopolski, A., Hoelzmann, P., and Pachur, H. J.: Simulation of an abrupt change in Saharan vegetation in the mid-Holocene, Geophys. Res. Lett., 26, 2037–2040, doi:10.1029/1999GL900494, 1999.

Claussen, M., Mysak, L. A., Weaver, A. J., Crucifix, M., Fichefet, T., Loutre, M. F., Weber, S. L., Alcamo, J., Alexeev, V. A., Berger, A., Calov, R., Ganopolski, A., Goosse, H., Lohmann, G., Lunkeit, F., Mokhov, I. I., Petoukhov, V., Stone, P., and Wang, Z.: Earth System Models of Intermediate Complexity: closing the gap in the spectrum of climate system models, Clim. Dynam., 18, 579–586, doi:10.1007/s00382-001-0200-1, 2002.

Collins, M. R. and Teh, H. C.: Neutron-scattering observations of critical slowing down of an Ising system, Phys. Rev. Lett., 30, 781–784, doi:10.1103/PhysRevLett.30.781, 1973.

Contamin, R. and Ellison, A. M.: Indicators of regime shifts in ecological systems: What do we need to know and when do we need to know it?, Ecol. Appl., 19, 799–816, doi:10.1890/08-0109.1, 2009.

Crucifix, M.: Oscillators and relaxation phenomena in Pleistocene climate theory, Phil. Trans. R. Soc. A, 370, 1140–1165, doi:10.1098/rsta.2011.0315, 2012.

Dakos, V., Scheffer, M., van Nes, E. H., Brovkin, V., Petoukhov, V., and Held, H.: Slowing down as an early warning signal for abrupt climate change, P. Natl. Acad. Sci. USA, 105, 14 308–14 312, doi:10.1073/pnas.0802430105, 2008.

Dakos, V., van Nes, E. H., Donangelo, R., Fort, H., and Scheffer, M.: Spatial correlation as leading indicator of catastrophic shifts, Theor. Ecol., 3, 163–174, doi:10.1007/s12080-009-0060-6, 2010.

Dakos, V., Kefi, S., Rietkerk, M., van Nes, E. H., and Scheffer, M.: Slowing down in spatially patterned ecosystems at the brink of collapse, Am. Nat., 177, E153–E166, doi:10.1086/659945, 2011.

Dakos, V., van Nes, E. H., D'Odorico, P., and Scheffer, M.: Robustness of variance and autocorrelation as indicators of critical slowing down, Ecology, 93, 264–271, doi:10.1890/11-0889.1, 2012.

de Saedeleer, B., Crucifix, M., and Wieczorek, S.: Is the astronomical forcing a reliable and unique pacemaker for climate? A conceptual model study, Clim. Dynam., online at http://dx.doi.org/10.1007/s00382-012-1316-1, doi:10.1007/s00382-012-1316-1, 2012.

Dekker, S. C., de Boer, H. J., Brovkin, V., Fraedrich, K., Wassen, M. J., and Rietkerk, M.: Biogeophysical feedbacks trigger shifts in the modelled vegetation-atmosphere system at multiple scales, Biogeosciences, 7, 1237–1245, doi:10.5194/bg-7-1237-2010, 2010.

deMenocal, P., Ortiz, J., Guilderson, T., Adkins, J., Sarnthein, M., Baker, L., and Yarusinsky, M.: Abrupt onset and termination of the African Humid Period: rapid climate responses to gradual insolation forcing, Quaternary Sci. Rev., 19, 347–361, doi:10.1016/S0277-3791(99)00081-5, 2000.

den Toom, M., Dijkstra, H. A., Cimatoribus, A. A., and Drijfhout, S. S.: Effect of atmospheric feedbacks on the stability of the atlantic meridional overturning circulation, J. Climate, 25, 4081–4096, doi:10.1175/JCLI-D-11-00467.1, 2012.

Dijkstra, H. A.: Characterization of the multiple equilibria regime in a global ocean model, Tellus A, 59, 695–705, doi:10.1111/j.1600-0870.2007.00267.x, 2007.

Ditlevsen, P. D. and Johnsen, S. J.: Tipping points: early warning and wishful thinking, Geophys. Res. Lett., 37, L19 703, doi:10.1029/2010GL044486, 2010.

d'Odorico, P., Laio, F., and Ridolfi, L.: Noise-induced stability in dryland plant ecosystems, P. Natl. Acad. Sci. USA, 102, 10 819–10 822, doi:10.1073/pnas.0502884102, 2005.

Donangelo, R., Fort, H., Dakos, V., Scheffer, M., and Van Nes, E. H.: Early warnings for catastrophic shifts in ecosystems: comparison between spatial and temporal indicators, Int. J. Bifurcat. Chaos, 20, 315–321, doi:10.1142/S0218127410025764, 2010.

Drake, J. M. and Griffen, B. D.: Early warning signals of extinction in deteriorating environments, Nature, 467, 456–459, doi:10.1038/nature09389, 2010.

Drijfhout, S. S., Weber, S. L., and van der Swaluw, E.: The stability of the MOC as diagnosed from model projections for pre-industrial, present and future climates, Clim. Dynam., doi:10.1007/s00382-010-0930-z, 2010.

Efron, B.: 1977 Rietz Lecture - Bootstrap Methods - Another Look At the Jackknife, Ann. Stat., 7, 1–26, doi:10.1214/aos/1176344552, 1979.

Fraedrich, K.: Structural and stochastic analysis of a zero-dimensional climate system, Q. J. Roy. Meteor. Soc., 104, 461–474, doi:10.1002/qj.49710444017, 1978.

Fraedrich, K.: Catastrophes and resilience of a zero-dimensional climate system with ice-albedo and greenhouse feedback, Q. J. Roy. Meteor. Soc., 105, 147–167, doi:10.1002/qj.49710544310, 1979.

Fraedrich, K.: A suite of user-friendly global climate models: hysteresis experiments, Eur. Phys. J. Plus., 127, doi:10.1140/epjp/i2012-12053-7, 2012.

Fraedrich, K., Kleidon, A., and Lunkeit, F.: A green planet versus a desert world: estimating the effect of vegetation extremes on the atmosphere, J. Climate, 12, 3156–3163, doi:10.1175/1520-0442(1999)012<3156:AGPVAD>2.0.CO;2, 1999.

Fraedrich, K., Jansen, H., Kirk, E., Luksch, U., and Lunkeit, F.: The Planet Simulator: towards a user friendly model, Meteorol. Z., 14, 299–304, doi:10.1127/0941-2948/2005/0043, 2005a.

Fraedrich, K., Jansen, H., Kirk, E., and Lunkeit, F.: The Planet Simulator: green planet and desert world, Meteorol. Z., 14, 305–314, doi:10.1127/0941-2948/2005/0044, 2005b.

Ganopolski, A., Kubatzki, C., Claussen, M., Brovkin, V., and Petoukhov, V.: The Influence of vegetation-atmosphere-ocean interaction on climate during the mid-Holocene, Science, 280, 1916–1919, doi:10.1126/science.280.5371.1916, 1998.

Gasse, F.: Diatom-inferred salinity and carbonate oxygen isotopes in Holocene waterbodies of the western Sahara and Sahel (Africa), Quaternary Sci. Rev., 21, 737–767, doi:10.1016/S0277-3791(01)00125-1, 2002.

Ghil, M.: Hilbert problems for the geosciences in the 21st century, Nonlin. Processes Geophys., 8, 211–222, doi:10.5194/npg-8-211-2001, 2001.

Goessling, H. F. and Reick, C. H.: What do moisture recycling estimates tell us? Exploring the extreme case of non-evaporating continents, Hydrol. Earth Syst. Sc., 15, 3217–3235, doi:10.5194/hess-15-3217-2011, 2011.

Guckenheimer, J. and Holmes, P.: Nonlinear Oscillations, Dynamical Systems, and Bifurcations of Vector Fields, vol. 42 of *Applied Mathematical Sciences*, Springer, 2 edn., 1983.

Guttal, V. and Jayaprakash, C.: Impact of noise on bistable ecological systems, Ecol. Model., 201, 420–428, doi:10.1016/j.ecolmodel.2006.10.005, 2007.

Guttal, V. and Jayaprakash, C.: Changing skewness: an early warning signal of regime shifts in ecosystems, Ecol. Lett., 11, 450–460, doi:10.1111/j.1461-0248.2008.01160.x, 2008.

Guttal, V. and Jayaprakash, C.: Spatial variance and spatial skewness: leading indicators of regime shifts in spatial ecological systems, Theor. Ecol., 2, 3–12, doi:10.1007/s12080-008-0033-1, 2009.

Hagemann, S.: An improved land surface parameter dataset for global and regional climate models, Tech. Rep. 336, Max-Planck-Institut für Meteorologie, 2002.

Hales, K., Neelin, J. D., and Zeng, N.: Sensitivity of tropical land climate to leaf area index: role of surface conductance versus albedo, J. Climate, 17, 1459–1473, doi:10.1175/1520-0442(2004)017<1459:SOTLCT>2.0.CO;2, 2004.

Hasselmann, K.: Stochastic climate models. Part I. Theory, Tellus, 28, 473–485, doi: 10.1111/j.2153-3490.1976.tb00696.x, 1976.

Hastings, A. and Wysham, D. B.: Regime shifts in ecological systems can occur with no warning, Ecol. Lett., 13, 464–472, doi:10.1111/j.1461-0248.2010.01439.x, 2010.

Held, H. and Kleinen, T.: Detection of climate system bifurcations by degenerate fingerprinting, Geophys. Res. Lett., 31, L23 207, doi:10.1029/2004GL020972, 2004.

Hoelzmann, P., Jolly, D., Harrison, S. P., Laarif, F., Bonnefille, R., Pachur, H.-J., and TEMPO: Mid-Holocene land-surface conditions in northern Africa and the Arabian Peninsula: a data set for the analysis of biogeophysical feedbacks in the climate system, Global Biogeochem. Cycles, 12, 35–51, doi:10.1029/97GB02733, 1998.

Horsthemke, W. and Lefever, R.: Noise-Induced Transitions, Springer, 1984.

Hély, C., Braconnot, P., Watrin, J., and Zheng, W.: Climate and vegetation: simulating the African humid period, CR. Geosci., 341, 671–688, doi:10.1016/j.crte.2009.07.002, 2009.

Irizarry-Ortiz, M. M., Wang, G. L., and Eltahir, E. A. B.: Role of the biosphere in the mid-Holocene climate of West Africa, J. Geophys. Res.-Atmos., 108(D2), 4042, doi: 10.1029/2001JD000989, 2003.

Jolly, D., Harrison, S., Damnati, B., and Bonnefille, R.: Simulated climate and biomes of Africa during the late quaternary: comparison with pollen and lake status data, Quaternary Sci. Rev., 17, 629–657, doi:10.1016/S0277-3791(98)00015-8, 1998a.

Jolly, D., Prentice, I. C., Bonnefille, R., Ballouche, A., Bengo, M., Brenac, P., Buchet, G., Burney, D., Cazet, J.-P., Cheddadi, R., Edorh, T., Elenga, H., Elmoutaki, S., Guiot, J., Laarif, F., Lamb, H., Lezine, A.-M., Maley, J., Mbenza, M., Peyron, O., Reille, M., Reynaud-Farrera, I., Riollet, G., Ritchie, J. C., Roche, E., Scott, L., Ssemmanda, I., Straka, H., Umer, M., Van Campo, E., Vilimumbalo, S., Vincens, A., and Waller, M.: Biome reconstruction from pollen and plant macrofossil data for Africa and the Arabian peninsula at 0 and 6000 years, J. Biogeogr., 25, 1007–1027, doi:10.1046/j.1365-2699.1998.00238.x, 1998b.

Kleinen, T., Held, H., and Petschel-Held, G.: The potential role of spectral properties in detecting thresholds in the Earth system: application to the thermohaline circulation, Ocean Dynam., 53, 53–63, doi:10.1007/s10236-002-0023-6, 2003.

Kroepelin, S., Verschuren, D., Lezine, A. . M., Eggermont, H., Cocquyt, C., Francus, P., Cazet, J. . P., Fagot, M., Rumes, B., Russell, J. M., Darius, F., Conley, D. J., Schuster, M., von Suchodoletz, H., and Engstrom, D. R.: Climate-driven ecosystem succession in the Sahara: the past 6000 years, Science, 320, 765–768, doi:10.1126/science.1154913, 2008.

Kuehn, C.: A mathematical framework for critical transitions: bifurcations, fast-slow systems and stochastic dynamics, Physica D, 240, 1020–1035, doi:10.1016/j.physd.2011.02.012, 2011.

Kutzbach, J. E.: Monsoon climate of the early Holocene: climate experiment with the earth's orbital parameters for 9000 years ago, Science, 214, 59–61, doi:10.1126/science.214.4516.59, 1981.

Kutzbach, J. E. and Liu, Z.: Response of the African monsoon to orbital forcing and ocean feedbacks in the middle Holocene, Science, 278, 440–443, doi:10.1126/science.278.5337.440, 1997.

Kéfi, S., Rietkerk, M., Alados, C. L., Pueyo, Y., Papanastasis, V. P., ElAich, A., and de Ruiter, P. C.: Spatial vegetation patterns and imminent desertification in Mediterranean arid ecosystems, Nature, 449, 213–217, doi:10.1038/nature06111, 2007.

Lenton, T. M.: Early warning of climate tipping points, Nature Clim. Change, 1, 201–209, doi:10.1038/NCLIMATE1143, 2011.

Lenton, T. M., Held, H., Kriegler, E., Hall, J. W., Lucht, W., Rahmstorf, S., and Schellnhuber, H. J.: Tipping elements in the Earth's climate system, P. Natl. Acad. Sci. USA, 105, 1786–1793, doi:10.1073/pnas.0705414105, 2008.

Lenton, T. M., Myerscough, R. J., Marsh, R., Livina, V. N., Price, A. R., and Cox, S. J.: Using GENIE to study a tipping point in the climate system, Phil. Trans. R. Soc. A, 367, 871–884, doi:10.1098/rsta.2008.0171, 2009.

Lenton, T. M., Livina, V. N., Dakos, V., and Scheffer, M.: Climate bifurcation during the last deglaciation?, Clim. Past, 8, 1127–1139, doi:10.5194/cp-8-1127-2012, 2012a.

Lenton, T. M., Livina, V. N., Dakos, V., van Nes, E. H., and Scheffer, M.: Early warning of climate tipping points from critical slowing down: comparing methods to improve robustness, Phil. Trans. R. Soc. A, 370, 1185–1204, doi:10.1098/rsta.2011.0304, 2012b.

Levis, S., Foley, J. A., Brovkin, V., and Pollard, D.: On the stability of the high-latitude climate-vegetation system in a coupled atmosphere-biosphere model, Global Ecol. Biogeogr., 8, 489–500, doi:10.1046/j.1365-2699.1999.00168.x, 1999.

Liu, Z., Gallimore, R. G., Kutzbach, J. E., Xu, W., Golubev, Y., Behling, P., and Selin, R.: Modeling long-term climate changes with equilibrium asynchronous coupling, Clim. Dynam., 15, 325–340, doi:10.1007/s003820050285, 1999.

Liu, Z., Otto-Bliesner, B., Kutzbach, J., Li, L., and Shields, C.: Coupled climate simulation of the evolution of global monsoons in the Holocene, J. Climate, 16, 2472–2490, doi:10.1175/1520-0442(2003)016<2472:CCSOTE>2.0.CO;2, 2003.

Liu, Z., Harrison, S. P., Kutzbach, J., and Otto-Bliesner, B.: Global monsoons in the mid-Holocene and oceanic feedback, Clim. Dynam., 22, 157–182, doi:10.1007/s00382-003-0372-y, 2004.

Liu, Z., Wang, Y., Gallimore, R., Gasse, F., Johnson, T., deMenocal, P., Adkins, J., Notaro, M., Prenticer, I. C., Kutzbach, J., Jacob, R., Behling, P., Wang, L., and Ong, E.: Simulating the transient evolution and abrupt change of Northern Africa atmosphere-ocean-terrestrial ecosystem

in the Holocene, Quaternary Sci. Rev., 26, 1818–1837, doi:10.1016/j.quascirev.2007.03.002, 2007.

Liu, Z. Y.: Bimodality in a monostable climate-ecosystem: the role of climate variability and soil moisture memory, J. Climate, 23, 1447–1455, doi:10.1175/2009JCLI3183.1, 2010.

Liu, Z. Y., Wang, Y., Gallimore, R., Notaro, M., and Prentice, I. C.: On the cause of abrupt vegetation collapse in North Africa during the Holocene: climate variability vs. vegetation feedback, Geophys. Res. Lett., 33, L22 709, doi:10.1029/2006GL028062, 2006.

Livina, V. N. and Lenton, T. M.: A modified method for detecting incipient bifurcations in a dynamical system, Geophys. Res. Lett., 34, L03 712, doi:10.1029/2006GL028672, 2007.

Livina, V. N., Kwasniok, F., and Lenton, T. M.: Potential analysis reveals changing number of climate states during the last 60 kyr, Clim. Past, 6, 77–82, doi:10.5194/cp-6-77-2010, 2010.

Lézine, A. M.: Timing of vegetation changes at the end of the Holocene Humid Period in desert areas at the northern edge of the Atlantic and Indian monsoon systems, C. R. Geosci., 341, 750–759, doi:10.1016/j.crte.2009.01.001, 2009.

Lézine, A.-M., Hély, C., Grenier, C., Braconnot, P., and Krinner, G.: Sahara and Sahel vulnerability to climate changes, lessons from Holocene hydrological data, Quaternary Sci. Rev., 30, 3001–3012, doi:10.1016/j.quascirev.2011.07.006, 2011a.

Lézine, A.-M., Zheng, W., Braconnot, P., and Krinner, G.: Late Holocene plant and climate evolution at Lake Yoa, northern Chad: pollen data and climate simulations, Clim. Past, 7, 1351–1362, doi:10.5194/cp-7-1351-2011, 2011b.

Marzin, C. and Braconnot, P.: Variations of Indian and African monsoons induced by insolation changes at 6 and 9.5 kyr BP, Clim. Dynam., 33, 215–231, doi:10.1007/s00382-009-0538-3, 2009.

May, R. M.: Thresholds and breakpoints in ecosystems with a multiplicity of stable states, Nature, 269, 471–477, doi:10.1038/269471a0, 1977.

Meehl, G. A., Stocker, T. F., Collins, W. D., Friedlingstein, P., Gaye, A. T., Gregory, J. M., Kitoh, A., Knutti, R., Murphy, J. M., Noda, A., Raper, S. C. B., Watterson, I. G., Weaver, A. J., and Zhao, Z.-C.: Global Climate Projections. In: Climate Change 2007: The Physical Science Basis. Contribution of Working Group I to the Fourth Assessment Report of the Intergovernmental Panel on Climate Change [Solomon, S., Qin, D., Manning, M., Chen, Z., Marquis, M., Averyt, K. B., Tignor, M. and Miller, H. L. (eds.)], Cambridge University Press, 2007.

Nicholson, S. E.: A revised picture of the structure of the "monsoon" and land ITCZ over West Africa, Clim. Dynam., 32, 1155–1171, doi:10.1007/s00382-008-0514-3, 2009.

North, G. R., Cahalan, R. F., and Coakley Jr., J. A.: Energy balance climate models, Rev. Geophys., 19, 91–121, doi:10.1029/RG019i001p00091, 1981.

Notaro, M., Wang, Y., Liu, Z., Gallimore, R., and Levis, S.: Combined statistical and dynamical assessment of simulated vegetation-rainfall interactions in North Africa during the mid-Holocene, Global Change Biol., 14, 347–368, doi:10.1111/j.1365-24866.2007.001495.x, 2008.

Notz, D.: The future of ice sheets and sea ice: between reversible retreat and unstoppable loss, P. Natl. Acad. Sci. USA, 106, 20 590–20 595, doi:10.1073/pnas.0902356106, 2009.

Otterman, J.: Baring high-albedo soils by overgrazing: a hypothesized desertification mechanism, Science, 186, 531–533, doi:10.1126/science.186.4163.531, 1974.

Oyama, M. D. and Nobre, C. A.: A new climate-vegetation equilibrium state for tropical South America, Geophys. Res. Lett., 30, CLM5–1–4, doi:10.1029/2003GL018600, 2003.

Patricola, C. M. and Cook, K. H.: Dynamics of the West African monsoon under mid-Holocene precessional forcing: regional climate model simulations, J. Climate, 20, 694–716, doi:10.1175/JCLI4013.1, 2007.

Patricola, C. M. and Cook, K. H.: Atmosphere/vegetation feedbacks: a mechanism for abrupt climate change over northern Africa, J. Geophys. Res.-Atmos., 113, D18 102, doi:10.1029/2007JD009608, 2008.

Petit-Maire, N. and Riser, J.: Holocene lake deposits and palaeoenvironments in Central Sahara, Northeastern Mali, Palaeogeogr. Palaeocl., 35, 45–61, doi:10.1016/0031-0182(81)90093-6, 1981.

Pierrehumbert, R. T.: Principles of Planetary Climate, Cambridge University Press, 2010.

Pinty, B., Roveda, F., Verstraete, M. M., Gobron, N., Govaerts, Y., Martonchik, J. V., Diner, D. J., and Kahn, R. A.: Surface albedo retrieval from Meteosat - 2. Applications, J. Geophys. Res.-Atmos., 105, 18 113–18 134, doi:10.1029/2000JD900114, 2000.

Politis, D. N.: The impact of bootstrap methods on time series analysis, Stat. Sci., 18, 219–230, doi:10.1214/ss/1063994977, 2003.

Prentice, I. C., Jolly, D., and participants, B. .: Mid-Holocene and glacial-maximum vegetation geography of the northern continents and Africa, J. Biogeogr., 27, 507–519, doi:10.1046/j.1365-2699.2000.00425.x, 2000.

Priestley, M. B.: Spectral Analysis and Time Series. Volume 1: Univariate Series, Academic Press, 1981.

Renssen, H., Brovkin, V., Fichefet, T., and Goosse, H.: Holocene climate instability during the termination of the African Humid Period, Geophys. Res. Lett., 30, 1184, doi:10.1029/2002GL016636, 2003.

Renssen, H., Brovkin, V., Fichefet, T., and Goosse, H.: Simulation of the Holocene climate evolution in Northern Africa: the termination of the African Humid Period, Quatern. Int., 150, 95–102, doi:10.1016/j.quaint.2005.01.001, 2006.

Rietkerk, M. and van de Koppel, J.: Regular pattern formation in real ecosystems, Trends Ecol. Evol., 23, 169–175, doi:10.1016/j.tree.2007.10.013, 2008.

Rietkerk, M., Stroosnijder, L., Prins, H., and Ketner, P.: Sahelian rangeland development: a catastrophe?, J. Range Manage., 49, 512–519, doi:10.2307/4002292, 1996.

Rietkerk, M., Boerlijst, M., van Langevelde, F., HilleRisLambers, R., van de Koppel, J., Kumar, L., Prins, H., and de Roos, A.: Self-organization of vegetation in arid ecosystems, Am. Nat., 160, 524–530, doi:10.1086/342078, 2002.

Rietkerk, M., Dekker, S. C., de Ruiter, P. C., and van de Koppel, J.: Self-organized patchiness and catastrophic shifts in ecosystems, Science, 305, 1926–1929, doi:10.1126/science.1101867, 2004.

Rietkerk, M., Brovkin, V., van Bodegom, P. M., Claussen, M., Dekker, S. C., Dijkstra, H. A., Goryachkin, S. V., Kabat, P., van Nes, E. H., Neutel, A.-M., Nicholson, S. E., Nobre, C., Petoukhov, V., Provenzale, A., Scheffer, M., and Seneviratne, S. I.: Local ecosystem feedbacks and critical transitions in the climate, Ecol. Complex., 8, 223–228, doi:10.1016/j.ecocom.2011.03.001, 2011.

Rudolf, B. and Schneider, U.: Calculation of gridded precipitation data for the global land-surface using in-situ gauge observations, in: Proceedings of the 2nd Workshop of the International Precipitation Working Group IPWG, pp. 231–247, 2005.

Salzmann, U. and Hoelzmann, P.: The Dahomey Gap: an abrupt climatically induced rain forest fragmentation in West Africa during the late Holocene, Holocene, 15, 190–199, doi:10.1191/0959683605hl799rp, 2005.

Scheffer, M., Carpenter, S., Foley, J. A., Folke, C., and Walker, B.: Catastrophic shifts in ecosystems, Nature, 413, 591–596, doi:10.1038/35098000, 2001.

Scheffer, M., Holmgren, M., Brovkin, V., and Claussen, M.: Synergy between small- and large-scale feedbacks of vegetation on the water cycle, Global Change Biol., 11, 1003–1012, doi:10.1111/j.1365-2486.2005.00962.x, 2005.

Scheffer, M., Bascompte, J., Brock, W. A., Brovkin, V., Carpenter, S. R., Dakos, V., Held, H., van Nes, E. H., Rietkerk, M., and Sugihara, G.: Early-warning signals for critical transitions, Nature, 461, 53–59, doi:10.1038/nature08227, 2009.

Schurgers, G., Mikolajewicz, U., Groger, M., Maier-Reimer, E., Vizcaino, M., and Winguth, A.: Dynamics of the terrestrial biosphere, climate and atmospheric CO2 concentration during interglacials: a comparison between Eemian and Holocene, Clim. Past, 2, 205–220, doi:10.5194/cp-2-205-2006, 2006.

Sellers, W. D.: A global climatic model based on the energy balance of the earth-atmosphere system, J. Appl. Meteor., 8, 392–400, doi:10.1175/1520-0450(1969)008<0392:AGCMBO>2.0.CO;2, 1969.

Sieber, J. and Thompson, J. M. T.: Nonlinear softening as a predictive precursor to climate tipping, Phil. Trans. R. Soc. A, 370, 1205–1227, doi:10.1098/rsta.2011.0372, 2012.

Simonnet, E., Dijkstra, H. A., and Ghil, M.: Bifurcation analysis of ocean, atmosphere and climate models, in: Handbook of Numerical Analysis, edited by Ciarlet, P., vol. Volume 14, pp. 187–229, Elsevier, doi:10.1016/S1570-8659(08)00203-2, 2009.

Stommel, H.: Thermohaline convection with two stable regimes of flow, Tellus, 13, 224–230, doi:10.1111/j.2153-3490.1961.tb00079.x, 1961.

Strogatz, S.: Nonlinear Dynamics and Chaos. With Applications to Physics, Biology, Chemistry, and Engineering, Perseus Books Group, 1994.

Stull, R. B.: An Introduction to Boundary Layer Meteorology, Reidel Publishing Co., 1988.

Thompson, J. M. T. and Sieber, J.: Climate tipping as a noisy bifurcation: a predictive technique, IMA J. Appl. Math., 76, 27–46, doi:10.1093/imamat/hxq060, 2011a.

Thompson, J. M. T. and Sieber, J.: Predicting climate tipping as a noisy bifurcation: a review, Int. J. Bifurcat. Chaos, 21, 399–423, doi:10.1142/S0218127411028519, 2011b.

Thompson, J. M. T., Stewart, H. B., and Ueda, Y.: Safe, explosive, and dangerous bifurcations in dissipative dynamical systems, Phys. Rev. E, 49, 1019–1027, doi:10.1103/PhysRevE.49.1019, 1994.

Tietsche, S., Notz, D., Jungclaus, J. H., and Marotzke, J.: Recovery mechanisms of Arctic summer sea ice, Geophys. Res. Lett., 38, L02 707, doi:10.1029/2010GL045698, 2011.

Timmermann, A. and Lohmann, G.: Noise-induced transitions in a simplified model of the thermohaline circulation, J. Phys. Oceanogr., 30, 1891–1900, doi:10.1175/1520-0485(2000)030<1891:NITIAS>2.0.CO;2, 2000.

Tjallingii, R., Claussen, M., Stuut, J.-B. W., Fohlmeister, J., Jahn, A., Bickert, T., Lamy, F., and Rohl, U.: Coherent high- and low-latitude control of the northwest African hydrological balance, Nature Geosci., 1, 670–675, doi:10.1038/ngeo289, 2008.

van Nes, E. H. and Scheffer, M.: Implications of spatial heterogeneity for catastrophic regime shifts in ecosystems, Ecology, 86, 1797–1807, doi:10.1890/04-0550, 2005.

van Nes, E. H. and Scheffer, M.: Slow recovery from perturbations as a generic indicator of a nearby catastrophic shift, Am. Nat., 169, 738–747, doi:10.1086/516845, 2007.

Veraart, A. J., Faassen, E. J., Dakos, V., van Nes, E. H., Lurling, M., and Scheffer, M.: Recovery rates reflect distance to a tipping point in a living system, Nature, 481, 357–359, doi:10.1038/nature10723, 2012.

Viana, R. L., Camargo, S., Pereira, R. F., Verges, M. C., Lopes, S. R., and Pinto, S. E. S.: Riddled basins in complex physical and biological systems, J. Comp. Int. Sci., 1, 73–82, doi:10.6062/jcis.2009.01.02.0007, 2009.

Vincens, A., Buchet, G., Servant, M., and Collaborators, E. M.: Vegetation response to the 'African Humid Period' termination in Central Cameroon (7 degrees N) - new pollen insight from Lake Mbalang, Clim. Past, 6, 281–294, doi:10.5194/cp-6-281-2010, 2010.

von Hardenberg, J., Meron, E., Shachak, M., and Zarmi, Y.: Diversity of vegetation patterns and desertification, Phys. Rev. Lett., 87, 198 101–1–198 101–4, doi: 10.1103/PhysRevLett.87.198101, 2001.

Waller, M. P., Street-Perrott, F. A., and Wang, H.: Holocene vegetation history of the Sahel: pollen, sedimentological and geochemical data from Jikariya Lake, north-eastern Nigeria, J. Biogeogr., 34, 1575–1590, doi:10.1111/j.1365-2699.2007.01721.x, 2007.

Wang, G. L.: A conceptual modeling study on biosphere-atmosphere interactions and its implications for physically based climate modeling, J. Climate, 17, 2572–2583, doi:10.1175/1520-0442(2004)017<2572:ACMSOB>2.0.CO;2, 2004.

Wang, G. L. and Eltahir, E. A. B.: Biosphere-atmosphere interactions over West Africa. II: Multiple climate equilibria, Q. J. Roy. Meteor. Soc., 126, 1261–1280, doi:10.1002/qj.49712656504, 2000.

Wang, Y., N. M. L. Z. G. R. L. S. and Kutzbach, J. E.: Detecting vegetation-precipitation feedbacks in mid-Holocene North Africa from two climate models, Clim. Past, 4, 59–67, doi: 10.5194/cp-4-59-2008, 2008.

Watson, A. J. and Lovelock, J. E.: Biological homeostasis of the global environment: the parable of Daisyworld, Tellus, 35B, 284–289, doi:10.1111/j.1600-0889.1983.tb00031.x, 1983.

Weldeab, S., Frank, M., Stichel, T., Haley, B., and Sangen, M.: Spatio-temporal evolution of the West African monsoon during the last deglaciation, Geophys. Res. Lett., 38, L13 703, doi: 10.1029/2011GL047805, 2011.

Wieczorek, S., Ashwin, P., Luke, C. M., and Cox, P. M.: Excitability in ramped systems: the compost-bomb instability, P. Roy. Soc. A - Math. Phy., 467, 1243–1269, doi: 10.1098/rspa.2010.0485, 2011.

Wiesenfeld, K.: Noisy precursors of nonlinear instabilities, J. Stat. Phys., 38, 1071–1097, doi: 10.1007/BF01010430, 1985a.

Wiesenfeld, K.: Virtual Hopf phenomenon - a new precursor of period-doubling bifurcations, Phys. Rev. A, 32, 1744–1751, doi:10.1103/PhysRevA.32.1744, 1985b.

Wiesenfeld, K. and McNamara, B.: Small-signal amplification in bifurcating dynamical systems, Phys. Rev. A, 33, 629–642, doi:10.1103/PhysRevA.33.629, 1986.

Williams, J. W., Blois, J. L., and Shuman, B. N.: Extrinsic and intrinsic forcing of abrupt ecological change: case studies from the late Quaternary, J. Ecol., 99, 664–677, doi:10.1111/j.1365-2745.2011.01810.x, 2011.

Wissel, C.: A universal law of the characteristic return time near thresholds, Oecologia, 65, 101–107, doi:10.1007/BF00384470, 1984.

Wolff, U.: Critical slowing down, Nucl. Phys. B-Proc. Sup., 17, 93—-102, doi:10.1016/0920-5632(90)90224-I, 1990.

Zeng, N. and Neelin, J. D.: The role of vegetation-climate interaction and interannual variability in shaping the African savanna, J. Climate, 13, 2665–2670, doi:10.1175/1520-0442(2000)013<2665:TROVCI>2.0.CO;2, 2000.

Zeng, N., Hales, K., and Neelin, J. D.: Nonlinear dynamics in a coupled vegetation-atmosphere system and implications for desert-forest gradient, J. Climate, 15, 3474–3487, doi:10.1175/1520-0442(2002)015<3474:NDIACV>2.0.CO;2, 2002.

Acknowledgements

I heartily thank everybody who helped me to accomplish this thesis. In particular, I am grateful to

my supervisor Martin Claussen for his providence, encouragement and reliability,

my supervisor Klaus Fraedrich whose profound and creative approach to science is an inspiration,

Jörn Behrens for his supervision as a panel chair and his exceedingly prudent advice,

the Max Planck Institute and Max Planck Society for the financial support to visit conferences, workshops and summer schools and to cover the service charges of publications,

the Deutsche Forschungsgesellschaft for the project funding within the Cluster of Excellence CliSAP,

the German Climate Computing Center (DKRZ) for the arrant computing time on tornado (R.I.P.),

the anonymous reviewers for helping to improve the manuscripts,

Reiner Lauterbach for his very kind and clear explanations (especially for a mathematician),

Holger Kantz, Steven Lade, Marten Scheffer, Vasilis Dakos, Zhengyu Liu and Andrea Cimatoribus for their altruistic and kind advice and the fruitful discussions,

Christian Reick, Hermann Held, Thomas Kleinen, Victor Brovkin, and Jin-Song von Storch for their helpful comments,

Helge for his meticulousness and persistency regarding scientific hobbies,

Helge, Fabio and Jessica for patience with my swearing, cheering, telephoning and permanent shutting of the blinds,

Daniel for his beneficial positive disrespectfulness,

all members of the MPI vegetation groups for the comfortable working atmosphere with the right mix of productivity and distraction,

Jörn-Peter Boll for creative stimulation,

Peter Beekmann for the faithful PENNY MOBIL relationship,

Robert Schoetter for the lunchtime lessons and exciting bets at the edge of moral integrity,

Dr. Sheldon Cooper for his singular remarks,

and Walter White for the display of his inspiring career.



ISSN 1614-1199